ADDIS ABABA INSTITUTE OF TECHNOLOGY

SCHOOL OF CIVIL AND ENVIRONMENTAL ENGINEERING

EVALUATION IMPACTS OF SCUFFING FORCES INDUCED DUE TO BRAKING AND TURNING OF VEHICLES ON THE FLEXIBLE PAVEMENT PERFORMANCE CAPACITY USING FINITE ELEMENT MODELING APPROACH

A Thesis Submitted to the School of Civil and Environmental Engineering Addis Ababa University in Partial Fulfillment for the Requirement of Degree of

Master of Science

(Road and Transport Engineering)

By: Girmaye Kebede

Advisor: Dr. Ephrem Taddesse

ADDIS ABABA UNIVERSITY

FEBRUARY, 2020

ADDIS ABABA INSTITUTE OF TECHNOLOGY

SCHOOL OF CIVIL AND ENVIRONMENTAL ENGINEERING

EVALUATION IMPACTS OF SCUFFING FORCES INDUCED DUE TO BRAKING AND TURNING OF VEHICLES ON THE FLEXIBLE PAVEMENT PERFORMANCE CAPACITY USING FINITE ELEMENT MODELING APPROACH

SUBMITTED BY:

GIRMAYE KEBEDE

APPROVED BY BOARD OG EXIMINERS

1.	Dr. Ephrem Taddesse	_____	_____
	Main advisor	signature	date
2.	Mr.Tewodros Nigatu	_____	_____
	Internal examiner	signature	date
3.	Mr.Atnafu Admas	_____	_____
	External examiner	signature	date
4.	Dr.Ing. Mebruk Mohammed	_____	_____
	Chairperson	signature	date

Acknowledgment

First of all, thanks God for strengthening me and the unlimited blessings to do this study.

I would like to express my sincere gratitude to my advisor Dr. Ephrem Taddesse for giving me his invaluable time and scientific direction in this study.

Special thanks to Dr. Bikila T. & Asres S., for their considerable effort and great help.

Finally, my sincere appreciation is also extended to Almaz .G , Desta. N , Elias.L & Gugsa.A for their encouragement, support and giving peer review of the study.

Abstract

The induced scuffing force is one of the major factors that significantly affect the distress resisting capacity of flexible pavement at vehicles stop or turn. Braking causes extra significant longitudinal load on the flexible pavement surface whereas turning causes additional significant lateral load on the pavement surface. These additional horizontal forces (scuffing) are controlled by tire slip ratio, road adhesion coefficient and tire turning angle/angle of steering

Thus the objective of this study was identification and evaluation of the major possible causes that responsible for the premature failure of flexible pavement mainly in vehicles' stopping and turning areas or stretches.

In this study, the flexible pavement responses to tire-pavement moving loads (vertical load, longitudinal load, and lateral load) at various rolling conditions were examined with developed (3-D) finite element model. The flexible pavement structure layers characterized as elastic materials, and the transient dynamic tire loadings were simulated using trapezoidal moving load for transient dynamic analysis. The analyses were mainly on the rolling conditions (braking load, turning load and free rolling load); affectivity of asphalt concrete thickness with shear stress-strain and influence of braking and cornering on pavement interface were investigated.

The study found that, top-down fatigue cracking and shoving are the main distress type observed at tire braking and turning. The damage ratio of fatigue cracking due to tire braking is, 2.04 times compared to free rolling condition; the shoving potential of asphalt due to tire turning is 1.93 times compared to free rolling condition and the shoving potential of asphalt due to tire braking is 2.85 times compared to free rolling condition.

The overall impacts of scuffing load due to braking and turning of vehicles is estimated. The combined relative damage ratio convenes that, braking of tire reduces the pavement distress resisting capacity approximately by 1.77 times, and turning reduces the capacity by 1.33 times compared to free rolling conditions.

Thickness optimization for shear stress-strain for typical flexible pavement structure (150mm, 170mm, 190mm, 210mm, and 240mm asphalt thickness) showed that the thickness barely increase carrying capacity of scuffing force unless it increased more; that is uneconomical. The effect of scuffing force is also significant at the interface of asphalt and base course that reduce the performance of flexible pavements.

Key words: Finite element model, moving load, scuffing force, relative damage & flexible pavement.

Contents

List of tables

List of figures

Chapter -1

1.1 Introduction

Road pavement deterioration has become a growing issue in Ethiopia, and the causes of these problems have not been fully identified; the solutions are not commonly understood (TEMESGEN, 2016). Most of the constructed roads failed prematurely before their service life, and the traffic loadings have the highest share factors for pavement failure (Asnake, 2015). Especially the traffic loading at intersections cause a significant pavement deterioration such as asphalt rutting, shoving, slippage cracking and so on, which offer a clear evidence that tire braking and turning imposed extra scuffing stress that might change the stress-state near the surface of a flexible pavement (Wang and Al-qadi, 2011).

Some special sections of the pavement more likely subjected to braking and turning would beer a great scuffing (horizontal) stresses, and these loads might cause adverse effects on the responses of pavement. At braking, concentrated longitudinal stresses push the material, thus, causing displacement of localized areas resulting in shoving and crescent cracking. This surface-related damage is directly related to the variation of tire-pavement contact results of tire braking and turning (Shakiba *et al.*, 2016).

The scuffing loads generated by vehicle movement are transferred to the pavement tires rolling friction, road sliding friction and lateral friction. The conventional (traditional) pavement design method can't differentiate the stresses distribution at tire pavement interface under different rolling conditions. And also the model(static) can't explain the phenomenon of the road damage intersection may appear damage phenomena earlier than roads, including deformation, rutting, fatigue cracking, etc. (Jin *et al.*, 2015).

Braking and turning of moving tires can cause sliding and deforming the surface of layers of pavement structures. The top layer absorbs the stresses due to slide/ deform and unable to transfer effectively to the entire depth of the pavement structures, thus, layer interface debonding/slippage often arise and fatigue life of the pavement is reduced because of the tangential shear load on the pavement. Effectiveness of asphalt thickness sensitively reduces this shear stress.

Thus, for clear understanding of lateral and longitudinal dynamics of tire-pavement interaction, at the sensitive areas of road sections, where braking and turning could usually take places, that might affect the critical responses of pavement and enhances the potential of pavement damage is a certain practical significance to be analyzed using finite element (3-D) model considering different rolling condition.

Asphalt thickness optimization for shear stress and asphalt base course interface condition also discussed based on the analysis from FE analysis.

1.2 Statement of Problem

The goal of structural design is to limit the level of distress, deformation and cracking to predetermined values that show appropriate remedial treatment at the end of the design period.

However, most of the roads constructed in Ethiopia fail prematurely before serving the design life due to various causes arises from many factors. The pavement extensive damage, rutting, shoving and slippage cracking are the major problems associated with flexible pavement in the area where vehicles stop or turn(RAZA, 2017).

These phenomena usually happen on pavements at signalized intersections, toll plaza, roundabouts, speed breaker, vehicle station etc. where braking and turning of the vehicle mostly taken place. This road sections are mostly under the excessive scuffing force due to vehicle tires breaking and turning that accelerates deterioration of pavement more severe than other road section.

The major problems at these regions are extensive damage, rutting, shoving and slippage crack of pavement as shown in figure 1. This deterioration of pavement may be caused by higher shear stress concentration /shear flow from scuffing force (horizontal load) due to certain maneuver of vehicles (braking and turning).

Figure1.0: pavement deform in turning area.

In response to this problem, this study propose to investigate why there was a persistent gap, despite the aim of structural pavement design, and to suggest improving material design, pavement design and maintenance technique based on findings.

1.3 General Objective

The main purpose of this study was to evaluate the effect of scuffing forces on flexible pavement through pavement critical responses with FE method and identify possible causes of premature damage of the pavement at vehicles turn and stop.

1.3.1 Specific Objective

1. The relative damage of pavement evaluation, using the calculated pavement responses and availed damage model.
2. Determine the effects, on lifetime of pavement structures using damage ratio.
3. Examine the effect of asphalt thickness to mitigate the influence of shear stress on pavement capacity.

1.4 Research Questions

1. What are the major factors of scuffing/ tangential load induction?
2. What are the impacts of scuffing forces at critical flexible pavement responses & its consequences on damage (deformation) relatively?
3. Does increase the asphalt thickness; has significant change on shear stress?
4. How the conditions of layers interface affect the performance of pavements?

1.5 Scope of the Study

The scope is focused on issues related to pavement response because of significant tangential loads (longitudinal and lateral tire force).

The research is also limited to the study of the impact of vehicles tire turning & braking conditions.

1.6 Motivation of the Study

Most academic researches on pavement analysis and design have concentrated on experimental performance of pavements under vertical loading and general problems on the whole portion of road sections rather than particular sections where certain maneuvers like braking and turning aggravate, premature damage of pavement sections.

Vehicle dynamic load transfer and stationary vehicle load transfer are completely different, that stated by Newton's law of motion that explained detail under longitudinal and lateral vehicle dynamics in chapter -2 of this study. Vehicle at braking situation, the load is transferred to the front wheel, and tire-pavement interaction produces large longitudinal scuffing force which is not considered during pavement design. Similarly, at the time of turning/cornering, the load transferred to the side and outer tire would be subjected to large centripetal forces, which in turn subject pavement to significant lateral force. These ignored forces in design load create motivation to investigate the effect in the context of Ethiopia.

Moreover, the motivation to conduct research on this area comes from practical problems encountered in daily life when traveling from place to place especially, in Addis Ababa city. Due to a huge number of traffic, excessive rate of pavement deterioration is observed at curved and accelerated/decelerated road sections. This pavement failure, in turn, causes the government to allocate budget for repair/maintenance before its design life.

In general these all situation initiate me to identify and understand the probable causes as well as to know how much our design specifications is responsible to withstand the coming shear stress from reaction force which is induced due to tire-pavement contact friction and also to suggest analytical analysis like finite element method beside experimental performance.

1.7 Significance of the Research

Nowadays, even though there are new merging flexible pavement analysis and design, very few is known about the tire-pavement interaction association with pavement deterioration & extent to consideration of longitudinal and transverse loads reduce the distresses of pavement layers.

The willingness to investigate the effect of dynamic loading at various loading and rolling conditions is the pushing force to conduct this research. The results of this research would provide a concept that considering vertical loading at these areas alone is not the primary cause for pavement distresses for decision-makers and pavement engineers.

In addition, it is the researcher's belief that the study possibility will be taken as input for further researches.

Chapter-2

2 Literature Review

2.1 General

Pavements are structures built to hold and maintain vehicular masses & categorized into:

- ♣ Rigid pavement
- ♣ Flexible pavement
- ♣ Unpaved (gravel or dirty) pavement (Adlinge and Gupta, 2009).

This study focused on flexible pavements which have be constructed as several layers of material of high quality at the top and lower quality at bottom. Strongest material at top, and weakest material at bottom would be used for the reason that at surface layer, tire load applied at small area as a result, high-stress level occurred whereas deeper portion of the pavement layers subjected to disperse load to large area as could be seen from figure 2, that results to small stress level (Adlinge and Gupta, 2009).

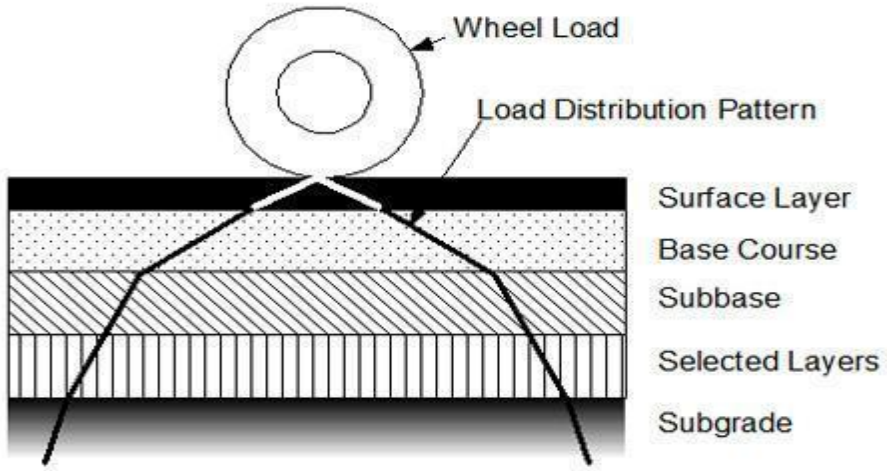

Figure 2.0: Load Distribution of Flexible Pavement (Adlinge and Gupta, 2009)

2.2 Pavement Deterioration (Distress) types

Pavement distress is defined as ”Any indication of poor or unfavorable pavement performance or signs of impending failure; any unsatisfactory performance of a pavement short of failure**”**(Rather and Lateef, 2016)**.** Researchers (Adlinge and Gupta, 2009) stated that the applied load on the pavement was often less than the strength of the material in the pavement structure. That implied, one load application couldn’t fail pavement but caucused small distress or deterioration, which gradually increased to reach an unacceptable level.

Pavement deterioration was a severe problem that causes distort pavement aesthetics, damage parts of vehicles, traffic accidents, and mainly lead to premature failure (damage) of the highway structural pavement (Zumrawi, 2015).

The main types of pavement deterioration are:

- Rutting
- Cracking
  - Fatigue cracking
  - Seasonal (frost heave) cracks
  - Joint construction cracking
  - Edge (verge) cracking
  - Block Cracking
  - Joint Reflection Cracking
- Potholes
- Bleeding
- Ravelling
- Stripping
- Corrugation and shoving
- Segregation
- Patching
- Polishing
- Depressions
- Slippage cracking
- Water bleeding and pumping

The common distresses at intersections and curved sections are rutting, shoving (corrugation), slippage and fatigue cracking in which this study focused on (Abdallah and Nazarian, 2011).

2.3 Causes of Pavement Deterioration

The main factors that contribute to pavement deterioration are environmental factors, material quality, construction quality, design standard, traffic and loading, and ages of pavement (Zumrawi, 2015).

2.3.1 Traffic volume and Loading

Roads are highway structures that to be built so as to hold and maintain vehicular masses. Therefore traffic is an important issue that has impacts overall pavement performance. Mostly, deterioration of pavements was because of vehicle loads and quantity. Each vehicle, which passes over a road, reasons a momentary but extensive deformation in the street shape. This is determined by way of the significance of every of its axle masses, the spacing among the axles, the number of wheels, the touch pressures of the tires and the touring velocity. The passage of many automobiles has a cumulative impact which reasons repeated flexing of the pavement main to fatigue cracking and structural failure(Huang, 2004)

2.3.2 Material properties and Composition

The selection of materials used for the construction of pavement layers may additionally cause road deterioration. This is due to inherent variability within the materials used for road construction in terms of soil properties together with strength or load-bearing ability, gradation; mix properties, elastic and resilience modulus.

If materials with low quality used for pavement layers, that will have an adverse effect on the strength of the layers and their subsequent performance (Huang, 2004).

The effect of moving load applications in the lateral and longitudinal direction and material properties were the main study areas in this paper.

2.4 Load of moving vehicle

Dynamics vehicle is engineering subject about its motion in relevant to the user operation (Pradko, 2016). It also concerned with the movement of vehicle, acceleration, braking, and cornering. The behavior of vehicles are determined by the imposed forces from tires, gravity and air load (Reif, 2014).

These behaviors could be expressed by Newton's second law of motion that govern longitudinal, lateral and yaw moments(Gillespie, 1992)

$$\begin{cases} \sum F_x = Ma_x \\ \sum F_y = Ma_y \\ \sum T_x = I_{xx}\alpha_x \end{cases} \quad (2.1)$$

. Where: M is total mass of the body

F_y: Lateral force

F_x : Longitudinal force

Tx: Torque about the x- axis

a_x: Longitudinal acceleration

a_y: Lateral acceleration

I_{xx}: Moment of inertia about x- axis

α_x: Angular acceleration

2.5 Load of Static Vehicle Distribution to the pavement.

Static load distribution takes the first step in analyzing of vehicle force that describe the dynamic behavior of the vehicle(Gillespie, 1992). Stationary vehicle on the road has the sprung mass at center of gravity (CG) tends to be transmitted to the ground through tires. Tires take the distributed load from axles and transmit it to the ground. Front and rear tires may have no the same weight distribution efficiency. Weight (load) distribution efficiency is affected by longitudinal distance of tire from center of gravity of vehicle body. If the (CG) is located at the middle of front and rear tires, load distribution factor is equal (50%) for both front and rear tires.

Static Loads distribution of four wheeled vehicles to ground:

a) To flat level ground

When vehicles stop on leveled ground, their weight distributed to front and rear tires through distribution factors & then to the ground.

$$\begin{cases} W_f = W\left(\frac{l_r}{L}\right) \\ W_r = W\left(\frac{l_f}{L}\right) \end{cases} \quad (2.2)$$

Where:W_f: front axle normal force.

W_r: Rear axle normal force.

l_f : Longitudinal distance from center of gravity (CG) to front axle.

l_r : Longitudinal distance from center of gravity (CG) to rear axle;

L: Wheelbase length (L=$l_f + l_r$) of vehicle.

b) To banked angle (α) ground

$$\begin{cases} W_i = \frac{W}{2} + \frac{Wh}{t}\alpha \\ W_o = \frac{W}{2} - \frac{Wh}{t}\alpha \end{cases} \quad (2.3)$$

Where: W_i: inner tire normal force.

W_o: Outer tire normal force;

h: height of CG above ground ;

t: rack width; & α: Bank angle in radian;

c) To gradient angled(θ) ground

$$\begin{cases} W_f = W\left(\frac{l_r}{L}\right) - W\frac{h}{L}\theta \\ W_r = W\left(\frac{l_r}{L}\right) + W\frac{h}{L}\theta \end{cases} \quad (2.4)$$

θ: Gradient angle in radian.

2.6 Load of Moving Vehicle Transfer to Pavement;

When the vehicle is in motion (dynamic) condition, static weight can transfer to front, rear or side a vehicle based on vehicle maneuver conditions (Rajamani, 2006) &(Gillespie, 1992).

- At braking condition the load can transfer to front axle tire;
- At accelerating condition, load can transfer to rear axle tire;
- At cornering (turning) condition, load can transfer to side to side.

(Gillespie, 1992) explained the governing equations as follow:

✓ During braking : $\begin{cases} W_f = \left(\frac{l_r}{L}\right)W + \frac{W}{g}\frac{h}{L}a_x \\ W_r = \left(\frac{l_f}{L}\right)W - \frac{W}{g}\frac{h}{L}a_x \end{cases}$ (2.5)

✓ During acceleration: $\begin{cases} W_f = \left(\frac{l_r}{L}\right)W - \frac{W}{g}\frac{h}{L}a_x \\ W_r = \left(\frac{l_f}{L}\right)W + \frac{W}{g}\frac{h}{L}a_x \end{cases}$ (2.6)

During cornering (turning):

Load transfer of turning vehicle is varied based on height of roll center which is called geometric load transfer and roll stuffiness that is called elastic load transfer (Doumiati et al., 2009). The steady-state equation for lateral load transfer if vehicle is turning to right, as could be seen in figure 2.1, the equation is given by

✓ $\Delta Fz = \begin{cases} = Fz_{fl} + Fz_{rl} - Fz_{fr} - Fz_{rr} \\ = -2\left(\frac{k_f}{ef} + \frac{k_r}{er}\right)\theta - \frac{2w}{g}a_y/L\,(\frac{l_f h_f}{ef} + \frac{l_f h_r}{er}) \end{cases}$ (2.7)

Where: h is height of center of gravity (CG)
h_f: Height of front roll center
h_r: Height of rear roll center
$e_f \& e_r$: $front\ and\ rear\ vehicl'strack$
θ: $rolling\ angle\ of\ body$
$k_f \& k_r$: Front and rear roll stiffness.
a_y: Lateral acceleration

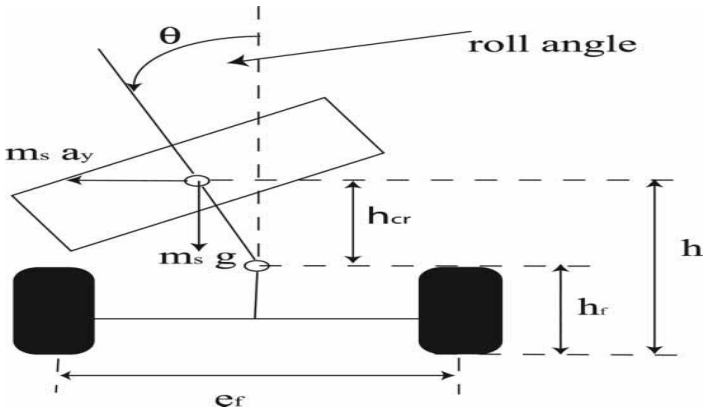

Figure 2.1: Roll Dynamics (Doumiati *et al.*, 2009)

2.7 The Major Categories of Vehicle Movement to Induce Scuffing forces on the Pavement.

2.7.1 Longitudinal Dynamics Movement Induced Forces.

Longitudinal dynamics is the forward movement of the vehicle that needed to generate torques on the tires as shown in fig 2.2. When the vehicle is in rectilinear motion; there are motive (driving/tractive) forces and retarding (resisting) forces.
The magnitudes of these forces are varying depending on vehicle operations such as acceleration, braking and normal movements (Hirz, 2015).

- During acceleration, motive force is governor.
- During braking, resistive force is governor.
- During normal (free rolling) movement, both are balancing each other.

Figure 2.2 shows that different type of forces acting on moving vehicle.

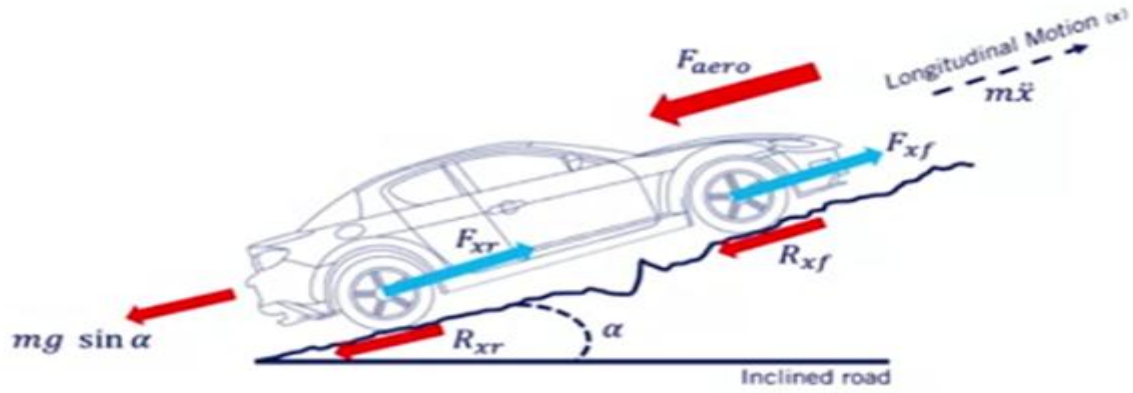

Figure 2.2: Balancing force along the vehicle longitudinal motion(x) yields(Rajamani, 2006)

Equation of motion could be developed by applying Newton's second law of motion.

$$Ma_x = F_{xf} + F_{xr} + F_{aero} + R_{xf} + R_{xr} + M_g sin\alpha \quad (2.8)$$

Where: F_{xf}, is the longitudinal tire force at the front tires

Fx, is the longitudinal tire force at the rear tires

F_{aero},, is the equivalent longitudinal aerodynamic drag force

$R_{xf,}$ is the force due to rolling resistance at the front tires

$R_{xr,}$ is the force due to rolling resistance at the rear tires

M, is the mass of the vehicle

g, is the acceleration due to gravity

To simplify the equation,(2.8)

Let Fx- total longitudinal force: $Fx= F_{fx} +F_{xr}$

Let Rx- total rolling resistance: $Rx=R_{xf} +R_{xr}$

Assume α is small angle: sinα=α

Then the simplified longitudinal dynamics become;

$$Ma_x = F_x + F_{aero} + R_x + M_g\alpha \quad (2.9)$$

2.7.1.1 Total Rolling Resisting Forces

As can see from the figure(2.2) above, there are two major opposing forces that determine the rectilinear motion of vehicle; these are motive(tractive) forces and resistive forces(Mannering and Washburn, 2012).

Resistance is defined as the forces that are impeding motion of vehicles.

There are three primary sources of vehicle resistance:

I. Aerodynamic resistance

Aerodynamics Resistance (F_{aero})

Aerodynamic force is dragging force which resisting motion of a traveling vehicle at a particular speed. This force resists the speed of vehicles that have significant impact on vehicle performance and composed from different sources(Mannering and Washburn, 2012).

- Turbulent air flow around vehicle body (85%)
- Friction of air over vehicle body (12%)
- Vehicle component resistance, from radiators and air vents (3%)

$$R_{aero} = \frac{\rho}{2} C_d A_f \, V^2 \qquad (2.10)$$

Where: ρ air density

C_d : drag coefficient

A_f: Vehicle's frontal area

V: Driving speed (taking account of the headwind speed)

2.7.1.2 Tires Rolling Resistance forces

Tire and road are subjected to deformation in contact batch while tire is rolling. As tire is loaded with vertical force, the components of tire materials deflect vertically. This loss energy considered as a force on tires called rolling resistance that opposes the longitudinal movement of the vehicle (Rajamani, 2006).

There are at least seven mechanisms responsible for rolling resistance:

1) Energy loss due to deflection of the tire sidewall near the contact area;

2) Energy loss due to deflection of the tread elements;

3) Scrubbing in the contact patch;

4) Tire slip in the longitudinal and lateral directions;

5) Deflection of the road surface;

6) Air drag on the inside and outside of the tire;

7) Energy loss on bumps.

Wide ranges of factors affects total rolling resistance are(Mannering and Washburn, 2012):

- Resistance from tire deformation (~90%)
- Tire penetration and surface compression (~4%)
- Tire slippage and air circulation around wheel (~ 6%)

Simplifying approximation:

$$R_x = f_{rl} W \quad , W = W_f + W_r \tag{2.11}$$

Where: $\boldsymbol{f_{rl}}$ is rolling resistance coefficient

W is weight of vehicle on front and rear tires..

To illustrate more, let as compute the balance moment for figure (2.3) and derive equation for rolling resistance of moving tire.

Summation of moment at center of contact patch is zero.

$$\begin{cases} \sum M = 0 \\ -R_X * r_{stas} - F_Z * \Delta x = 0 \\ -R_X = F_Z * \frac{\Delta x}{r_{stas}} \quad , \quad \frac{\Delta x}{r_{stas}} = \ f_{rl} \end{cases} \tag{2.12}$$

$$frl = fo + fs\left(\frac{v}{100}\right)^{2.5} \tag{2.13}$$

Where: V is speed of vehicle in km/hr, and f_0 and *fs* depend on inflation pressure of the tire.

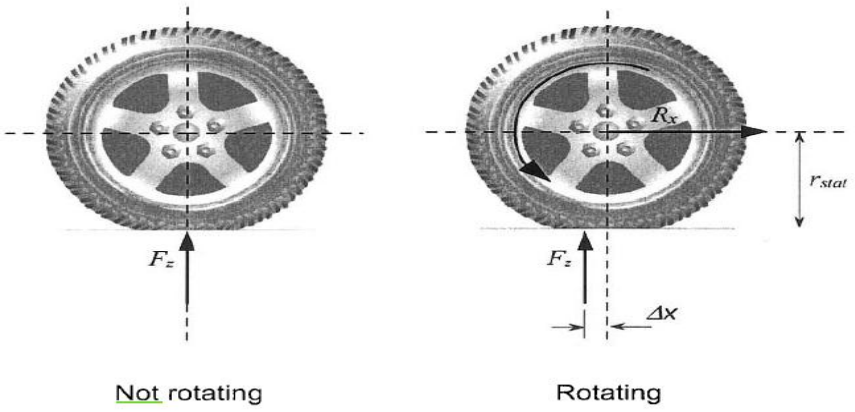

Figure 2.3: Description of rolling resistance

Some general relation with speed and tire types would have been developed from(Wong, 2001).

Radial-ply passenger car: $frl = 0.0136 + 0.04.10^{-6}.v^2$

Bias-ply passenger cars: $frl = 0.0169 + 0.19.10^{-6}.v^2$

Radial-ply truck : $frl = 0.006 + 0.23.10^{-6}.v^2$

Bias-ply truck: $frl = 0.007 + 0.45.10^{-6}.v^2$

Table2.1: Rolling resistance coefficient (Wong, 2001)

Rolling Resistance Coefficients

Conditions	Rolling resistance coefficient
Car tires on concrete or asphalt	0.013
Car tires on rolled gravel	0.02
Tar macadam	0.025
Unpaved road	0.05
Field	0.1–0.35
Truck tires on concrete or asphalt	0.006–0.01
Wheels on rail	0.001–0.002

Grading Resistance

At a vehicle move up or down on inclined road, its weight decomposed and produce a force which is directed downward.

$Rg = \pm Wsin\alpha$

2.7.1.3 Tractive force and braking force

- **Tractive force**

Tractive force is the force available, at pavement to perform work.
It is a motiving force that would be needed to overcome the total rolling resistance forces.
Tractive forces(Ftf+Ftr) are longitudinal force that comes from portion of vehicle weight and influenced by location of vehicle center of gravity(CG),tire slip ratio, normal load and tire-pavement friction coefficient(Wong, 2001). Figure 2.4 shows the phenomena that would happen during straight line moving of vehicle with tractive (drive) force.

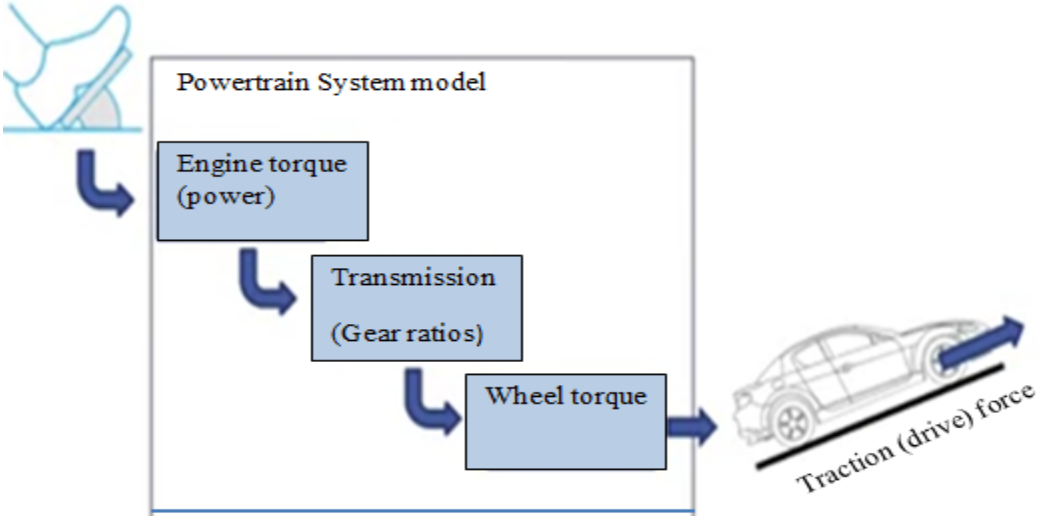

Figure2.4: Traction pedal system of vehicle (Reif, 2014).

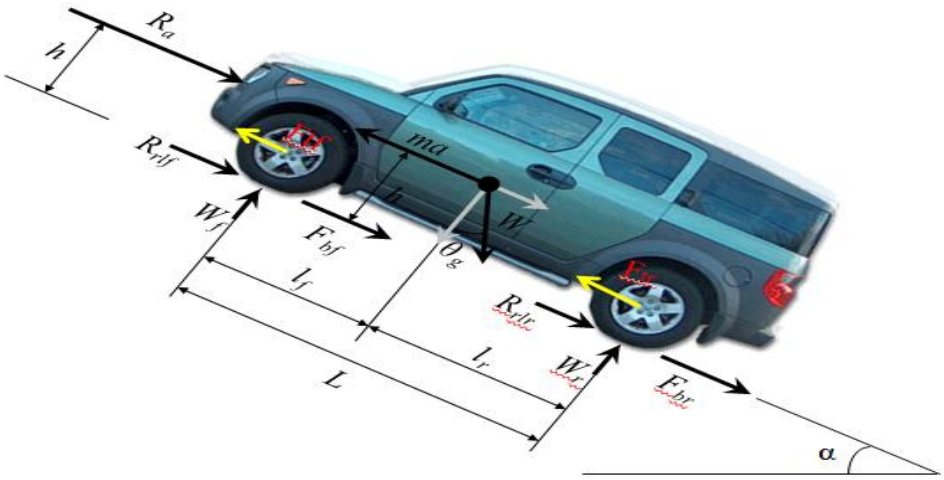

Figure2.5: Free body diagram of vehicle in motion

Ra = aerodynamic resistance,

W = total vehicle weight in,

R_{rlf} = rolling resistance of the front tires,

θg = angle of the grade in degrees,

R_{rlr} = rolling resistance of the rear tires,

M = vehicle mass,

F_{tf} = available tractive effort of the front tires,

a = acceleration

F_{tr} = available tractive effort of the rear tires,

Newton's second law for vehicle traction

$$\frac{dv}{dt} = \sum \frac{[Ft - Fr]}{Mv\varepsilon}$$

V: vehicle speed

ε:mass factor

The dynamic equation of vehicle motion along the longitudinal direction is expressed by:

$$M(\frac{dv}{dt}) = (Ftf + Ftr) - (Frf + Frr + Ra + Rg) \qquad (2.14)$$

Where $\frac{dv}{dt}$or $a_x$is acceleration along the longitudinal direction and M is vehicle mass;

Summation of the moment at center of (rear &front) tire contact patch respectively, the vertical force on front axle (Wf) and rear axle (Wr) can be computed as:

✓
$$\begin{cases} Wf = \frac{\{Wl_r cos\theta - h(Rg + Ra + Ma_x)\}}{L} \\ Wr = \frac{\{Wl_f cos\theta + h(Rg + Ra + ma_x)\}}{L} \end{cases} \qquad (2.15)$$

Summing the forces along the vehicle's longitudinal axis provides the basic equation of vehicle motion

$$\checkmark \begin{cases} (Ftf + Ftr) = Fa + Rx \pm Rg + ma_x \ \ , ignoring\ brake\ forces \\ Ft - Rx = Fa \pm Rg + ma_x \ \ , if \ \ F_{tf} + F_{tr} = Ft\ \ total\ trac \\ Wf = \frac{\{Wl_r cos\theta - h(Ft-Rx)\}}{L} \\ Wr = \frac{\{Wlf cos\theta + h(Ft-Rx)\}}{L} \\ Ftmax = \mu Wf = \ \mu\left[\frac{\{Wl_r cos\theta - h(Ft-Rx)\}}{L}\right] \\ F_{tfmax} = \left\{\frac{\frac{\mu W cos\theta[l_r + f_{rl}h]}{L}}{1+\mu\frac{h}{L}}\right\} \qquad , Rx = f_{rl}W \end{cases} \tag{2.16}$$

Where: f_{rl} is the coefficient of the rolling resistance, coefficient of road adhesion μ.

Coefficient of tire-pavement frictions are different based on pavement and vehicle movement condition as shown in table 2.2(Mannering and Washburn, 2012).

Table2. 2: typical values of coefficient frictoin (Wong, 2001)

	Coefficient of road adhesion	
Pavement	Maximum	Slide
Good, dry	1.00*	0.80
Good, wet	0.90	0.60
Poor, dry	0.80	0.55
Poor, wet	0.60	0.30
Packed snow or ice	0.25	0.10

Similarly For **a rear-wheel-drive** vehicle,

$$\checkmark \begin{cases} F_{tmax} = \mu Wr = \mu\left[\frac{\{Wl_f cos\theta + h(Ft-Rx)\}}{L}\right] \\ F_{trmax} = \left\{\frac{\frac{\mu W cos\theta\left[l_f - f_{rl}h\right]}{L}}{1-\mu\frac{h}{L}}\right\} \end{cases} \tag{2.17}$$

Summary during acceleration, the maximum tractive forces of front and rear tires (F_{tfmax}&F_{trmax}) are significantly different. The magnitude maximum tractive force on the rear tire is larger than that of front tire force. These imbalance forces accelerate pavement distresses of road section where acceleration of vehicles would have taken place.

2.7.1.4 Braking force

As can be seen in figure (2.6) that, the braking forces and tractive forces in the opposite direction because the braking forces are counteracting the forward motion.

The brake pad is pressed against the brake plat, thus developing a frictional torque on the brake plate, as shown in figure bellow.

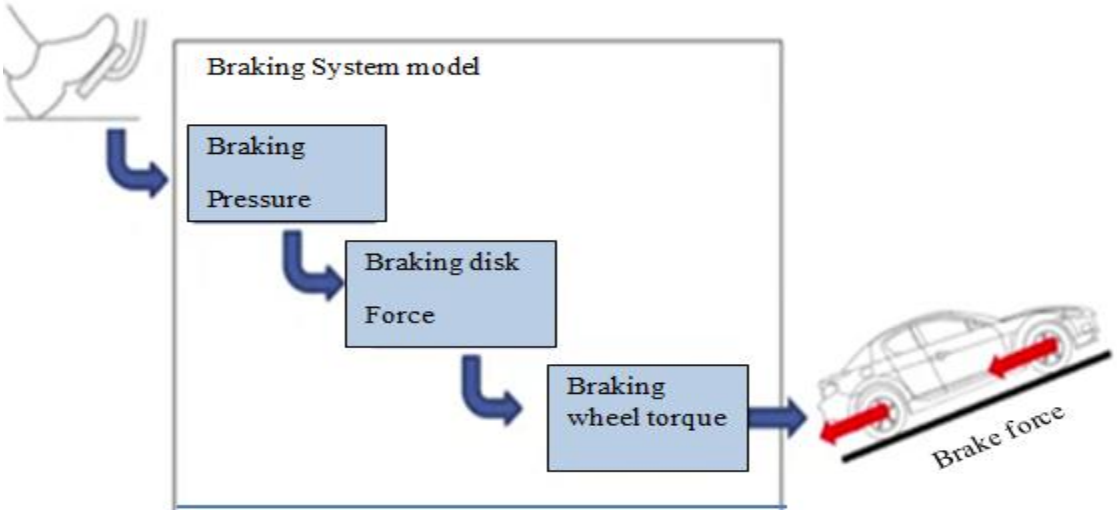

Figure 2.6: Braking pedal system (Reif, 2014)

✪ Derivative of braking force from fig, 2.5

Maximum braking force equation can derived in same fashion of traction force using equilibrium condition; at this time ignore tractive forces.

$$\checkmark \begin{cases} Wf = \frac{(Wl_r cos\theta + h(ma_x - Ra \pm Rg))}{L} \\ Wr = \frac{(Wlf cos\theta - h(ma_x - Fa \pm Rg))}{L} \end{cases} \quad (2.18)$$

Summing forces along the longitudinal axis gives;

$Fb + Rx = m\vec{a} - Fa \pm Rg$

Where: $Fb = Fbf + Fbr$

Substituting into (2.19) equation,

$$\checkmark \begin{cases} wf = \frac{Wl_r cos\theta}{L} + \frac{h(Fb+Rx)}{L} \\ wr = \frac{Wl_f cos\theta}{L} - \frac{h(Fb+Rx)}{L} \\ Rx = frW, Fbf\ max = \mu wf, Fbr\ max = \mu wr \\ F_{bfMax} = \frac{\mu W l_r cos\theta (lr + h(\mu + f_{rl}))}{L} \\ F_{brMax} = \frac{\mu W lf cos\theta (l_f - h(\mu + f_{rl}))}{L} \end{cases} \quad (2.19)$$

Summary: comparing, front tire and rear tire braking force(F_{bfMax} & F_{brMax}) would show us, front tires braking force is greater than rear tires braking forces. I.e. front tire longitudinal (scuffing) force increase while rear tire force is decreasing at braking times.

It is also improved from equation (2.19) & (2.17) that, maximum braking force of front axle wheels (tires) is greater than the whole longitudinal (scuffing) forces induced due to accelerating and braking operation of vehicle. Therefore, front tire braking force is considered for this study because the pavement section subjected to this scuffing horizontal force may be shorten the service life of flexible pavement significantly.

2.7.2 Lateral Vehicle Movement Induced Forces

The lateral motion of vehicle is due to steering input from driver to lane change, cornering, turning, collision avoidance etc.

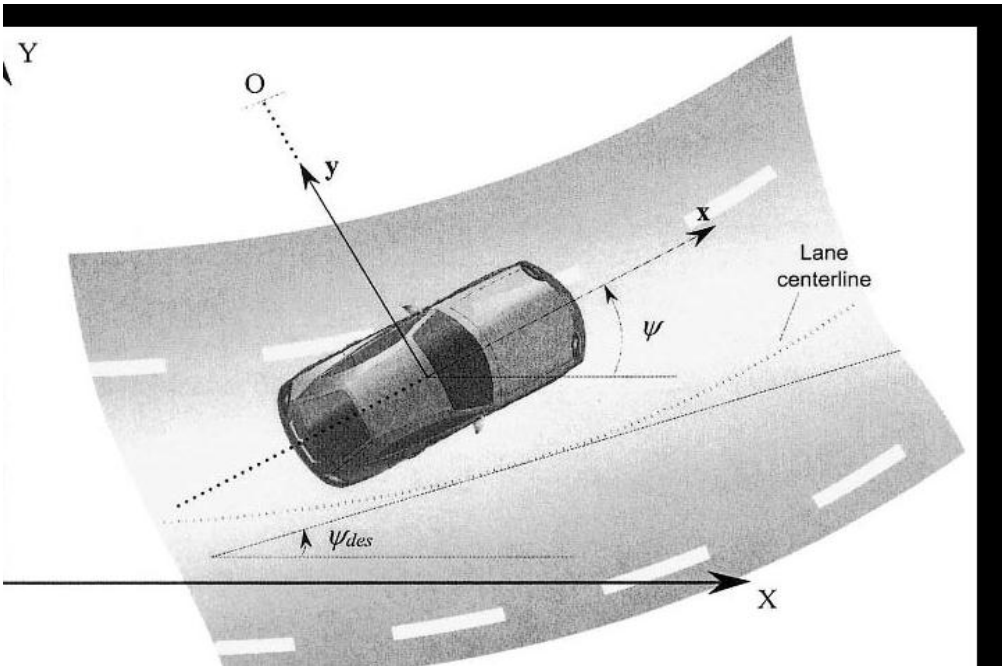

Figure 2.7: Vehicle lateral dynamics (Rajamani, 2006)

Using Newton's second law of motion to derive lateral scuffing forces;

Vehicle lateral dynamics could be described with bicycle model as shown figure 2.8 and equation 2.20 would be developed based on Newton's law of motion(Ji *et al.*, 2019).

✓
$$\begin{cases} Ma_y = F_{yf} + F_{yr} \\ a_y = \ddot{y} + \Psi'^2 R = \ddot{y} + v_x \Psi' \\ m(\ddot{y} + v_x \Psi') = F_{yf} + F_{yr} \\ I_z \psi'' = l_f F_{yf} - l_r F_{yr} \end{cases} \quad (2.20)$$

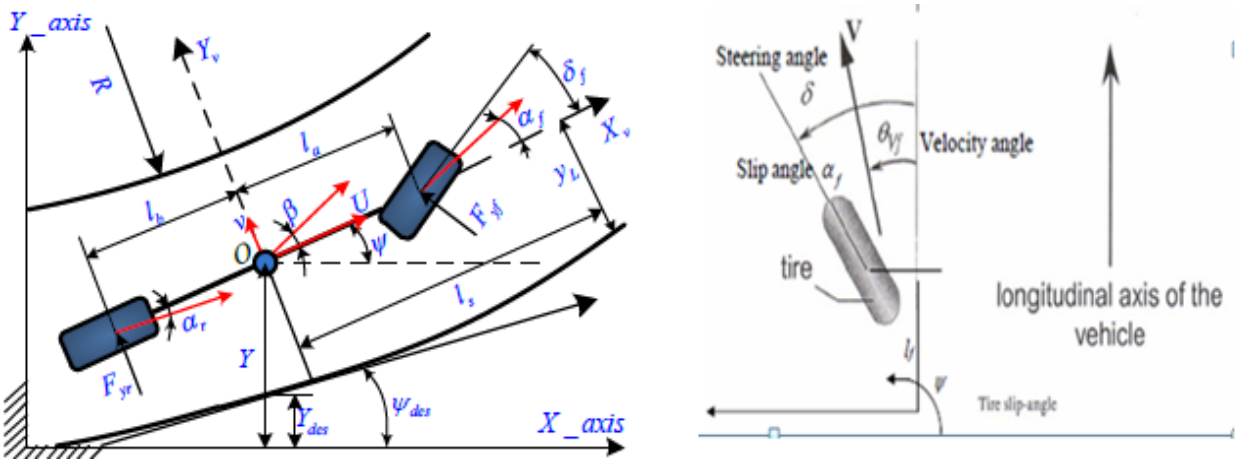

Figure 2.8 Vehicle lateral dynamics mode From (Ji *et al.*, 2019).

Slip angle of tire ($\alpha_{f,r}$) is the difference of steering angle and velocity angle;

✓
$$\begin{cases} \alpha_f = \delta - \theta_{vf} \\ \alpha_r = -\theta_{vr} \\ F_{yf} = 2C_{\alpha f}(\delta - \theta_{vf}) \\ F_{yf} = 2C_{\alpha r}(-\theta_{vr}) \ , where C_{\alpha f}, C_{\alpha r} \ are \ cornering \ stiffness \end{cases} \quad (2.21)$$

$$tan\theta_{vf} = \frac{v_y + l_f\psi'}{v}$$

$$tan\theta_{vr} = \frac{v_y - l_r\psi'}{v}$$

When velocity angle of front and rear tire are small, $tan\theta_{vf} = \theta_{vf}$ & $tan\theta_{vr} = \theta_{vr}$ by substituting these values in to equation (2.21), the lateral forces become:

✓
$$\begin{cases} F_{yf} = 2C_{\alpha f}\left(\delta - \frac{v_y + l_f\psi'}{v}\right) \\ F_{yr} = 2C_{\alpha r}\left(-\frac{v_y - l_r\psi'}{v}\right) \end{cases} \quad (2.22)$$

Cornering stiffness of tire is the slop of lateral force versus slip angle as shown figure below and which the function of friction of coefficient.

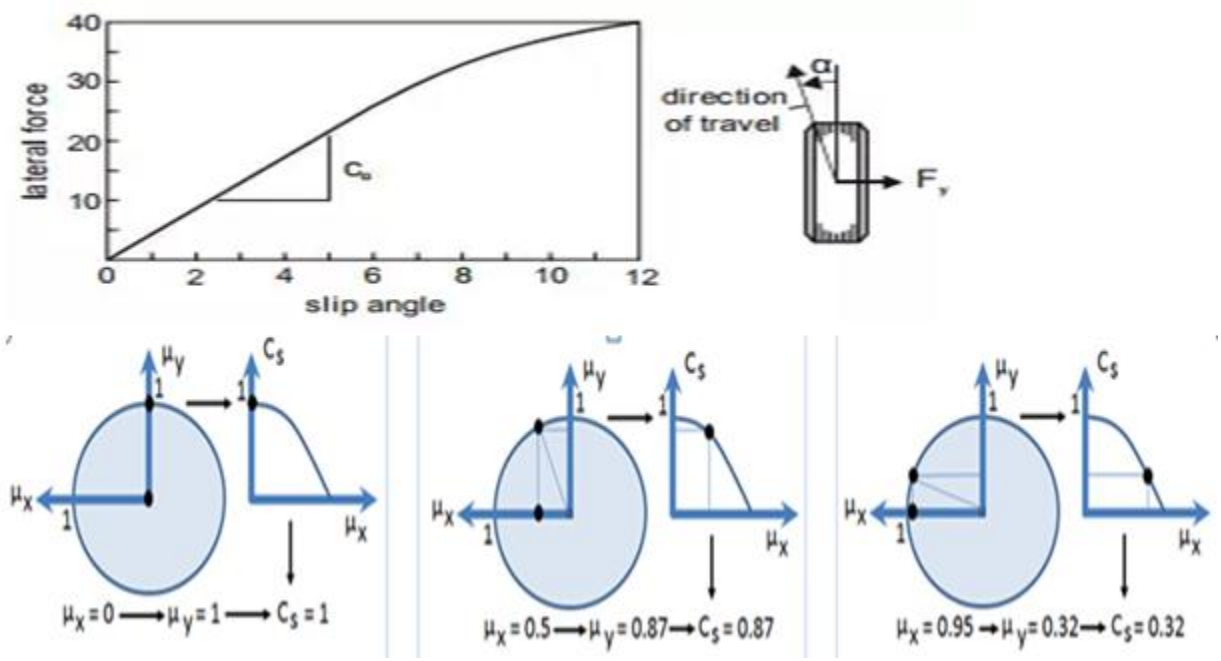

Figure 2.9: Relationship of lateral tire stiffness with slip angle & coefficient of friction (Rajamani, 2006).

2.7.3 Tire under Different Rolling Conditions

The tires transfer the horizontal and vertical forces performing at the car as a result of steering, braking and driving in aggregate with possible road disturbances or outside disturbances like aerodynamic forces because of as an instance pass-wind (Pauwelussen, Dalhuijsen and Merts, 2007).

Tire under free rolling condition

With the tread entering and shifting the contact region, the radius of tire changes for loaded and unloaded situation. Loaded situation reduce tire radius to form effective radius.at the entering and leaving contact area, tire radius compressed and elongated. These different radii produce different peripheral speed (R.Ш &Re. Ш) on contact area. The peripheral speed with recognize to the wheel center is proven in the lowest graph in figure (2.10), lowering from the unloaded pace Ш.R just before the touch region to the velocity Ш.Re inside the contact location. The whole longitudinal net force, derived from integrating the shear stress over the touch area could be a nonzero, small negative value, known as the rolling resistance force.

This rolling resistance force corresponds to a second performing around the wheel Centre, being balanced by the moment because of the tire load. Consequently, the net tire load ought to act along a force line, barely in the front of the wheel center (Pauwelussen, Dalhuijsen and Merts, 2007).

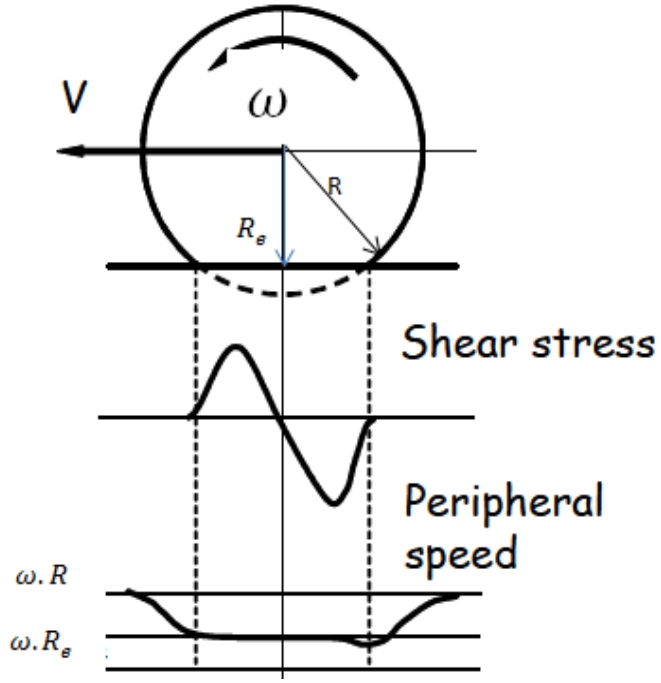

Figure 2.10: Free rolling tire (Pauwelussen, Dalhuijsen and Merts, 2007)

Tire under Braking Condition

During tire braking, the angular velocity of a tire is slower than the angular velocity at the free rolling condition due to the applied braking torque on the tire.

Now take into account a tire under a braking torque, as indicated in figure 2.11. The brake torque My as to be balanced by means of moments because of a brake force –Fx and the tire load Fz. The offset of the tire load in front of the wheel center will increase with appreciate to the free rolling tire. The tire will enjoy a slip speed of wheel w.r.t. ground, decreasing the angular velocity and consequently growing the effective rolling radius Re. If My is large sufficient, Re, braking will exceed the loaded radius. The entire longitudinal shear stress in the contact area now includes a part because of free rolling (dashed in figure 2.11) and a superimposed shear stress resulting from braking (Pauwelussen, Dalhuijsen and Merts, 2007).

As a result, the main part of the tire in the touch region is stretched because of the braking torque. Tread elements entering the contact area first try to adhere to the road surface, with the longitudinal deflection and consequently the shear stress increasing linearly alongside the contact zone. At a certain point, the shear stress reaches the limit of friction (μ.σz with local road friction μ and normal force underneath Coulomb law) and the treads begin to slide. As an end result, the shear stress drops down along the rear part of the touch region.

In a comparable manner as discussed for a free rolling tire, one arrives at a distribution of the peripheral speed of treads (w.r.t. the wheel center) as shown in the bottom part of figure 2.11. Observe that, in general, sliding starts at the rear of the contact areas and extends in the direction of the front part of the contact location for increasing brake torque, till subsequently sliding is apparent along the total touch region (Pauwelussen, Dalhuijsen and Merts, 2007).

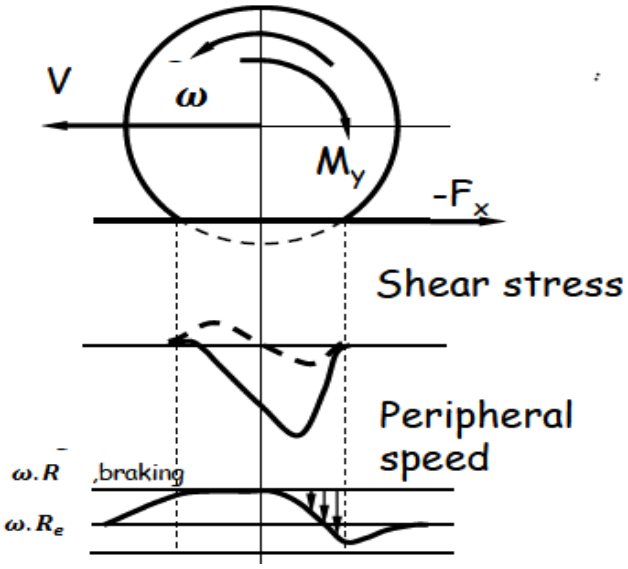

Figure 2.11: Braking rolling tire (Pauwelussen, Dalhuijsen and Merts, 2007)

Longitudinal Slip

Longitudinal slip ratio(S) or (k) is the ratio of the difference of vehicle longitudinal speed (v_x) and tire speed ($\omega.re$) to longitudinal speed.

$$K = \frac{V_x - \omega R_e}{V_X} \qquad (2.24)$$

Where: ω the wheel-spin velocity of the wheel is, R_e is the effective rolling radius, and V_X is the forward speed of the wheel center.

Pure Longitudinal force (Fx) is the forward horizontal scuffing force which is a function of normal tire force, slip ratio and different behavior of road surface coefficient at zero angle of turn.

$$F_X = \frac{\mu}{\mu_o} FX(Fz, \frac{\mu_o}{\mu} k) \qquad \{\text{For } \alpha=0)$$

Coefficient of friction related by road condition and speed of vehicle as shown in figure 2.12b.

(Gohring, Von Glasner and Pflug, 1991)concluded that induced scuffing forces at braking depended on tire normal force and slip ratio as parameter (figure: 2.12a)

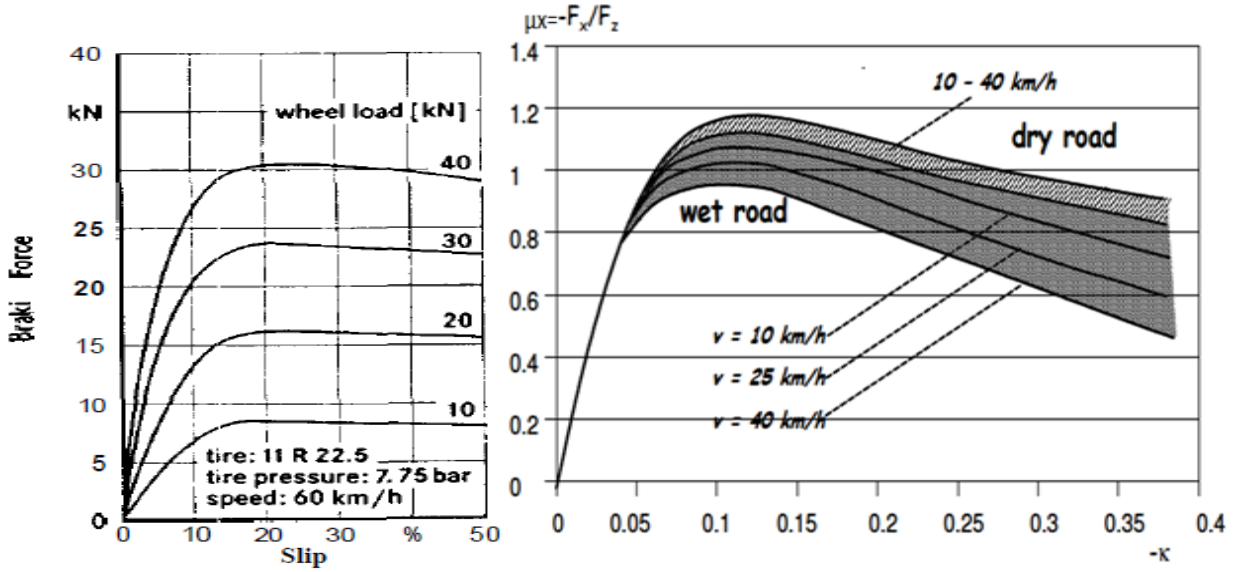

Fig.2.12a: Braking force /slip characteristics(Gohring et al., 1991), Fig 2.12b: effect of road condition and speed on (μx).(Pauwelussen et al., 2007)

Tire under Cornering

As the tire is cornering, the friction between the tire and road surface restricts the lateral movement of the tire and results in lateral deformation of the tire tread elements within the contact patch.

Let us take into account a tire under cornering situations, as indicated in figure2.13 (Pauwelussen, Dalhuijsen and Merts, 2007). Under cornering situations, there exists a local velocity vector, being in general no longer parallel to the wheel center plane. This wheel center plane is described as the symmetry plane of the tire such that forces acting within the symmetry plane do not contribute to the lateral force for the tyre.in the front a part of the contact are, the treads of the tire attempt to comply with this local speed course, ensuing in a displacement alongside the tire circumference inside the contact are, increasing linearly from zero (simply in

the front of the contact area) up to a situation where the induced lateral shear stress just reaches the maximum viable shear stress level, i.e. μ. σz with nearby road friction μ and normal stress σz underneath Coulomb law. We have discussed a comparable phenomenon for braking and driving (traction) of the tire. Beyond that point, the treads of the tire will slide main to a reduction of the shear stress in the course of the touch area rear end. Certainly, when sliding and in the absence of longitudinal slip, the lateral shear strain might be equal to μ. σsz. With σz decreasing to zero at the edges of the contact area, the friction limits for the shear stress will decrease in addition, and sliding is likely to increase until the contact area rear end.

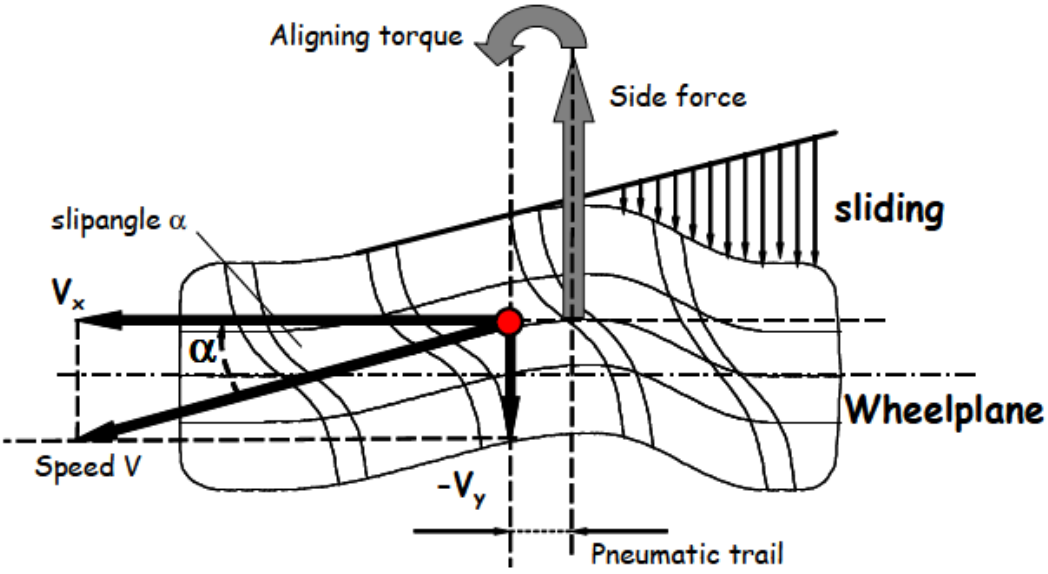

Figure 2.13: Tire under cornering conditions (Pauwelussen, Dalhuijsen and Merts, 2007)

Slip angle is the arc tangent ratio:

$$\alpha = tan^{-1}(\frac{V_y}{V_X})$$

$$F_y = \frac{\mu}{\mu_o} FY\left(Fz, \frac{\mu_o}{\mu}\alpha\right) \qquad \{fork = 0\}$$

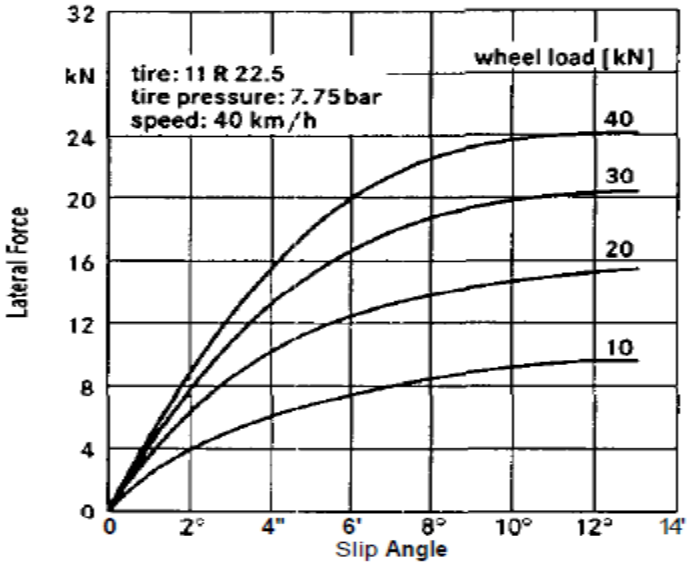

Figure 2.14 Lateral force/slip angle characteristics (Gohring, Von Glasner and Pflug, 1991).

2.8 Pavement Response to Tire Force

Responses of flexible pavement to tire loads were predicted by techniques of multi-layer elastic theory or finite element method (Holanda *et al.*, 2015).

2.8.1 Layered elastic theory method

In 1940s, the theory of elastic layer system developed to determine flexible pavement responses to traffic loading (tire force) with the following major assumptions(Huang, 2004).

- Uniform circular area of the pavement system is loaded statically;
- Stresses and strains compatibility is assumed to be satisfied at all layers interfaces;
- Native soil is assumed to be semi-finite layer with same elastic modulus;
- All materials are assumed to be weightless (no effect of inertia);
- Each layer is horizontally infinite, isotropic, mass homogeneous, and linear elastic;

Boussinesq's equation was restricted for homogeneous soil deposit of one layer. The general theory of stress and displacement for two-layer system was more applicable. So that evaluation of layer displacement (settlement) equation for a simple case has been modified to the first series (Burmister, 1945). Burmester's two-layer system later extended to three-layer system.

Pavement response model is one of the key components in analyzing flexible layers used to estimate internal loads of materials stress, strain and displacement that caused by external loading of traffic (tire loads) taking account the behavior of materials and prevailing environmental condition (Erlingsson and Ahmed, 2013).

2.8.2 Finite element method

Finite element method is a numerical method for solving problems of engineering and mathematical physics. The idea of the Finite element changed into coined by Clough inside the early 16th in his book entitled “The finite element method in plane strain analysis”(PRADHAN and CHAKRAVERTY, 2019).The Finite element analysis method, originally brought through Turner et al. (1956), was an effective technique for answers to a selection of "real-world" engineering issues having complex domains subjected to general boundary conditions. FEA has become an essential step in the design or modeling of a physical phenomenon in engineering disciplines. A physical phenomenon commonly occurs in a solid, liquid, or fuel regarding field variables (Madenci and Guven, 2006).

Two-Dimensional (2-D) FE models were the first examples of the software of the FE method in pavement analysis. The axisymmetric modeling approach assumes that the pavement machine has constant material and geometric residences in horizontal planes, and the site visitors loading is circular load applied on the pavement surface. ILLI_PAVE is one of the most common software programs that used in an axisymmetric FE model(Thompson and Elliott, 1985).

With the improvement of computer systems, using 3-D FE analysis has grown to be massive in pavement structural evaluation(WHITE and ZAGHLOUL, 1993).In assessment to the exceedingly easy layered elastic principle the 3-D FE version can perform many analysis, along with non-uniform tire-pavement contact. Dimensional finite element packages have been employed two decades before for examining road pavement responses. In recent time three dimensional (3D) finite element analyses emerged as effective tool that is successful of capturing pavement responses (Melaku, S.1, 2016).

There are a lot of applications of finite element techniques in various fields (Seoyoung CHO, 2018). Finite element method stands strong in the field of structural analysis and the trend of making use it into asphalt pavement in widespread. This suggested that finite element method was one of the strategic tools that could be used for the precise mechanical design of pavement structure for mechanistic analysis so as to estimate accurate pavement responses. Determination of pavement mechanical behavior such as stresses strains and deflections due to traffic load with finite element method showed that finite element method (FEM) offers the potential for comprehensive analysis of pavement strictures (Leonardi, Palamara and Sarah, 2017).(Gupta and Kumar, 2015) described finite element method (FEM) as analysis technique that could support to obtain various structural parameters like stress, strain and deflection flexible pavement layers.

Finite element (FE) method efficiently estimates the responses of flexible pavement if pavement material properties and tire/pavement contact regime are known(R.M. Mulungye, P.M.O Owende and Mellon, 2005). This paper suggested that the values obtained from model analysis could be used to assess the expected performance of pavement and improve on design

characteristics of pavement structure before construction.

In the pavement evaluation and design strategies, for simplicity, vehicle loading was normally modeled as a static or transferring (moving) single load with constant amplitude on multilayered elastic structures; but, in fact, the pavements ware subjected to transferring multiple axles as properly and in any dynamic pavement analysis, tire–pavement interplay load and HMA belongings ware time based so dynamic analysis was more approach to the actual condition (Sarkar, 2015).

2.9 Dynamic responses of flexible pavement

(Holanda *et al.*, 2015)Analyzed the dynamic responses of flexible pavement using FEM in four ways quasi-static, quasi-static elastic, dynamic viscoelastic and dynamic elastic to insure the importance of inertia forces in stress-strain analysis and found that normal displacement and normal stresses enhanced as the loading duration on the pavement increased which implied lower speed of vehicle cause larger rutting this mostly occurred in urban area.

They also noted the horizontal stresses bottom of surface layers have different properties from vertical stresses and displacements at the top of sub-grade when loading time increased or decreased. Horizontal stresses were sensitive to the duration that pavement subjected to tire load. Short duration caused significant tangential tresses for both quasi-static and dynamic consideration.

A similar study by (Khavassefat, 2014) found that compared to quasi static analysis and dynamic analysis showed that, as frequency increase, the horizontal stresses at top and bottom of the HMA layer increased for dynamic analysis.

That result implied the importance of tire-pavement interaction in the analysis of flexible pavement and influences of horizontal responses could have considerable effect on service life of flexible pavement. Furthermore(`P. Khavassefat, Jelagin, & Birgisson, 2015) noted that dynamic responses of pavement based on moving quarter car model examination numerically with finite element method(FEM) for same vehicle model moved on two different road profile(rougher& smoother) and forwarded the transient dynamic effect had noticeable influence on the induced horizontal stress-strain of flexible pavement responses; therefore, for the estimation of road cracking resistance, dynamic effects needed to be taken into account.

The FEM is hired and used within the time domain with the useful resource of the general motive computer software ANSYS to determine responses of pavement to moving vehicle (Beskou, Tsinopoulos and Theodorakopoulos, 2016).

They found, that the dynamic reaction is constantly higher than the corresponding static one and that increasing values of car speed boom the dynamic pavement response. moreover, it became also found that a series of transferring point loads or a disbursed moving load consequences in a lower response than a single point transferring load of intensity identical to the sum of those of the weight series or to the resultant force of the distributed load.

(Yoo and Al-Qadi, 2007) Studied moving load effect with transient dynamic analysis developed in finite element software ABAQUS used for 3-D pavement modeling; 275/80R22.5 tire assembly and 720kpa tire inflation pressure. The comparison of quasi-static and transient dynamic had shown that, quasi-static under estimate the responses of pavement to tire loads as seen in figure 3 and results were agreed with field data of Virginia Smart Road. The study reported that small dynamic variation in tire/pavement contact stresses might increase pavement damage which affect service life of the flexible pavement. Thus, transient dynamic model was successfully estimate the responses of pavement **during one pass** of tire load and this enhance the accuracy of model to predict the pavement capacity well.

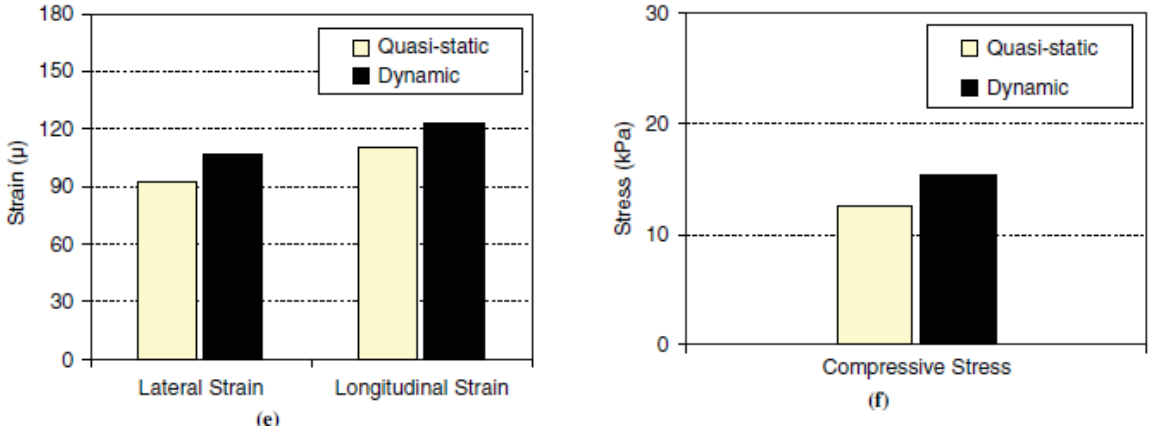

Figure 2.15: Calculated dynamic versus quasi-static pavement responses at bottom of HMA at 25C: (e) Peak strains at bottom of HMA, and (f) peak stresses at top of subgrade (Yoo and Al-Qadi, 2007).

Summary

3-D finite element analysis method was more applicable in engineering service to analyze any structural response and considers more varieties of parameters in analysis and design purpose.

Statics and dynamics were techniques (models) of load application system on pavement during pavement response analysis. However, statics load unless used for simplicity doesn't represent the actual phenomena that pavement subjected to vehicle maneuvering load. Therefore, transient dynamic moving load represent more actual situations.

This paper used (3-D) FE transient dynamic analysis that consider generally moving load of vehicle as input parameter.

2.10 Tire- Pavement Contact Stress Distribution

2.11 Tire-Pavement Interaction

Tire –pavement contact behavior plays an essential role in pavement capacity (performance) analysis and driving safety of vehicles that basically caused by rolling problems & the friction attire-pavement interface. Accurate prediction of tire-pavement interaction also contributes to estimating pavement response and stopping distance of vehicle (Hao Wang, 2010).

Aside from supporting the vehicle, tires have some other undertaking; that is exerting forces in a pavement tangent to the ground. Longitudinal forces are essential for riding and braking the car, whilst lateral ones for controlling the trajectory. Compliant, usually pneumatic tires, like those used on motor automobiles, can produce large longitudinal and lateral forces, even larger than the force the wheel exerts at the floor in everyday route. To do so they need to perform with non-negligible slip in each guideline. The presence of slip does not mean that the wheel slides on the surface(Gillespie, 1992).

The forces are longitudinal or tractive force (Fx), lateral force (Fy), and vertical or normal force (Fz). The moments are overturning second (Mx), rolling resistance moment (My), and vertical moment or aligning second (Mz). These forces and moments are in particular due to the tire-pavement interaction and its elastic deformation (Chae, 2006)&(Wong, 2001).

- ✓ **Vertical force of the tire (Fz)**

While a vehicle is placed on a road, it is obvious that vertical contact stress exists among tires and road surfaces. It's a static pressure because of gravity. But, while the automobile is moving on a hard street, the tire and sprung mass have vertical accelerations. The vertical pressure on the tire is affected in general by way of the vertical acceleration of the sprung mass alternatively than by using the vertical acceleration of the tire itself because the weight of the sprung mass is much higher than that of the tire.

- ✓ **Longitudinal scuffing force of tire (Fx).**

While tires are rolling or sliding along the longitudinal direction, longitudinal force is applied to the tire on the contact area.

During free rolling along a straight direction, the rolling resistant force is applied to the tire at the contact area against the tire rolling direction. The rolling resistant force or rolling resistance of tires is primarily caused by the hysteresis (inflation pressure) in tire materials due to the carcass deflection of rolling tires.
Free rolling condition is defined as the rolling condition without traction or braking torques applied on a tire. Here the pavement surface is mainly subjected to vertical load transferred from tires.

Friction is the main factors or causes of pavement scuffing forces in different pavement surface condition that is roughness and smoothness. The more application of friction occurred at the time of acceleration and braking of vehicle deriving condition. As the vertical load on the tire will increase under the equal operational situation, the longitudinal force also increases.

In braking operations, there is a speed difference between the rolling speed of a tire and its traveling speed, which results in a certain degree of slip between the tires tread and road surface. Without acceleration and braking efforts, no-slip will occur. With a certain amount of slip, a frictional force is developed in the tire-road contact area that enables the vehicle to be accelerated and decelerated. In the case of a braking operation, the degree of the slip can be

expressed in the slip ratio according to the equation 3.2. When the braking effort is so excessive that the wheel is locked and slides on the road surface, the slip ratio is described as 100%. The longitudinal force in response to a braking maneuver is known as a longitudinal scuffing force.

- ✓ **Lateral (transverse) scuffing force (Fy).**

Whilst automobile undertakes cornering (turning) operation, lateral force is evolved on the tire-pavement touch vicinity. The lateral forces for the duration of a cornering maneuver are dynamic because of the lateral acceleration of the vehicle. The lateral force in response to a cornering maneuver is known as a cornering scuffing force. The cornering force is tremendously structured of tire vertical load. As the vertical load on the tire will increase under the equal cornering operational situation, the cornering pressure also increases. Meanwhile, all through cornering maneuvers, a better vertical load is exerted on the right tires due to lateral load transfer. Consequently, higher cornering forces are also carried out to the same right tires while a tire is recommended and the car is under cornering situations, the tire is subjected to a lateral deflection due to a lateral force on the tire resisting the centrifugal force of the vehicle sprung mass

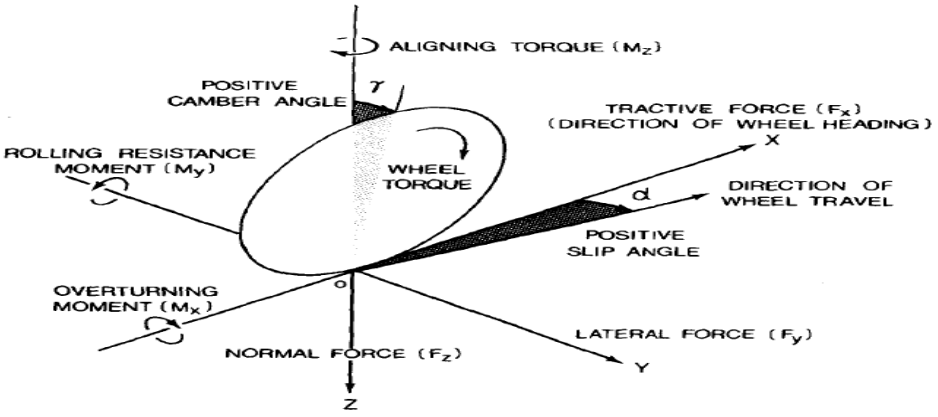

Figure 3.2: Tire axis system (Wong, 2001)

The contact stress distribution of tire-pavement interactions, in pavement design, is assumed to be uniformly distributed in circles or rectangles (Guo and Zhou, 2019). they studied tire-pavement contact distribution using finite element software ABAQUS under free rolling, braking, acceleration deriving condition with tire slip ratio. For this analysis, the following (2.1-2.5) equations had proposed accordingly.

$$S_a = \left(1 - \frac{v}{r\omega}\right) * 100\% \qquad 2.1$$

Where: Sa is the ratio of tire sliding in acceleration condition
v: is longitudinal speed
r: is tire effective radius
ω :is angular velocity of tire

$$S_b = \left(1 - \frac{v}{r\omega}\right) * 100\% \qquad 2.2$$

Sb: the ratio of tire sliding at braking time

When the tire was free rolling condition, longitudinal speed and angular velocity related as:

$v = r\omega \ , S = 0$ 2.3

$F = \mu N$ 2.4

F: the maximum induced scuffing longitudinal forces at critical tire slip ratio.

$\mu = \mu k + (\mu s - \mu k)e^{-\alpha s}$ 2.5

μ_k: kinetic coefficient friction at highest sliding speed;

μ_s: at zero sliding speed, static coefficient of friction;

α: exponential decay coefficient & S: sliding velocity.

Based on the result obtained, the researchers observed that the contact stresses were affected by vehicle moving conditions (free rolling, accelerating, braking and turning) of driving situations. The scuffing longitudinal force for braking and acceleration rapidly increased with tire slip ratio and then decreased after critical point of slip ratio.

In a similar study, (Shakiba *et al.*, 2016)studied tire-pavement contact stresses by developing incorporated realistic tire-pavement interface contact area & stresses into Pavement Analysis Non-linear Damage Approach(PANDA) software user interface with finite element.

They forwarded that, non-uniform vertical stresses and surface tangential shear stresses at tire–pavement interface, tire braking and accelerating motive extensive longitudinal contact stresses on pavement surface. Those stresses extensively have an effect on the pavement response at close to-surface and boost up pavement deterioration.

Flexible pavement distress mechanisms had been becoming the more prevalent as surface rutting and initiated pavement cracking (Nega and Nikraz, 2017).

They investigated contact stress distribution of tire-pavement interaction using the most powerful software **ABAQUS & ANSYS**; results validated with field measured data. For that evaluation, 40kN vertical load was assumed to be uniformly distributed over an equivalent rectangular area between tire and road as shown figure bellow and various tire inflation pressures (350,490,360 & 700) kpa for dual tires of 295/80R22.5 and 315/80R22.5 were considered in the investigation. They concluded that as tire increased more and more, lateral strain increased that would be caused for the reduction of fatigue life of flexible pavements. Such data could be used to investigate the expected fatigue performance of pavement to improve pavement analysis and design characteristics.

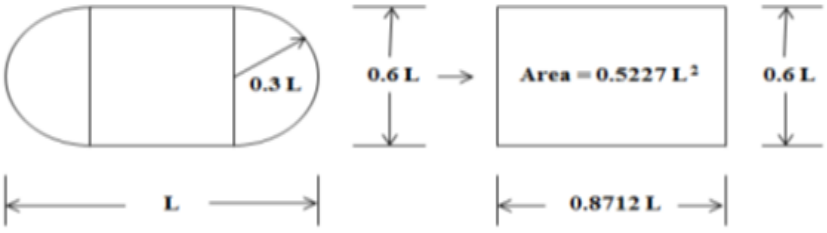

Actual and equivalent contact area After (Nega and Nikraz, 2017)

The exact modeling of tire-pavement contact stress distribution played an essential role in controlling vehicle stability and analysis of pavement capacity (Wang *et al.*, 2014). They studied

tire-pavement interaction to analyzed forces and contact stresses induced at the time of tire free rolling, braking and cornering situations using Arbitrary Lagrangian Eulerian (ALE) formulation in finite element method; considering influence of sliding-velocity dependent coefficient of friction at contact behavior incorporated with equation (2.5) of friction model and constant coefficient of friction. They concluded that, values of contact stresses were affected by vehicle movement and tire-pavement surface friction condition. At braking time, longitudinal/ tangential contact stresses increased as the coefficient of friction enhanced but lateral contact stresses were decreased.
For cornering conditions, vertical and transverse/lateral increased significantly.

Summary: the tire contact area, tire inflation pressure, turning angle and adhesion coefficient of friction were the main parameters that influence pavement responses under moving load. Braking and turning affects the stress-strain distribution than free rolling vehicle maneuvering, especially in horizontal direction (transverse & longitudinal). Significant scuffing forces were induced due to braking and turning of vehicles.

2.12 Concept and factors of scuffing force

Definition of scuffing forces

"*The pavement scuffing force is the horizontal shear force that reacts to the applied tyre scrubbing force*" (Taramoeroa and Pont, 2008).

They studied scuffing forces (cornering) with respect to axle load, axle group spread, wheelbase, and turn geometry (turning radius and steer angles) at constant speed using Yaw-Roll simulation software and validated with field test. Tire type 245/70819.5 dual and 385/65R22.5 wide-single were involved and equations (2.6-) have proposed to calculate the amount of lateral load transferred to tires.

$$\Delta zp = \left(\frac{fzp}{fzo} - 1\right) * 100\% \qquad 2.6$$

Where: Δzp is percentage of vertical load transferred
fzp is vertical force on tire
fzo is static vertical force on tire

$$\Delta ypt = \left(\frac{fypt}{fypo} - 1\right) * 100\% \qquad 2.7$$

Where: Δyp is change in peak scuffing force of tire configuration t
fypt is peak scuffing force;
fypo is peak scuffing force of tire configuration t;

$$-\mu fz \leq fy \leq \mu fz \qquad 2.8$$

Where: μ is friction coefficient.

The concluded points from the study were:

- Higher scuffing force could be generated from single tire;

- Axle groups have direct proportion with scuffing forces;
- Radius of turning has inverse proportion with scuffing force;

As seen from the above factors, pavement distress from scuffing force would be relayed on overall pavement design, pavement condition and different environmental factors.

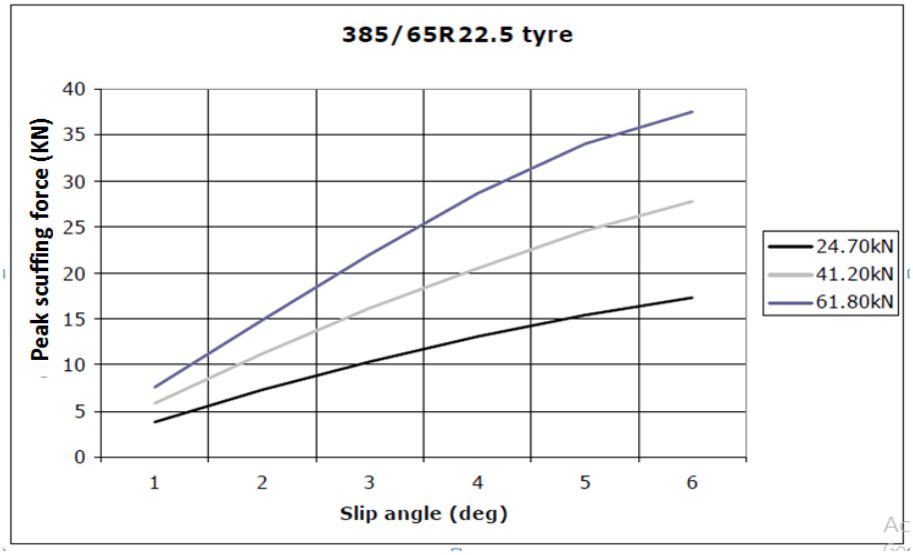

Figure 2.18: Relationship between cornering force and slip angle by vertical load

"*Friction coefficient has been used as an indicator for the initiation and propagation of scuffing*" (Blau, Qu and Truhan, 2005).

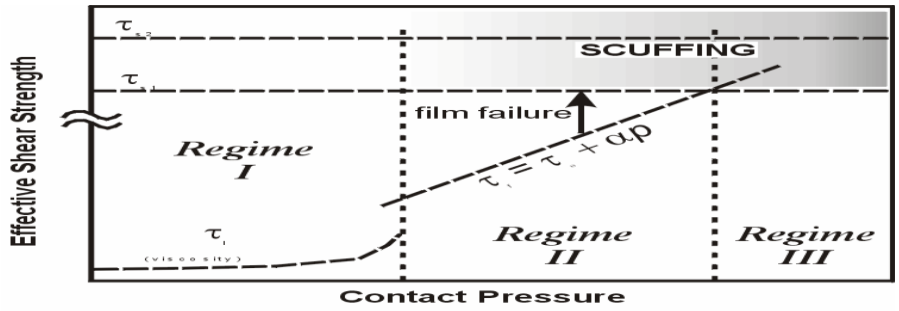

Figure 2.20: Conceptual scuffing model (Blau, Qu and Truhan, 2005)

Coulomb friction law

$\tau = \tau_o + \alpha\rho$ 2.9

Where: τ is effective shear stress.

τo is initial shear stress

α is pressure coefficient of shear strength

p is contact stress

The friction force (F) acting over an area (A) is proportional to the shear strength:

$F = \tau A$ 2.10

The friction coefficient is defined as the ratio of friction force to normal force P:

$\mu = F / P$ *2.11*

Combining (2.10), (2.11), and (2.12) gives:

$$\mu = \frac{(\tau_o + \alpha\rho)A}{P} \qquad 2.12$$

The variation of scuffing (transverse) force coefficient of tire and pavement as a function of time has two phases; linear and non-linear (Selig et al., 2014).

The forwarded figure (9), illustrated the relation of time, slip Angele & lateral coefficient that drawn from normal force equal to 5000N.

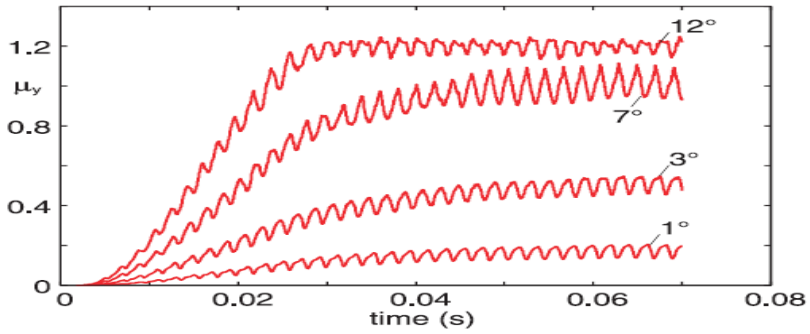

Figure 2.21: Tire lateral coefficient of friction versus time (Selig *et al.*, 2014)

(Zhu, 2011), investigated friction characteristics in conditions where lateral and longitudinal frictions were combined with the proposed equation (2.13) and drawn the following figures.

$$F^{SS} = F_n \mu_i{}^{ss} \quad , \quad i=xy \qquad 2.13$$

Where: $\mu_i{}^{ss}$ are the steady-state tire friction coefficient.

$$s = \begin{cases} \frac{v_{rx}}{R\omega} & for\ v\cos(\alpha) < R\omega, acceleration \\ \frac{-v_{rx}}{v\cos(\alpha)} & for\ R\omega > v\cos(\alpha), Braking \end{cases} \qquad 2.14$$

S: longitudinal slip
V: longitudinal speed
R: effective tire radius
ω: tire angular speed
α: tire slip angle

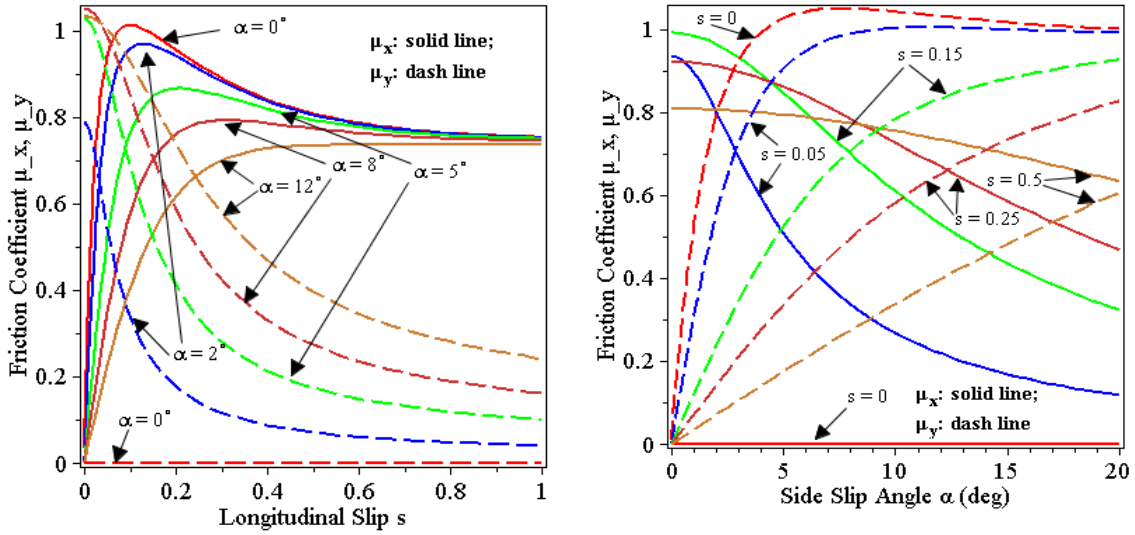

a) Longitudinal and lateral friction coefficients vs. longitudinal slip
bLongitudinal and lateral friction coefficients vs. side slip angle
from(Zhu, 2011)

Figure 2.22: combined friction coefficient model

2.13 Effects of scuffing force on pavement responses

Turning and braking maneuver of vehicles generated the most extreme shear stresses and vertical strains on the structures of flexible pavement (Hu et al., 2017).this study investigated that the effect of tire slip angle (turning) maneuver and longitudinal movement (acceleration and braking), under different dynamic loading & environmental conditions on flexible pavement capacity responses (stresses-strains) using finite element modeling approach. The modeling and sensitivity evaluations were performed for two input cases. The first case was tire slip angles to simulate turning; second case was dynamic loading to simulate longitudinal traffic. Results of turns (curved) with slip angles of(0,5,10 deg) simulation illustrated with figure 2.23 below. Stresses and strains diminished down with depth of the pavement structure and shear stresses increased with slip angles but vertical strains increased up to critical point and then decreased angle increased.

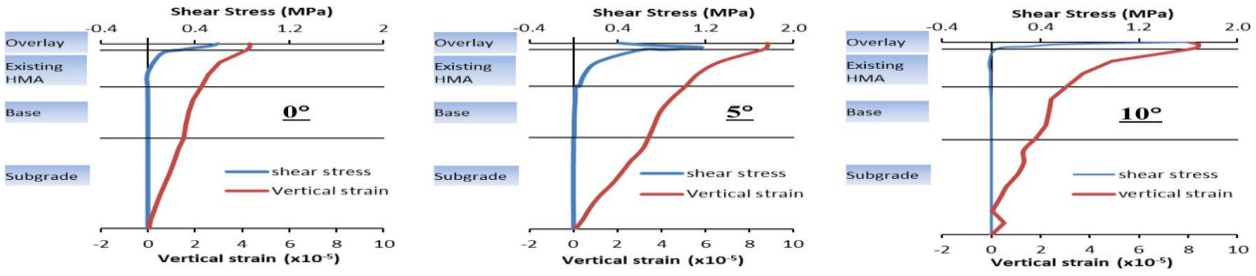

Figure 2.23: pavement response to inclination (slip) angles (Hu et al., 2017)

The influences of accelerating, steady rolling and braking were conducted for a single tire with 690kpa inflation moving over 12m long with speeds of $6.7 m/_{s^2}$,96.6km/h & $6.7 m/_{s^2}$ respectively. The maximum shear stresses occurred at tire braking compared to other scenarios. It could be observed in figure 2.24 that the maximum shear stress (1000kpa) induced for braking and the less shear stress (540kpa) for free rolling and 650kpa for accelerating.

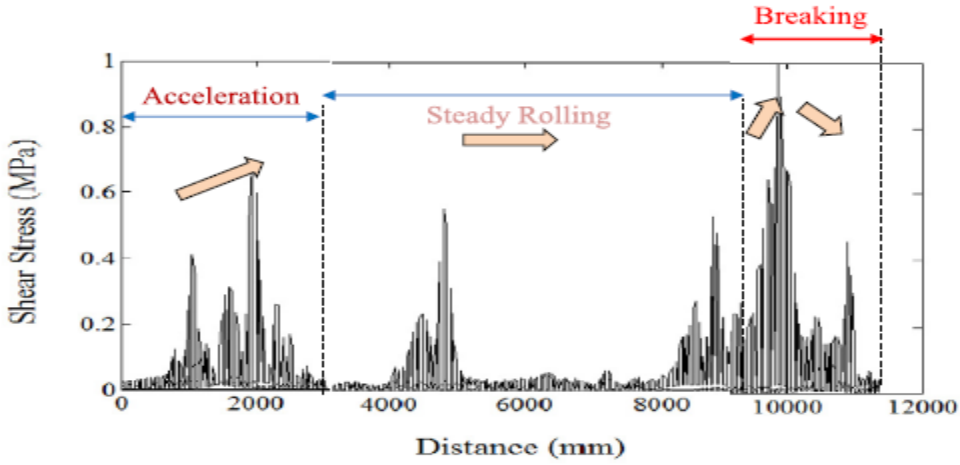

Figure 2.24: Maximum shear stresses for steady rolling, and decelerating From (Hu *et al.*, 2017).

Similarly (Shakiba *et al.*, 2016) investigated effect of scuffing(longitudinal) force on flexible pavement responses under three different scenarios of braking, traction/acceleration and free rolling by PANDA user interface(PUI) in FE for 3-D pavement modeling, as seen in figure (13) and responses evaluations. The investigation was considered 275/80R22.5 dual tire assembly, 44.5KN tire vertical force & 758kpa inflation tire pressure and proposed equations(2.15-2.16) to calculate slip ratios for braking and traction. The author found that compared pavement responses of scuffing forces of all scenarios; the stress and strain affected by braking and traction that significantly seen in the traffic movement direction which might generate greater shoving or corrugation. The responses of pavement diminished in depth of asphalt as shown in figure 15.

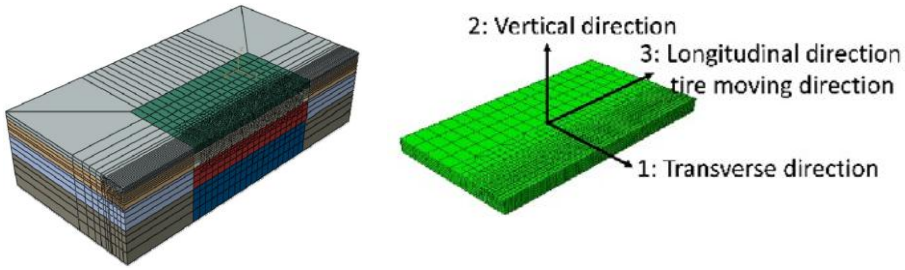

Figure 2.25: Sample of constructed FE representation of pavement using PUI.

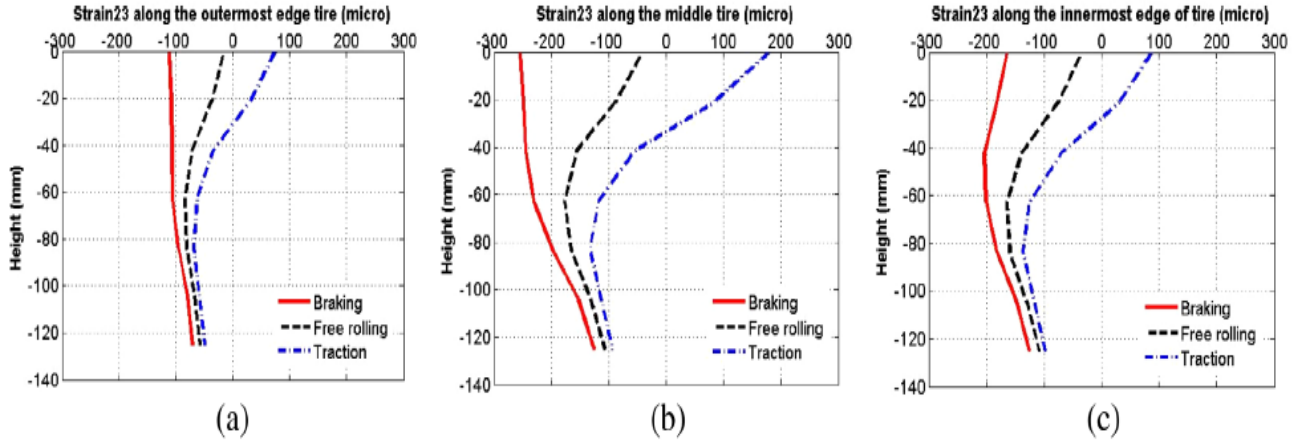

Figure 2.25: shear strain (23) along depth at the (a) outermost edge, (b) middle and (c) innermost edge of tire.

(Alkaissi et al., 2019)analyzed the effect of horizontal traction on response of flexible pavement using finite element software to assess top-down cracking.

Pavement model was constructed as 3-D elastic solid mode with two pavement layers (asphalt and sub-grade). Table 1 showed dimensions and material properties of the pavement structures. The model was loaded with moving load of one tire (40kN) at equivalent rectangular area shown in figure 13 with 690kpa uniform contact pressure.

Fatigue cracking and damage analysis were carried out with equations (2.15 &2.16) taken from Asphalt institute.

$$N_f = 0.0796\left[\frac{1}{\epsilon t}\right]^{3.295} * \left[\frac{1}{E1}\right]^{0.854} \qquad 2.15$$

Where:N_f: Number of load repetitions to cause fatigue cracking.

ϵt: Tensile strain at the bottom of asphalt layer.

E1: Elastic modulus of asphalt layer (psi).

$$D_i = \frac{1}{N_i} \qquad 2.16$$

Where: D_i is damage ratio, N_i is wheel load repetition

Based on the result, they concluded that top surface of asphalt was subjected to concentrated horizontal stresses due to horizontal traction. This traction had significant impact to increase tensile strains at asphalt layer that in turn increased the damage ratio of fatigue failure of surface of flexible pavement.

Table2. 3: pavement material properties

Pavement Layers	Elastic Modulus (MPa)	Poisson's ratio (v)	Density (Kg/m³)
Asphalt	508	0.35	2240
Local Subgrade Layer	211.53	0.4	1870

Source (Alkaissi, Al-badran and Wasif, 2019)

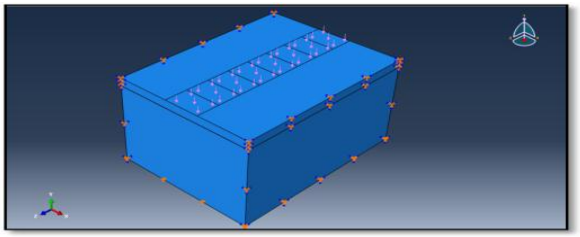

Figure 2.26: 3-D model and pavement responses (Alkaissi, Al-badran and Wasif, 2019)

Braking operation of vehicle, significantly increase the responses of flexible pavement such as normal stresses, normal displacement (rutting)and tangential shear stresses of asphalt pavement i.e. the maximum longitudinal/ horizontal stresses during brake operation were four times of free rolling conditions(Jin *et al.*, 2015).The conducted analysis on the effects of vehicle braking used finite element analysis software ANSYS to 3-D pavement model and analysis pavement performances.

Developed equations were:

$F_{xbmax} = F_z\varphi$ 2.17

Fxb max: maximum braking force between the wheel and the road

FZ: wheel vertical forces acting on the road

Φ: road adhesion coefficient

$a = \varphi g$ 2.18

a: maximum braking acceleration

$s = \frac{1}{2}at^2$ 2.19

S: stopping distance

t: braking time($t = \frac{v_o}{a}$) , v_o is braking speed

$T_i = \frac{s'}{v_o - 2s'}$ 2.20

Ti: the actuation duration of the i-th step loading

s': Rectangular length of wheel contacting with the road

2.14 Pavement Failure Mechanisms

Generally, the layers of flexible pavement structure such as HMA layer, base/sub-base layer, and sub-grade layer exhibit a unique failure mode that related to the critical response of each layer. The main load-associated flexible pavement distresses are fatigue cracking, HMA rutting (primary), HMA shoving (shear flow), rutting unbound base layer, and sub-grade rutting(secondary) (Habin Wang, 2010).

In this study, relative pavement damage caused by rolling condition were used to convey the

intensity of pavement damage caused by scuffing loads in relation to critical pavement response and the allowed number of load application before failure. Relative damage caused by scuffing force with respect to free rolling of vehicles such as HMA rutting due to densification & shoving(shear flow), subgrade rutting and HMA fatigue cracking.

The main failure mechanisms of each layer of flexible pavement were presented below.

Fatigue cracking of HMA

Fatigue cracking is caused by repeated load applications mostly lower than the strength of paving material. It is commonly bottom-up fatigue cracking but recently there is also cracking which is top to bottom fatigue cracking (NCHRP, 2004).

Bottom-up fatigue cracking: is alligator cracking start at the bottom of the asphalt layer and propagate to the surface of the pavement under the load application, which is the result of the bending of HMA under loading. With continued vertical deflection, the tensile stress and strain cause crack to initiate and propagate to top of the pavement.
Surface –down fatigue cracking: in this type of fatigue cracking, the crack instated at the surface of HMA and propagates to the bottom of the asphalt layer. It is mainly caused by tensile strain at the top surface and transverse shear strain developed at a shallow depth of HMA layer. In this study, bottom-up fatigue cracking was taken to evaluate relative damage.

The proposed AASHTO 2002 MEPDG (ARA, 2004) expressed the allowable number of application load for bottom-up cracking as follows.

$$N_f = 0.00432.K.C\left(\frac{1}{\varepsilon_t}\right)^{3.9492}.\ \left(\frac{1}{E}\right)^{1.281} \quad (3.11)$$

Where: E is elastic modulus of asphalt concrete

ε_t: Horizontal tensile strain at the bottom of the asphalt
K: is a parameter related to the asphalt layer thickness
C: is related to asphalt mixture volumetric properties

HMA rutting
Rutting is permanent deformation or unrecoverable depression in the wheel path of moving vehicles that mainly caused by the densification of HMA materials. The permanent deformation property of asphalt and unbound materials are mainly analyzed in laboratory tests. But AASHTO 2002MEPDG (ARA, 2004) proposed the following transfer equation

$$\log\left(\frac{\varepsilon p}{\varepsilon r}\right) = -3.74938 + 0.4262\log(N) + 2.02755\log(T) \quad (3.12)$$

Where: ε_p is accumulative permanent strain?

ε_r is compressive elastic strain

N is allowable number of load application

T is pavement temperature

Equation (3.12) may be re-written as follow (Al-Qadi and Wang, 2009a)

$$N = \left(\frac{15}{h\varepsilon_{vr.}.10^{x}}\right)^{1.74} \quad (3.13)$$

Where: h is asphalt thickness (mm)

$\varepsilon_{vr.}$: Compressive elastic strain of AC

The accumulation of permanent deformation in the asphalt layer is very sensitive to shear flow (down and upward) of pavement material which is known as **pavement shoving**. (Monismith and Popescu, 2007)

Correct the rutting (shear) to shear stress and shear strain instead of compressive strain and develop the following equation.

$$\gamma = aexp(b\tau)\gamma_e n^c \quad (3.14)$$

Where: γ is permanent shear strain of asphalt

γ_e: is elastic shear strain

τ: Corresponding shear stress in Asphalt

n^c: Number of load application

a,b,& c experimental coefficient(b=0.0072is used for this study from (Habin Wang, 2010)& (Wang and Al-qadi, 2011) .

Permanent Deformation of Unbound Base Layer

The granular material of the base undergoes permanent deformation due to insufficient stability of constituent material because of heavy loading or drainage condition. The loss of particle-to-particle interlock force causes the base layer to shear failure. The south Africa Mechanistic Design(SA-MDM) takes into account the permanent deformation of base layer related to the ratio of working stress and yield strength(THEYSE, BEER and RUST, 1996).

$$N = 10^{(2.605122F+3.480098)} \quad (3.15)$$

$$F = \frac{\sigma_3\left[k\,tan^2\left(45+\frac{\emptyset}{2}\right)-1\right]+2kctan\left(45+\frac{\emptyset}{2}\right)}{\sigma_1-\sigma_3} \quad (3.16)$$

Where: N is number of allowable load application;
F is safety factor; $\sigma_1 and\ \sigma_3$ are major and minor principal stress, k is constant of drainage condition(0.65 for saturated,0.8 for moderate and 0.95 for normal condition is cohesion coefficient
$\emptyset$ is angle of internal friction(c =0, φ =30° & k=0.95 are used for this study).

Rutting of sub-grade

Sub-grade rutting (secondary rutting) is permanent deformation developed due to compressive stress because of repetitive traffic loading. Mostly, vertical compressive strain at the top of sub-grade is related to this rutting type. The Asphalt Institute(ASPHALT INSTITUTE and No.2(Ms-2), 1970) proposed a rutting damage model based on the vertical compressive strain with the maximum threshold of 12.5mm rutting on sub-grade (equation 3.17). Where N is allowed load repetition until failure, and $\varepsilon_{v.}$is maximum vertical compressive strain on top of sub-grade.

$$N = 1.365 * 10^{-9}(\varepsilon_{v.})^{-4.477} \quad (3.17)$$

Summary and gap:

Vehicle maneuvering (braking and turning) are the main causes of scuffing forces that, in turn, significantly affect the responses of pavement such as stress, strain, and deformation. Most Researchers used different approaches to investigate the impacts of turning angle and slip ration of moving vehicles for assessing pavement performance. They assume tangential loads simply as the product of vertical load with friction coefficient (longitudinal or lateral) that hadn't included the inertial effect of moving vehicles. But in this study, the inertial effect of the moving vehicle is included through tire slip ratio and slip angle during braking and turning of vehicles to compute the scuffing forces (tangential).

To take in consideration of the moving vehicle in finite element analysis, the most powerful finite element software ANSYS and ABAQUS were used. ANSYS software could be selective to analyze and develop pavement models. Because ANSYS is one of the powerful like ABAQUS but not programming (language) sensitive at the time of running like ABAQUS. So ANSYS can accurately estimate the internal response of structure of material subjected to external loading easily.

Chapter- 3

3 Methodology

The model in this study utilizes transient dynamic loading, linear finite element model, and simple 3-D pavement structure with of finite element approach. To achieve this mission, finite element software ANSYS is used from modeling to analyzing. Single front tire was used with incorporates of standard axle load (80KN) and subjected to scuffing forces on the time of braking and turning maneuver of the vehicle as stated in the literature. The movement of a vehicle is governed by using the forces generated between the tire and the Pavement.

3.1 Data source

This study based on secondary data that were taken from the Ethiopian Road Authority office and(ERA, 2013) manual, Addis Ababa City Road Authority office and (AACRA, 2004)manual and the CarSim2017 software package.

- **From ERA**: In the ERA specification manual 2013, the properties of the layers are numerically defined.

Those values are: elastic modulus (E) & Poisson ratio (v).

As shown in table (1), ERA recommends elastic modulus and Poisson's ratio according to material types and California bearing ratio of used materials for road construction.

Table3. 1: Material characteristic for mechanistic analysis

Material	Parameter	Value	Comment
Asphaltic concrete wearing course and binder course	Elastic modulus (MPa)	3000	A balance between a value appropriate for high ambient temperatures and the effect of ageing and embrittlement
	Volume of bitumen	10.5%	
Asphaltic concrete roadbase	Elastic modulus (MPa)	3000	
	Volume of bitumen	9.5%	
Granular roadbase	Elastic modulus (MPa) Poisson's ratio	300 0.30	For all qualities with CBR > 80%
Granular sub-base	Elastic modulus (MPa) Poisson's ratio	175 0.30	For CBR ≥30%
Capping layer	Elastic modulus (MPa) Poisson's ratio	100 0.30	For CBR ≥15%
Subgrades S1 S2 S3 S4 S5 S6	Elastic modulus in MPa	 28 37 53 73 112 175	Poisson's ratio for all subgrades was assumed to be 0.4
Hydraulically stabilised material	Elastic modulus (MPa)	CB1 = 3500 CB2 = 2500 CS =1500	Poissons ratio assumed to be 0.25 The modulus of CS is assumed to decrease with time hence a conservative low value of 1000MPa has been used

❖ **From AACRA**:

Some data are taken from the (AACRA, 2004)manual and AACRA office. Laboratory results of material and soil test reports contain test results of quarry sites such as Bulbula and Ayer Tena that covers the source of most construction materials for Addis Ababa & surround road construction.

The laboratory test was carried out by STAGIA Engineering Works Consultant in a joint venture with GANDY.

In addition to laboratory material test results, the report contains traffic data & recommended pavement design under a topic of "traffic study and pavement design report" for various road segments of Addis Ababa City.

Table3. 1: Summary of Projected Traffic, Cumulative ESA of each Class of Vehicles in one direction Over the Design Period of 20-years

Project name	**20 Year Design period**		
	% direction	**CESAin(million tons)**	**Traffic class**
CMC Ayat Road Junction – Gurd Sholla Summit Road	60	12,860,985	T7
CMC Summit /DawitKitfo / -Meri Road	60	12,860,985	T7
Tulu Dimtu Condominium access road	60	16,453,642	T7
Fafa Food Factory-Dama Hotel road	60	6,198,812	T6
Dima Hotel-Beheretsege road	60	12,860,985	T7
BeheretsegeSeneZetegn School- DZ road	60	6,198,812	T6
Gofa Military Camp-GofaMebrat Hail Condominium road	60	12,860,985	T7
GofaMebrat Hail Condominium-NOC Fuel Station Junction road	60	12,860,985	T7
Lebu Roundabout- Jemo Roundabout road	60	24,506,210	T8
Piazza Junction at Churchill Road –Minilik Square (First section)	60	16,453,642	T7
Piaza Junction at Churchill Road –Minilik Square (Second section)	60	16,453,642	T7

Table3. 2 Summary of Design Sub grade CBR & Sub grade Strength Class

Project Name	**Design sub grade CBR (improved sub grade)**	**Sub grade strength class (improved sub grade)**
CMC Ayat Road Junction – GurdSholla Summit Road	15	S5
CMC Summit /DawitKitfo / -Meri Road	15	S5
Tulu Dimtu Condominium access road	15	S5
Fafa Food Factory-Dama Hotel road	15	S5
Dima Hotel-Beheretsege road	15	S5
BeheretsegeSeneZetegn School- DZ road	15	S5
Gofa Military Camp-GofaMebrat Hail Condominium road	15	S5
GofaMebrat Hail Condominium-NOC Fuel Station Junction road	15	S5
Lebu Roundabout- Jemo Roundabout road	15	S5
Piazza Junction at Churchill Road – Minilik Square (First section)	15	S5
Piaza Junction at Churchill Road –Minilik Square (Second section)	15	S5

Table3. 3: Summary of Pavement Structures Recommended

No.	Project Road Name	ecommended Pavement Layers Thickness (mm)			
		AC Surface Course		Granular Road Base (GB1)	Sub-base(GS)
		WC	**BC**		
I	At CMC Ayat road junction –GurdSholla Summit road	40	60	200	150
II	CMC Summit – Meri Road(DwwitKitfo)	40	60	200	150
III	Tulu Dimtu Condominium access road	50	75	200	150
IV	Fafa Food Factory-Dama Hotel road	40	60	150	150
V	Dima Hotel-Beheretsege road	40	60	200	150
VI	BeheretsegeSeneZetegn School- DZ road	40	60	150	150
VII	Gofa Military Camp-GofaMebrat Hail Condominium road	40	60	200	150
VIII	GofaMebrat Hail Condominium-NOC Fuel Station Junction road	40	60	200	150
IX	Piaza Junction at Churchill Road –Minilik Square(first section)	40	60	200	150
X	Piaza Junction at Churchill Road –Minilik Square(first section)	40	60	200	150
XI	Lebu Roundabout- Jemo Roundabout road project	75	75	200	300

The highlighted road name (route) in the table was taken for this study. Because it consist roundabout and intersection where vehicle maneuver (deceleration, braking and turning) taken place.

Table3. 5: Summary of Pavement material parameters for model

materials	Thickness(cm)	Elastic modulus(Mpa)	Density(kg/m^3)	Poisson's ratio(v)
Asphalt	15	3000	2400	0.35
Base course	20	300	2150	0.3
Sub-base course	30	175	2070	0.3
Sub-grade course	infinite	112	180	0.3

3.2 Variable categories

The following variables are considered in this study.

I. Independent variables:
- Thickness of the pavement layers.
- Vertical load(Fz)
- Pavement interaction friction coefficient
- Temperature
- Density
- Elastic modulus
- Poisson's ratio

II. dependent variables:
- stresses
- strains
- deformations
- damage ratio
- slip angles(alpha)
- slip ratio(kappa)

3.3 Research Design

The research method used for this study follows the logical activities and procedures of research that has addressed credibly of the study achievement. Therefore, the descriptive research design used to fit the objective of research and the research approach.

The study employed a quantitative research approach that enables data collection, analysis and interpretation of results.

Data obtained from analysis in the form of numbers helps to arrive at the conclusion and recommendations for the study.

The study design can be represented by flow chart that clearly show the herarical steps and activities in each rows.

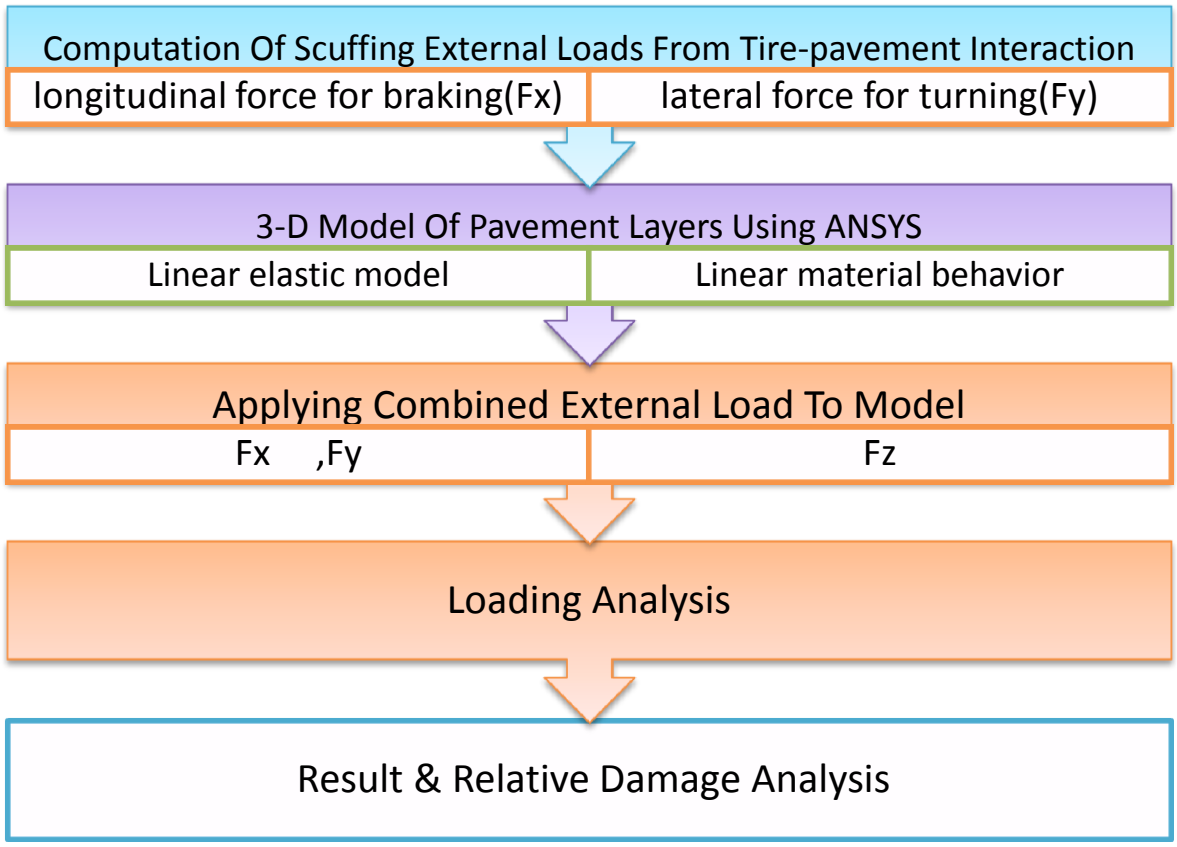

Figure 3.1: Flow chart of method

3.4 Computation of Scuffing Forces

Some aspects, such as transient contact with non-linear frictional behavior at contact patch, make rolling contact problems difficult than if it might appear at first glance. Therefore, it was reasonable to use a sliding-velocity-dependent friction model to estimate tire braking force and cornering force with a slip angle(Hao Wang, 2010).

Mechanical Car Simulation (Carsim2017.1) Software: used to model and calculate tire forces**.**

Tire model in this software is based on different theories, such as combined slip theory and friction similarity incorporated in VS Math Models of Carsim2017.1.

Pure longitudinal and lateral slip

Fx=FX (Fz,k) {α=0} 3.1

For pure longitudinal slip, longitudinal force is modeled as a **table function** of vertical force and longitudinal slip (k).

Longitudinal slip: longitudinal slip ratio (k) defined as:

$$Slip\ ratio(kabba)[k] = \left(1 - \frac{Re*\omega}{v}\right) \quad 3.2$$

Where:
Re: tire effective rolling radius,
ω: wheel angular velocity,
v: tire speed
Slip ratio always generates a maximum longitudinal braking force between 10% and 30% (Chae, 2006).
For different surface, function similarity would be used.

$$Fx = \frac{\mu}{\mu_o} FX\left(Fz, \frac{\mu}{\mu_o} k\right) \qquad \{for\ \alpha = 0\} \qquad 3.3$$

For pure lateral slip, lateral force is modeled as the table function of vertical force (Fz) and lateral slip angle (α).

$$Fy = FY\ (Fz, \alpha) \qquad \{k=0) \qquad 3.4$$

Lateral slip: the slip angle (α) for each tire is defined in terms of X & Y velocity. The slip angle is the arc tangent of ratio.

$$\alpha = \tan^{-1}(v_y/v_x). \qquad 3.5$$

$$Fy = \frac{\mu}{\mu_o} FY\left(Fz, \frac{\mu}{\mu_o} \alpha\right) \qquad \{for\ k\ = 0\} \qquad 3.6$$

For this study, tire assembly of 265R/75/16 was modeled with CarSim2017.1 software to calculate tire-pavement interaction forces.

Optimization the loads in Carsim have carried out.

Input data:

- Effective rolling radius (Re);
- Unloaded (free) radius(R);
- Vertical (normal) force;
- Reference vertical force
- Maximum allowable force(100KN by default)
- Slip ratio (k)
- Slip angle (α)
- Tire width
- friction coefficient

Other data were taken from the software data set and library.

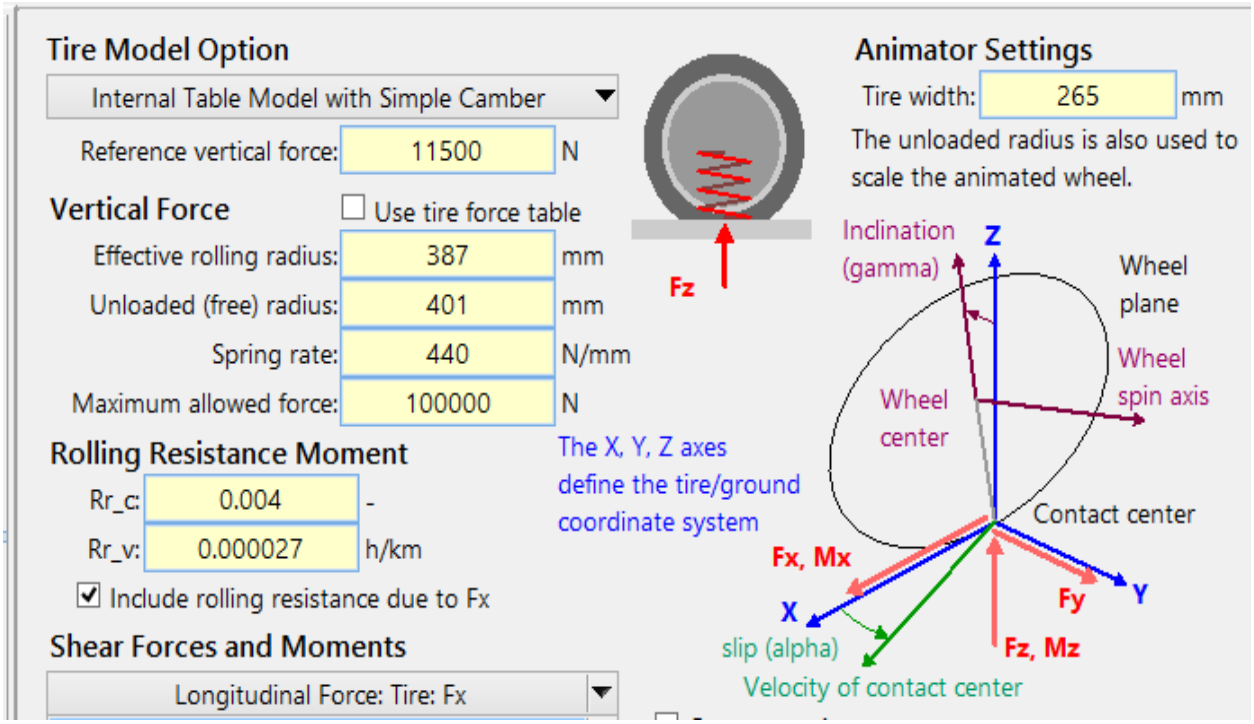

Figure 3.3: Data field screen of tire model

VS Math Models of Carsim2017.1 software prepare models of tire and gives the result and draws graphs of the result, as can be seen in figure 3.5. Results can be linked to an excel sheet for more elaboration and observe the relationship of parameters

The following figures that Cleary show that, vehicle in turning or braking, the front tire subjected large load components that need to caramelize. Because the nature of dynamics increases all loads due to movement of the body in all three direction (up, down & forth).

- Notice free rolling condition of vehicle

- Notice the front tires **while turning** operations of vehicle

- Notice the front tires while **braking** operations of vehicle**.**

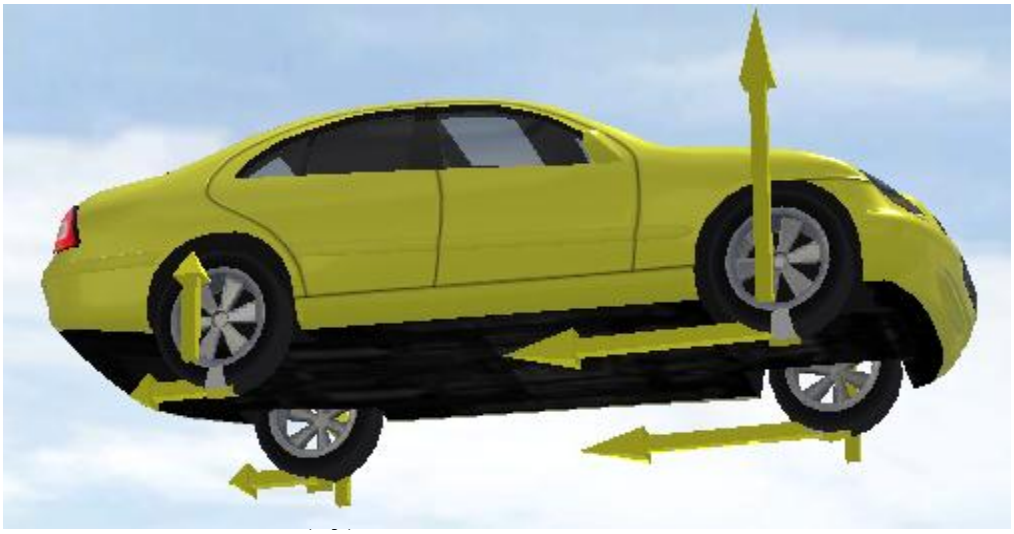

Table3. 6: Lateral scuffing force

Top row: vertical tire load Fz (N); X axis: slip angle (degree); rest: **lateral force** Fy(N).

X	1	2	3	4	5	6	7	8	9	10
0	***FZ 2819.41***	***FZ 5638.82***	***FZ 8458.2***	***FZ 11278***	***FZ 14097.1***	***FZ 16916***	***FZ 19736***	***FZ 20000.00***	***FZ 22555.3***	***FZ 40000.00***
0.5	329.58	633.8	909.33	1154.7	1369.28	1553	1706	1741.40	1828.89	3261.61
1	648.04	1246.9	1790	2274.4	2698.83	3062.9	3366.9	3436.37	3611.83	6441.84
1.5	945.81	1821.35	2617.1	3328.6	3953.62	4491.5	4942.5	5043.56	5307.63	9467.54
2	1215.89	2343.97	3372	4294	5106.92	5809.4	6401.3	6530.64	6883.54	12280.33
2.5	1454.34	2807.04	4043.5	5156.5	6141.82	6997.3	7722.3	7876.22	8317.22	14840.09
3	1659.96	3208.03	4627.7	5910.5	7051.03	8046.4	8895	9069.82	9596.91	17125.37
3.5	1833.72	3548.45	5126.2	6557.2	7835.24	8956.4	9918.3	10110.32	10720.1	19131.33
4	1978.06	3832.57	5544.4	7102.9	8500.93	9733.6	10798	11003.72	11691.5	20866.09
4.5	2096.12	4066.18	5890.3	7556.9	9058.15	10388	11544	11760.67	12520.9	22346.79
5	2191.36	4255.65	6172.4	7929.7	9518.74	10933	12168	12394.44	13220.9	23595.92
5.5	2267.11	4407.27	6399.7	8232	9894.93	11382	12687	12919.22	13805.4	24638.39
6	2326.48	4526.89	6580.4	8474.1	10198.5	11746	13111	13349.06	14288.5	25499.34
6.5	2372.2	4619.73	6721.7	8665.2	10440.3	12039	13455	13697.15	14683.6	26202.81
7	2406.62	4690.32	6830.3	8813.5	10629.9	12271	13731	13975.44	15003	26770.89
7.5	2431.75	4742.52	6911.7	8926.2	10775.8	12452	13948	14194.54	15257.7	27223.40
8	2449.26	4779.59	6970.6	9009.2	10885.1	12590	14116	14363.68	15457.5	27577.76
8.5	2460.54	4804.23	7010.9	9067.6	10964	12692	14243	14490.79	15610.7	27849.09
9	2466.74	4818.71	7036	9105.7	11017.7	12763	14335	14582.66	15724.8	28050.42
9.5	2468.82	4824.88	7048.6	9127.1	11050.4	12810	14397	14645.04	15805.8	28192.81
10	2467.54	4824.29	7050.9	9134.8	11065.8	12835	14435	14682.80	15859	28285.74
10.5	2463.55	4818.2	7044.9	9131.1	11066.9	12844	14453	14700.02	15888.9	28337.21
11	2457.38	4807.65	7032.1	9118.2	11056.3	12838	14454	14700.15	15899.4	28353.97
11.5	2449.45	4793.52	7013.7	9097.8	11036	12820	14441	14686.09	15893.5	28341.77
12	2440.13	4776.5	6990.9	9071.2	11007.8	12792	14417	14660.28	15874	28305.40
12.5	2429.71	4757.19	6964.5	9039.7	10973.2	12757	14382	14624.76	15843.2	28248.94
13	2418.42	4736.06	6935.2	9004.1	10933.4	12715	14340	14581.26	15803.1	28175.83
13.5	2406.46	4713.53	6903.7	8965.4	10889.4	12667	14292	14531.23	15755.1	28089.04
14	2394	4689.91	6870.5	8924.3	10842	12616	14238	14475.87	15700.8	27990.95
14.5	2381.18	4665.49	6835.9	8881.1	10792	12561	14179	14416.23	15641.3	27883.64
15	2368.09	4640.49	6800.3	8836.5	10740	12503	14118	14353.15	15577.5	27768.88
15.5	2354.84	4615.09	6764.1	8790.8	10686.4	12443	14053	14287.38	15510.4	27648.17
16	2341.5	4589.44	6727.4	8744.4	10631.8	12382	13987	14219.52	15440.6	27522.74
16.5	2328.13	4563.69	6690.4	8697.5	10576.3	12319	13919	14150.09	15368.7	27393.66
17	2314.78	4537.92	6653.3	8650.3	10520.4	12256	13850	14079.54	15295.2	27261.84
17.5	2301.5	4512.23	6616.3	8603.1	10464.2	12192	13780	14008.21	15220.5	27128.02
18	2288.3	4486.68	6579.4	8555.9	10407.9	12128	13709	13936.43	15145.1	26992.89
18.5	2275.23	4461.33	6542.7	8509	10351.8	12064	13639	13864.45	15069.2	26856.93
19	2262.31	4436.23	6506.3	8462.3	10296	12000	13568	13792.48	14993.1	26720.62
19.5	2249.54	4411.41	6470.3	8416.1	10240.5	11937	13497	13720.71	14916.9	26584.37
20	2236.94	4386.91	6434.7	8370.3	10185.5	11873	13427	13649.30	14841	26448.48
20.5	2224.53	4362.74	6399.5	8325	10131.1	11811	13358	13578.36	14765.4	26313.22
21	2212.32	4338.92	6364.8	8280.3	10077.2	11749	13288	13508.00	14690.2	26178.82
21.5	2200.29	4315.46	6330.7	8236.1	10024	11687	13220	13438.30	14615.6	26045.48
22	2188.47	4292.38	6297	8192.6	9971.53	11627	13152	13369.77	14541.7	25914.27
22.5	2176.85	4269.68	6263.9	8149.8	9919.75	11567	13085	13301.16	14468.5	25782.52
23	2165.43	4247.36	6231.3	8107.6	9868.7	11508	13019	13233.81	14396.1	25653.13
23.5	2154.22	4225.42	6199.2	8066	9818.42	11450	12954	13167.49	14324.5	25525.50

X	1	2	3	4	5	6	7	8	9	10
0	***FZ 2819.41***	***FZ 5638.82***	***FZ 8458.2***	***FZ 11278***	***FZ 14097.1***	***FZ 16916***	***FZ 19736***	***FZ 20000.00***	***FZ 22555.3***	***FZ 40000.00***
24	2143.21	4203.87	6167.7	8025.2	9768.9	11392	12889	13101.75	14253.8	25398.95
24.5	2132.4	4182.7	6136.7	7985	9720.15	11336	12826	13037.07	14184	25274.28
25	2121.78	4161.9	6106.2	7945.4	9672.17	11280	12763	12973.31	14115.1	25151.26

When tire undergoes steering (tilted in some angles), the vehicle forced to turning condition that subjects the tire to lateral deflection because of lateral force on tire resisting centrifugal force vehicle sprung mass.

As can be seen from figures below, the larger normal force(Fz) induce larger lateral force(Fy) taking slip angles as the consistent variable for all normal forces which is similar to (Gohring, Von Glasner and Pflug, 1991) study.

The lateral induced force and slip angle have a linear and non-linear relationship, as one can note from graphs. In other words, lateral force increased with a slip angle linearly up to some point and then started to increase non-linearly up to a maximum point (in a stable zone) and finally decreased in an unstable zone.

At zero slip angle (straight with constant speed), there was an insignificant lateral force, which implied that free rolling conditions only subjected to vertical load. But some road sections, such as intersection, roundabout, and flat small curved roads, are subjected to lateral forces.

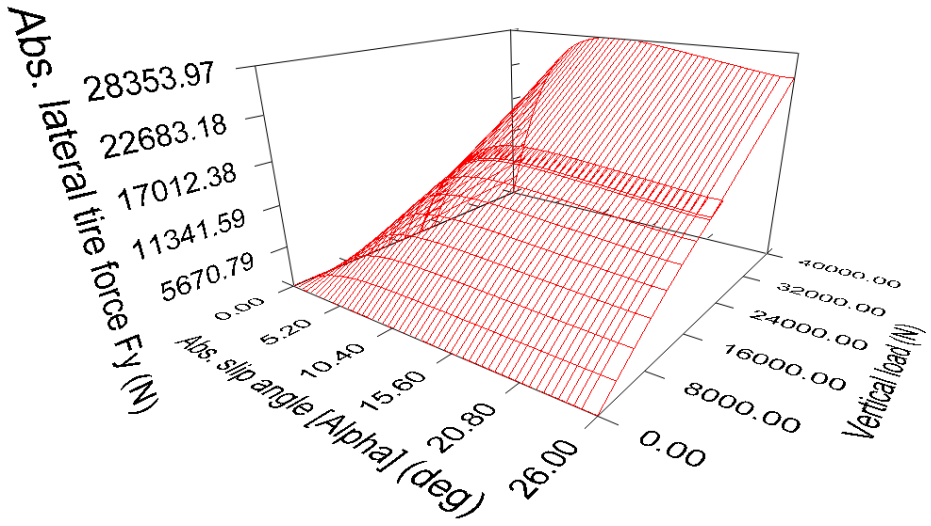

Figure 3.6: 3-D lateral forces

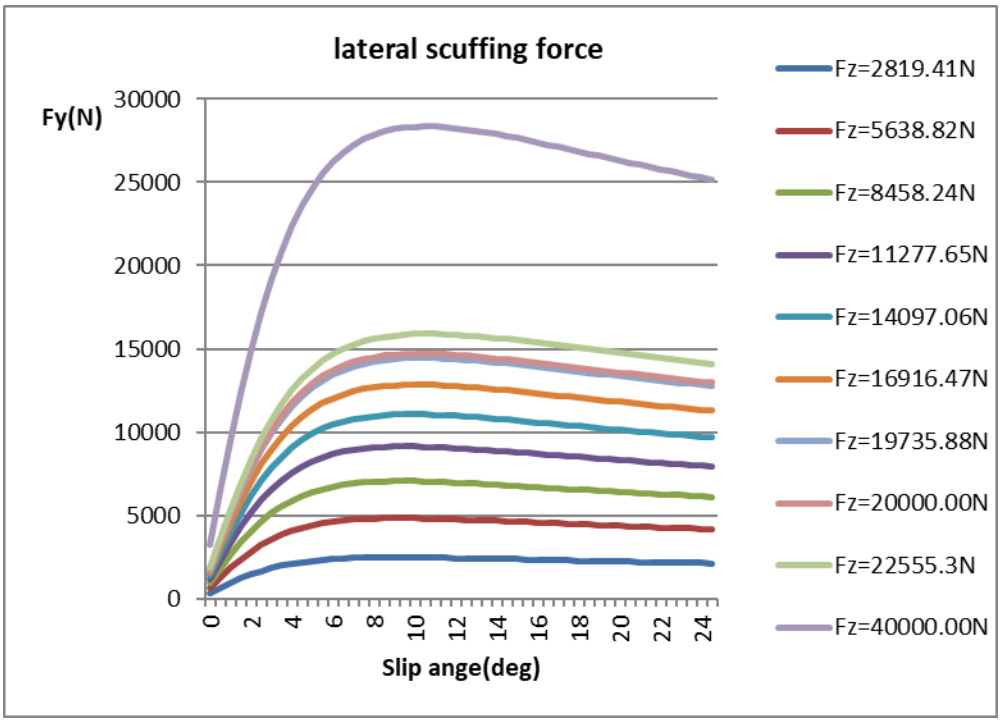

Figure 3.5: predicted lateral turning force

Table3. 7: Braking forces

Top row: vertical tire load (N);X axis: absolute slip ratio[kappa](-);rest: abs l**ongitudinal force** Fx(N).

X	1	2	3	4	5	6	7	8	9	10
0	***FZ 2819.41***	***FZ 5638.82***	***FZ 8458.24***	***FZ 11277.65***	***FZ 14097.06***	***FZ 16916.47***	***FZ 19735.88***	***FZ 20000.00***	***FZ 22555.3***	***FZ 40000.00***
0.02	659.98	1310.49	1949.71	2576.32	3189.21	3787.34	4369.71	4432.79	4935.36	8769.18
0.04	1213.62	2408.05	3579.67	4725.96	5844.79	6934.2	7992.38	8108.69	9017.56	16024.19
0.06	1619.31	3210.25	4767.62	6287.9	7768.15	9205.77	10598.36	10754.06	11943.63	21226.14
0.08	1893.6	3751.15	5566.2	7334.49	9052.54	10717.34	12326.12	12508.73	13876.34	24663.02
0.1	2072.48	4103	6084.23	8011.39	9880.67	11688.8	13432.84	13633.16	15110.11	26857.43
0.12	2187.92	4329.57	6416.99	8445.04	10409.72	12307.6	14135.69	14347.55	15891.24	28246.96
0.14	2262.4	4475.42	6630.65	8722.77	10747.62	12701.71	14582	14801.36	16385.75	29126.74
0.16	2310.35	4569.09	6767.52	8900.16	10962.77	12951.84	14864.31	15088.54	16697.45	29681.37
0.18	2340.84	4628.48	6854	9011.81	11097.64	13107.96	15039.71	15267.08	16890.18	30024.4
0.2	2359.6	4664.84	6906.65	9079.39	11178.75	13201.2	15143.7	15373.56	17003.56	30234.4
0.22	2370.27	4685.35	6936.06	9116.71	11222.99	13251.38	15198.83	15429.31	17062.69	30331.66
0.24	2375.27	4694.74	6949.15	9132.81	11241.4	13271.38	15219.76	15450.82	17083.89	30369.56
0.26	2376.19	4696.14	6950.56	9133.73	11241.33	13269.85	15216.3	15447.53	17078.07	30359.41
0.28	2374.15	4691.75	6943.48	9123.62	11227.86	13252.7	15195.17	15426.27	17052.68	30314.44
0.3	2369.92	4683.08	6930.15	9105.4	11204.54	13224.08	15161.08	15391.83	17012.97	30243.99
0.32	2364.06	4671.23	6912.16	9081.15	11173.91	13186.98	15117.42	15347.65	16962.69	30154.74
0.34	2356.98	4657	6890.71	9052.42	11137.85	13143.57	15066.65	15296.24	16904.58	30051.55
0.36	2348.99	4640.99	6866.67	9020.34	11097.75	13095.47	15010.61	15239.46	16840.68	29938.05
0.38	2340.31	4623.65	6840.69	8985.77	11054.65	13043.91	14950.7	15178.74	16772.53	29817
0.4	2331.13	4605.33	6813.3	8949.37	11009.35	12989.83	14887.97	15115.15	16701.31	29690.47
0.42	2321.58	4586.3	6784.87	8911.66	10962.48	12933.96	14823.25	15049.58	16627.94	29560.75
0.44	2311.76	4566.76	6755.72	8873.04	10914.53	12876.85	14757.19	14982.55	16553.12	29427.18
0.46	2301.77	4546.88	6726.1	8833.81	10865.88	12818.96	14690.27	14914.68	16477.41	29292.64
0.48	2291.67	4526.8	6696.18	8794.24	10816.83	12760.65	14622.92	14846.37	16401.26	29157.33

X	1	2	3	4	5	6	7	8	9	10
0	***FZ 2819.41***	***FZ 5638.82***	***FZ 8458.24***	***FZ 11277.65***	***FZ 14097.06***	***FZ 16916.47***	***FZ 19735.88***	***FZ 20000.00***	***FZ 22555.3***	***FZ 40000.00***
0.5	2281.52	4506.62	6666.14	8754.51	10767.63	12702.19	14555.44	14777.92	16325.02	29021.85
0.52	2271.35	4486.43	6636.09	8714.8	10718.46	12643.81	14488.09	14709.6	16248.97	28886.69
0.54	2261.2	4466.28	6606.13	8675.22	10669.5	12585.69	14421.08	14641.62	16173.33	28752.28
0.56	2251.1	4446.25	6576.34	8635.89	10620.85	12527.97	14354.56	14574.41	16098.29	28618.91
0.58	2241.08	4426.36	6546.78	8596.88	10572.62	12470.78	14288.66	14507.28	16023.99	28486.86
0.6	2231.15	4406.66	6517.51	8558.26	10524.89	12414.2	14223.5	14441.16	15950.53	28356.3
0.62	2221.32	4387.18	6488.57	8520.09	10477.73	12358.3	14159.15	14375.87	15878.01	28227.41
0.64	2211.61	4367.93	6459.99	8482.4	10431.17	12303.14	14095.67	14311.45	15806.5	28100.31
0.66	2202.03	4348.93	6431.79	8445.23	10385.27	12248.77	14033.11	14246.91	15736.04	27958.82
0.68	2192.58	4330.21	6404	8408.59	10340.05	12195.23	13971.51	14185.46	15666.69	27851.81
0.7	2183.26	4311.76	6376.62	8372.52	10295.53	12142.52	13910.9	14123.95	15598.46	27730.54
0.72	2174.1	4293.6	6349.68	8337.03	10251.73	12090.68	13851.29	14063.46	15531.38	27611.3
0.74	2165.07	4275.73	6323.17	8302.11	10208.65	12039.71	13792.7	14004	15465.45	27494.12
0.76	2156.2	4258.16	6297.11	8267.79	10166.31	11989.61	13735.13	13944.57	15400.69	27378.99
0.78	2147.47	4240.88	6271.49	8234.05	10124.71	11940.4	13678.58	13888.18	15337.09	27265.94
0.8	2138.89	4223.89	6246.31	8200.9	10083.84	11892.07	13623.05	13831.77	15274.65	27154.82
0.82	2130.46	4207.21	6221.57	8168.35	10043.71	11844.61	13568.54	13776.48	15213.36	27045.85
0.84	2122.18	4190.82	6197.28	8136.38	10004.3	11798.02	13515.03	13722.18	15153.22	26939.09
0.86	2114.04	4174.72	6173.43	8104.99	9965.61	11752.28	13462.52	13668.88	15094.2	26834.18
0.88	2106.05	4158.91	6150	8074.17	9927.63	11707.4	13410.99	13616.58	15036.29	26731.24
0.9	2098.2	4143.39	6127.01	8043.92	9890.36	11663.35	13360.43	13565.25	14979.48	26630.25
0.92	2090.5	4128.15	6104.43	8014.23	9853.78	11620.13	13310.82	13514.9	14923.75	26531.18
0.94	2082.94	4113.19	6082.27	7985.08	9817.89	11577.72	13262.15	13465.49	14869.08	26434
0.96	2075.51	4098.51	6060.52	7956.48	9782.66	11536.11	13214.39	13417.02	14815.45	26338.65
0.98	2068.22	4084.09	6039.17	7928.41	9748.09	11495.28	13167.55	13369.47	14762.84	26245.14
1	2061.06	4069.94	6018.22	7900.86	9714.16	11455.21	13121.59	13322.81	14711.23	26153.39

When tire undergoes braking pedal, the vehicle forced to deceleration condition that subjects the tire to longitudinal deflection because of total rolling resistance force on tire resisting braking torque applied by the driver.

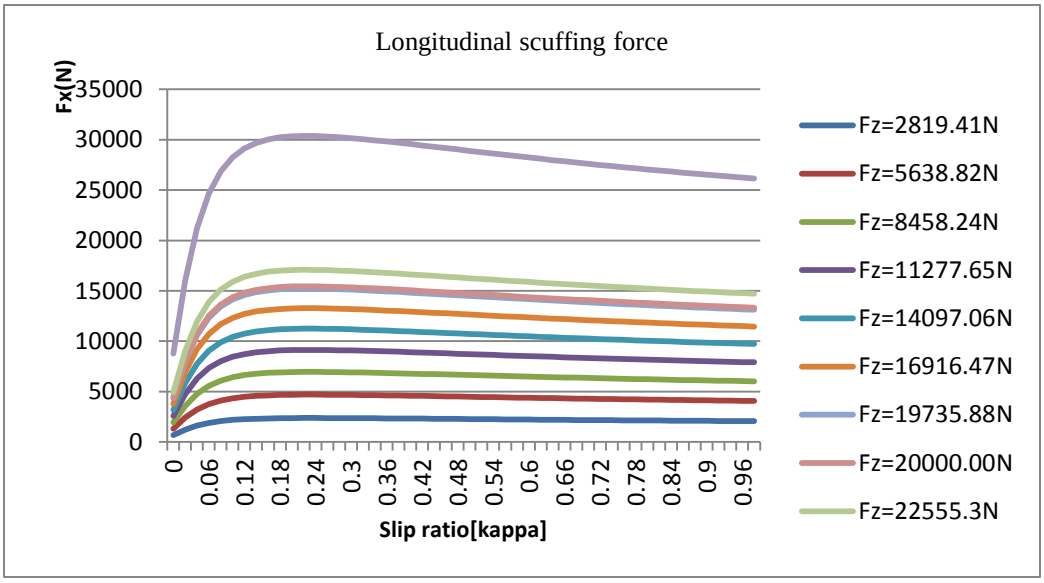

Figure 3.9: Longitudinal scuffing force

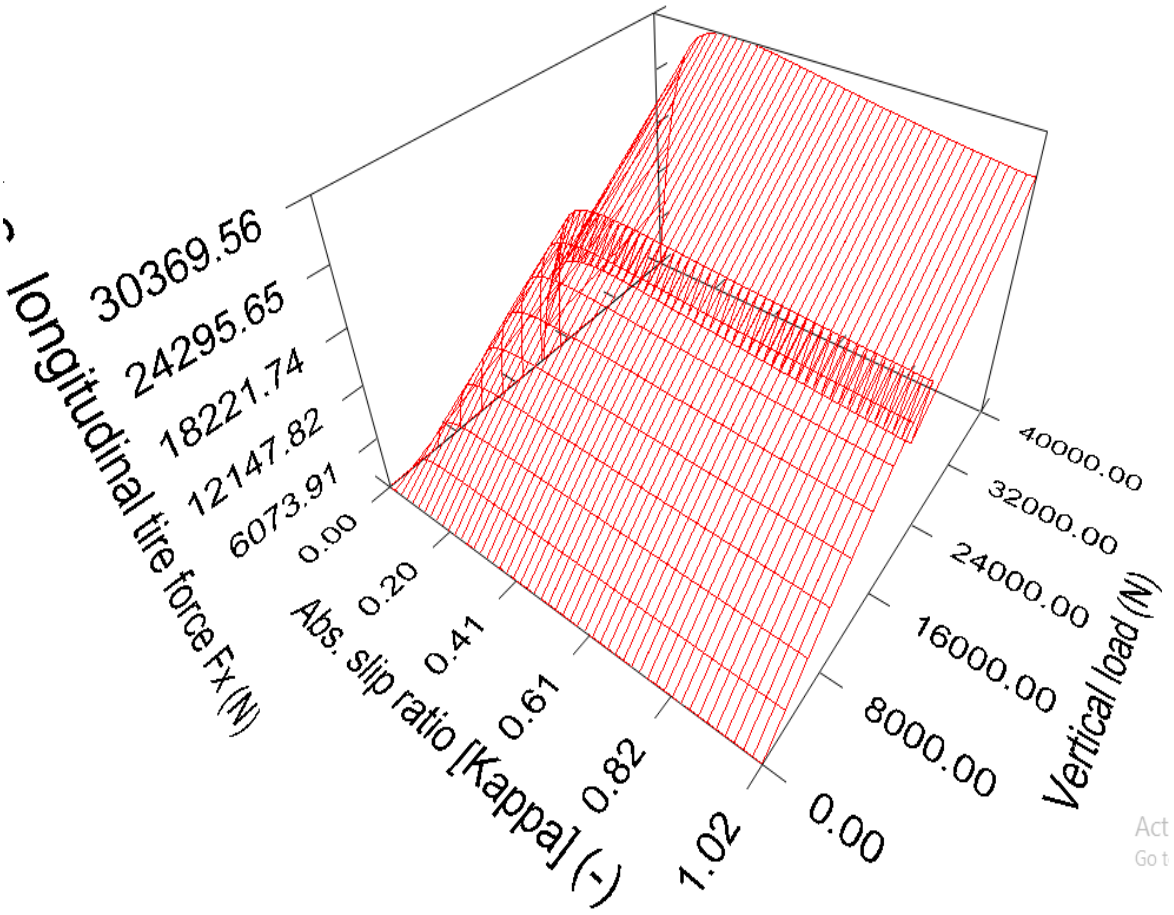

Figure 3.10: 3-D predicted longitudinal force

Pavement road section, such as legs of intersection and roundabout, vehicle station and speed barker hump where full braking or partial braking could have carried out, the pavement is subjected to this significant horizontal or tangential force of tire that causes pavement deterioration and lead to premature failure. In contrast, the free rolling is free from this horizontal force. As can be seen from the graph, similar to lateral forces, longitudinal force linearly increased up to some specific point of slip ratio and; started to decrease as slip ratio increased further. So the relationship of forces and slips were both linear & non-linear.

Table3. 8: Summary of computed tire-pavement interaction forces

Estimated tire-pavement contact forces	Maximum forces
Vertical Force(Fz)	40kN
Braking longitudinal force(Fx)	30.36956kN
Cornering Lateral force(Fy)	28.35397 kN

3.5 Finite Element Modeling of Flexible Pavement

3-D finite element (FE) flexible pavement model was built using ANSYS 8.1.

The 3-D FE model was an appropriate choice compared to 2-D plane model; because3-D model considers 3Dcontact stress distribution at tire contact batch and allows transient dynamic loading associated with a moving vehicle(WANG, 2011).

The pavement model requires choosing material and a structure a good way to withstand cyclic loading and weather conditions over a design period. Materials used in pavement construction require superior constitutive models that can be capable of taking pictures of the complexities observed of their conduct.

The technique for computational modeling the use of the FEM consists of the following steps:

- Geometric modeling.
- Contact type and definition.
- Meshing and detail definition.
- boundary conditions
- Martial property Assignment.
- Loading circumstance application.
- Analysis and solution.
- Visualization

Geometric Model and Boundary Conditions

The pavement geometric model was built through the use of ANSYS design modeler each solid part represented one layer within the pavement shape.

The geometric model was created in three dimensions (3-D) with a tire-pavement contact area along the longitudinal line of the model.

Table3. 9: Material Data and thickness of 3-D model

Object name	Thickness cm	Young's Modulus MPa	Density kg m^-3	Poisson's Ratio
Asphalt	15	3000	2400	0.35
Base	20	300	2150	0.3
Sub-base	30	175	2070	0.3
Sub-grad	infinite	112	1800	0.4

Stiffness Behavior	Flexible			
Material				
Assignment	sub-grade	sub-base	base	Asphalt
dimension				
Length X	300cm			
Length Y	100cm.	30cm	20cm	15cm
Length Z	99.4cm			

Figure 3.11: dimension of pavement model

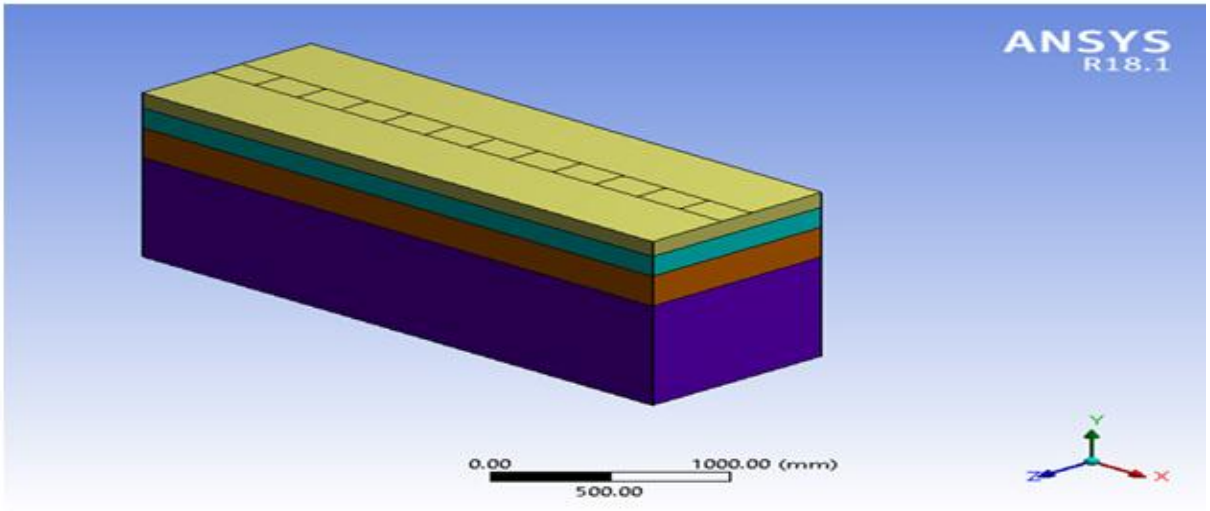

Figure 3.12: three dimensional geometry of pavement model

Figure 3.11&12 Dimension of pavement model

Contacts Types

In ANSYS software, there are five types of contact.

Bonded contact type: as its name indicate, target and contact bodies are neither move vertically nor move horizontally. They are strongly bonded to each other.

Separate contact type: in this type of contact, vertical movement is restricted but excessive tangential slide is allowed.

Frictional contact type: in this type of contact, vertical movement (separation) is not allowed but the tangential slide is allowed with strong resistance that comes from friction coefficient.

Rough contact type: vertical separation is allowed however, a tangential slide is restricted with an infinite coefficient of friction.

Frictionless contact type: as its name show, there is no restriction of movements in both directions. So starting from this definition, bonded contact type is taken for this study.

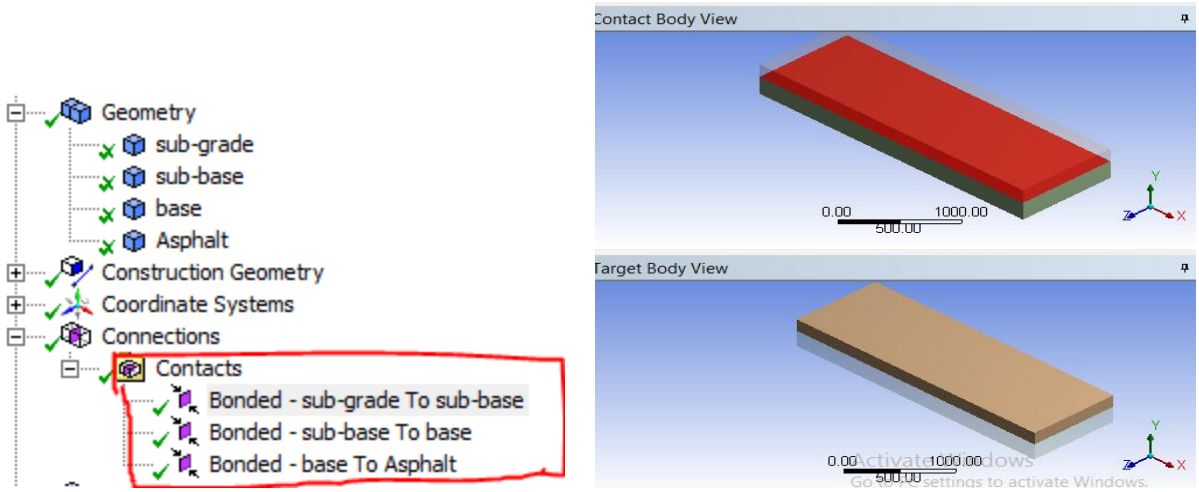

Meshing and Detail Definition

The meshing process divides the hassle area into the set of factors linked at nodes. The density of elements in a given place of the hassle controls the accuracy of the effects. Inside the case of modeling a pavement subjected to a tire load, excessive element density (20 x 25 mm) is desired close to the weight. The meshing method generally requires numerous iterations to outline on top of the line number of factors as a way to produce a sufficiently correct solution at a nearly sensible computational effort.

The element type and the respective number of nodes are described throughout the meshing technique. The range of nodes defines the type of feature that may be used to approximate the solution within an individual element.

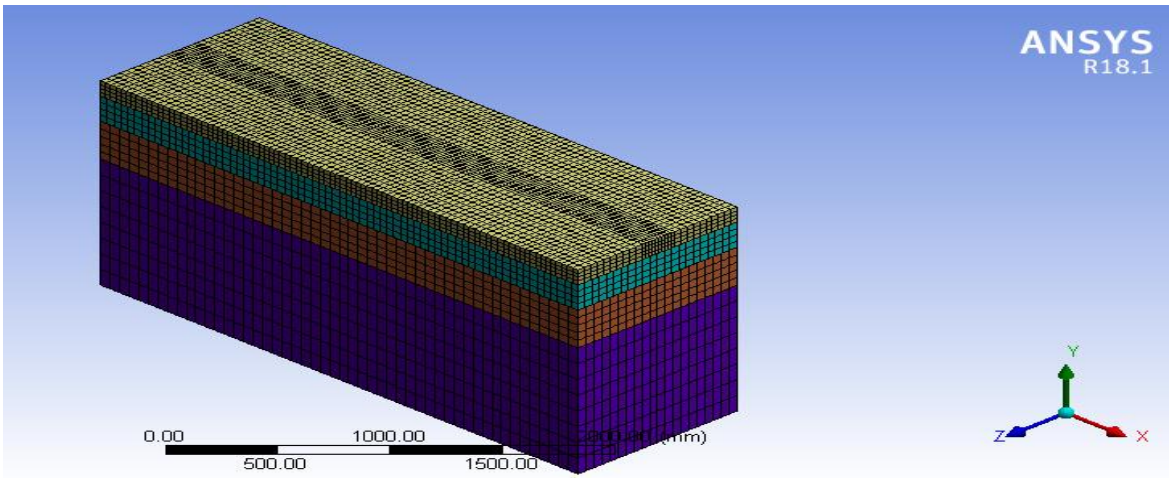

Figure 3.13: Meshing model

Table3. 10: number of elements and nodes

Statistics	
Nodes	144000
Elements	29840

Boundary condition

Boundary conditions had been completed to all faces of the geometric model to restriction displacement within the path perpendicular to the face. The bottom of the layer modeling the subgrade becomes constrained (fixed support) to no displacement in all guidelines. The other sides of the model were orthogonally restricted.

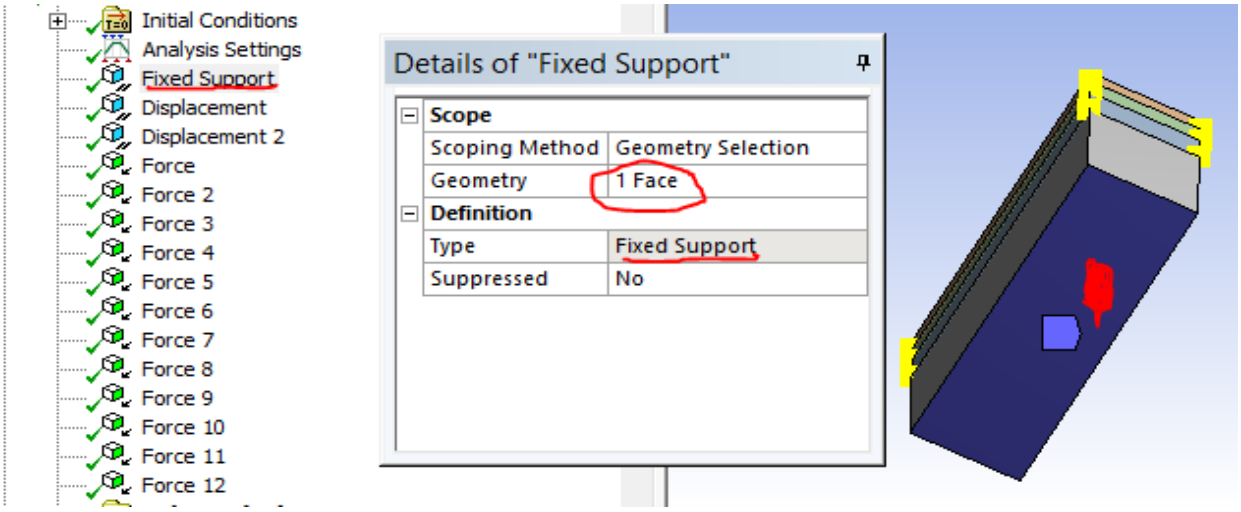

Figure 3.14: Fixed support lower face re

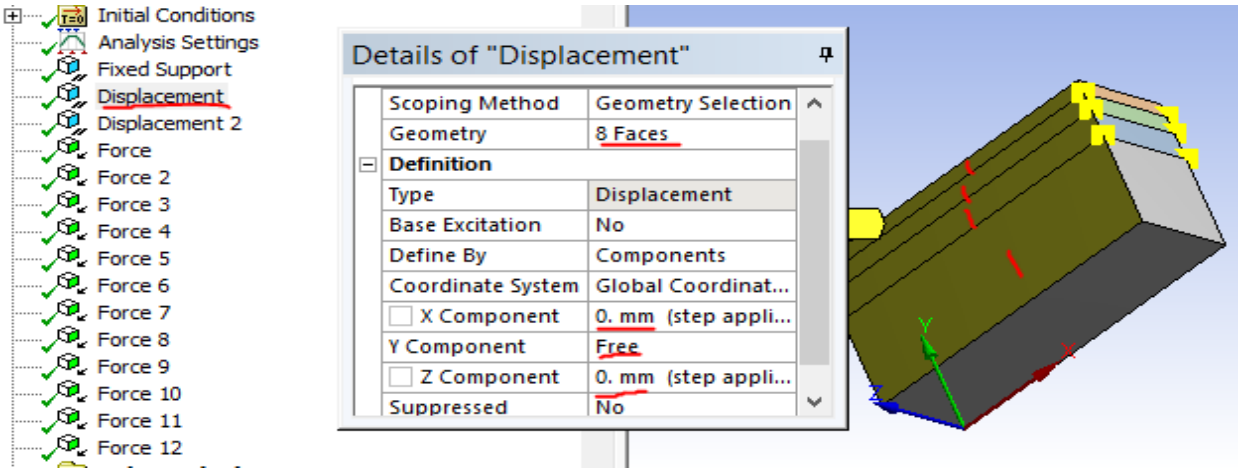

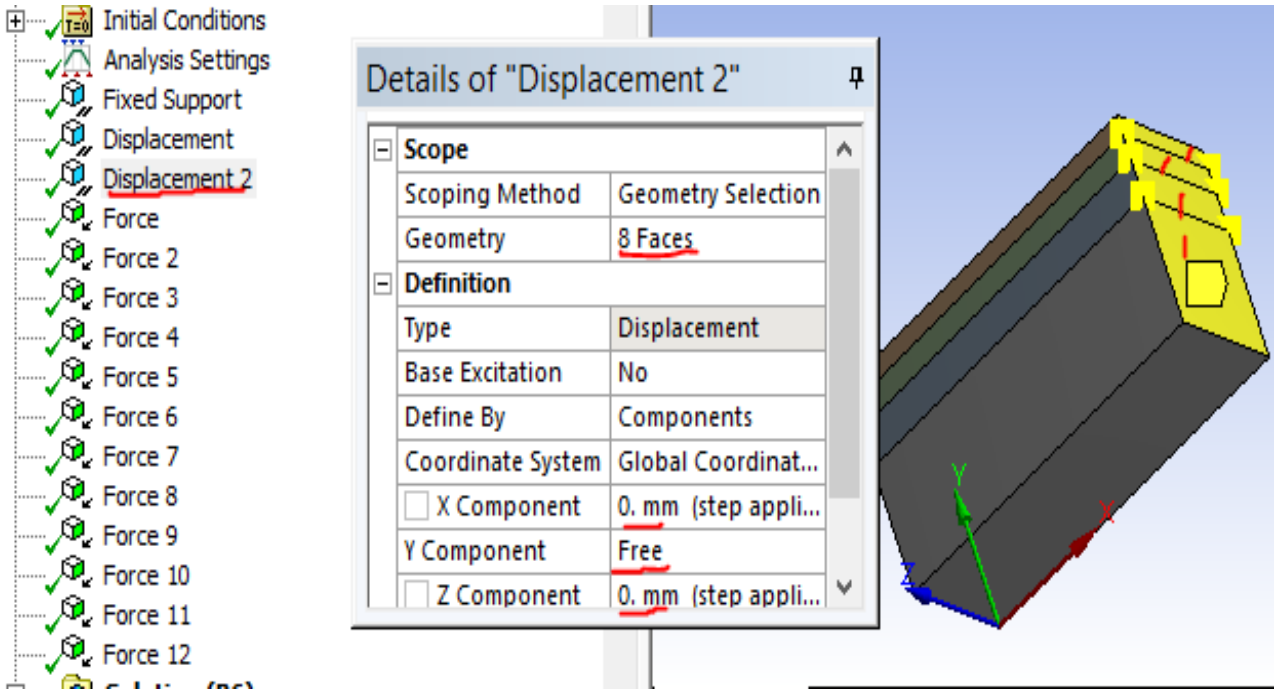

Figure 3.15: orthogonal restriction for side faces

Martial property Assignment

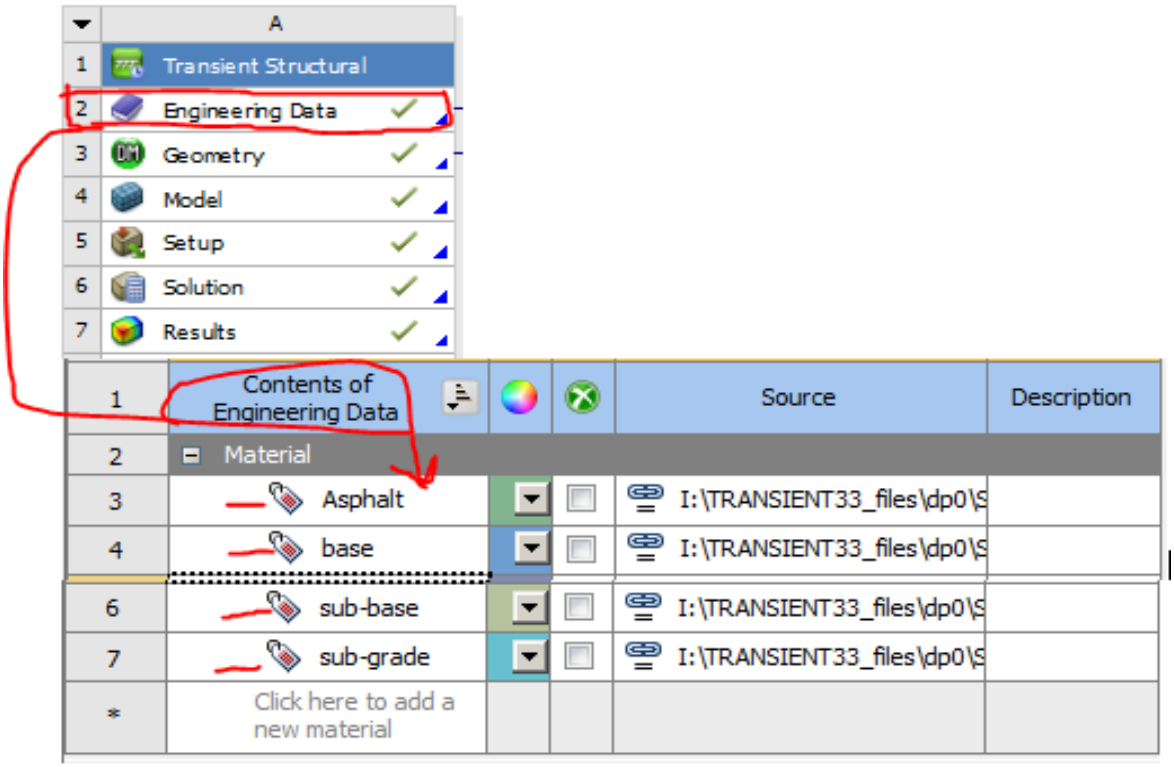

Properties of Outline Row 3: Asphalt

	A	B	C	D	E
1	Property	Value	Unit		
2	Material Field Variables	Table			
3	Density	24000	kg m^-3		
4	Isotropic Elasticity				
5	Derive from	Young's ...			
6	Young's Modulus	3000	MPa		
7	Poisson's Ratio	0.35			
8	Bulk Modulus	3.3333E+09	Pa		
9	Shear Modulus	1.1111E+09	Pa		

Properties of Outline Row 4: base

	A	B	C	D	E
1	Property	Value	Unit		
2	Material Field Variables	Table			
3	Density	2150	kg m^-3		
4	Isotropic Elasticity				
5	Derive from	Young's ...			
6	Young's Modulus	300	MPa		
7	Poisson's Ratio	0.3			
8	Bulk Modulus	2.5E+08	Pa		
9	Shear Modulus	1.1538E+08	Pa		

Properties of Outline Row 6: sub-base

	A	B	C	D	E
1	Property	Value	Unit		
2	Material Field Variables	Table			
3	Density	2070	kg m^-3		
4	Isotropic Elasticity				
5	Derive from	Young's ...			
6	Young's Modulus	175	MPa		
7	Poisson's Ratio	0.3			
8	Bulk Modulus	1.4583E+08	Pa		
9	Shear Modulus	6.7308E+07	Pa		

Properties of Outline Row 7: sub-grade

	A	B	C	D	E
1	Property	Value	Unit		
2	Material Field Variables	Table			
3	Density	1800	kg m^-3		
4	Isotropic Elasticity				
5	Derive from	Young's ...			
6	Young's Modulus	112	MPa		
7	Poisson's Ratio	0.4			
8	Bulk Modulus	1.8667E+08	Pa		
9	Shear Modulus	4E+07	Pa		

Figure 3.16: Material assignment

Loading condition

Determination of the tire contact area

For simplification, the imprint wheel contact area of road surface for uniform distributed load, considered as equivalent rectangular area with width 0.6L, length 0.8712L, then the rectangular area is 0.5227L 2 and As the stiffening effect of the tire wall is neglected, in pavement design, the contact pressure is considered to be equal with tire pressure(Huang, 2004).

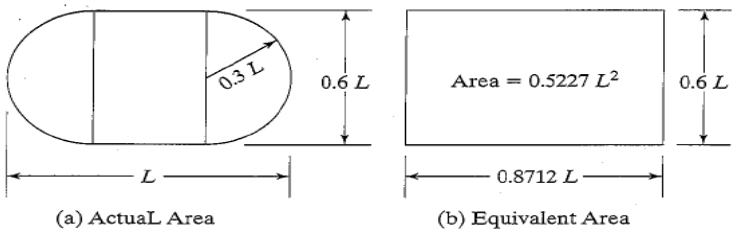

Figure3.17a: Contact area between tire and pavement surface. Figure4b: Equivalent contact area.

$$L = \sqrt{\frac{F}{0.5227P}} = \sqrt{\frac{40}{0.5227*930}} = 0.287\text{m} \quad (3.7)$$

Where: F is vertical tire force and P is tire pressure and take F=40kN& P=0.93Mpa.

Rectangle length L = 0.8712L= 250mm; width B = 0.6L' = 172mm.

Figure : contact area

This paper takes a single tire footprint length of 0.25 m and a width of 0.172 m. When meshing, there are 12 rectangle units in the one tire contact area in X-direction where the load is moving.

Transient moving load

Traffic loading is the acyclic application of moving tire loads which is in nature characterized by moving load as vehicle is moving in certain speed (Hao Wang, 2010). Moving transient load is one of the options to simulate vehicular loading.

To simulate a moving tire with a certain speed, the contact patch area of the tire was gradually shifted over loading area until a single tire pass was completed. Trapezoidal loading step can be used if contact pressure was assumed to be uniform (Yoo *et al.*, 2006). The loading was operated on the first contact area and then transferred to the next parts of the contact area.

In this study, the vehicle speed 11.25 km/h was considered in finite element analysis.

When the vehicle is in uniform motion (free rolling), the vehicle speed is 11.25km / h, the time that load acting on each contact length is 0.08seconds.i.e t=(L/Vo).
Assume there is no lateral force when the vehicle is braking so that the vehicle can reach a maximum braking deceleration (a) and adhesion coefficient (μ).

$$a = \mu g \quad (3.8)$$

Assume adhesion coefficient is 0.8,a=7.84m/s2

This paper studies the braking distance at continuous braking phase, and assuming the acceleration is the same during acceleration, then braking time can be obtained using equation

$$L = V_o t - \frac{1}{2} a t^2 \quad (3.9)$$

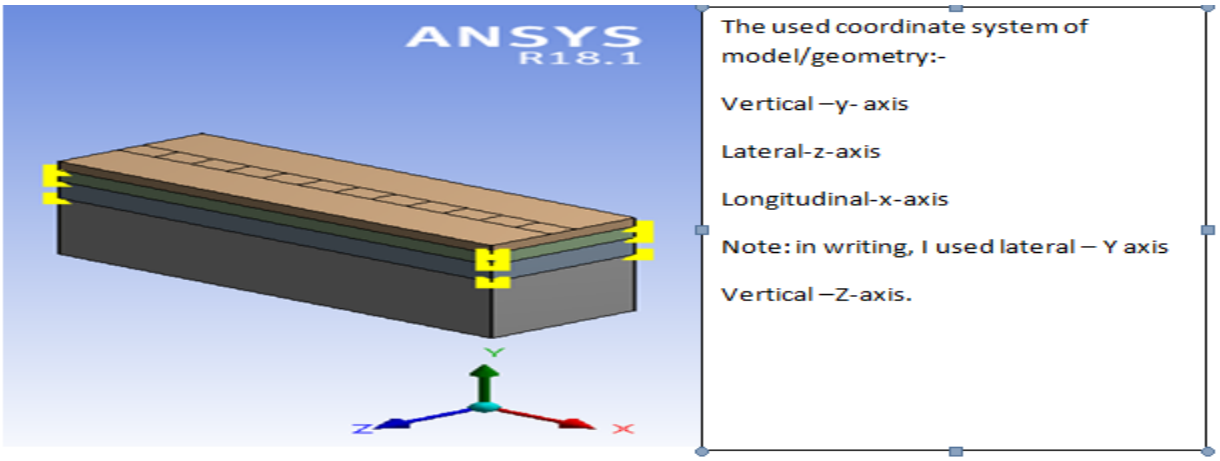

Used coordinate system of geometry

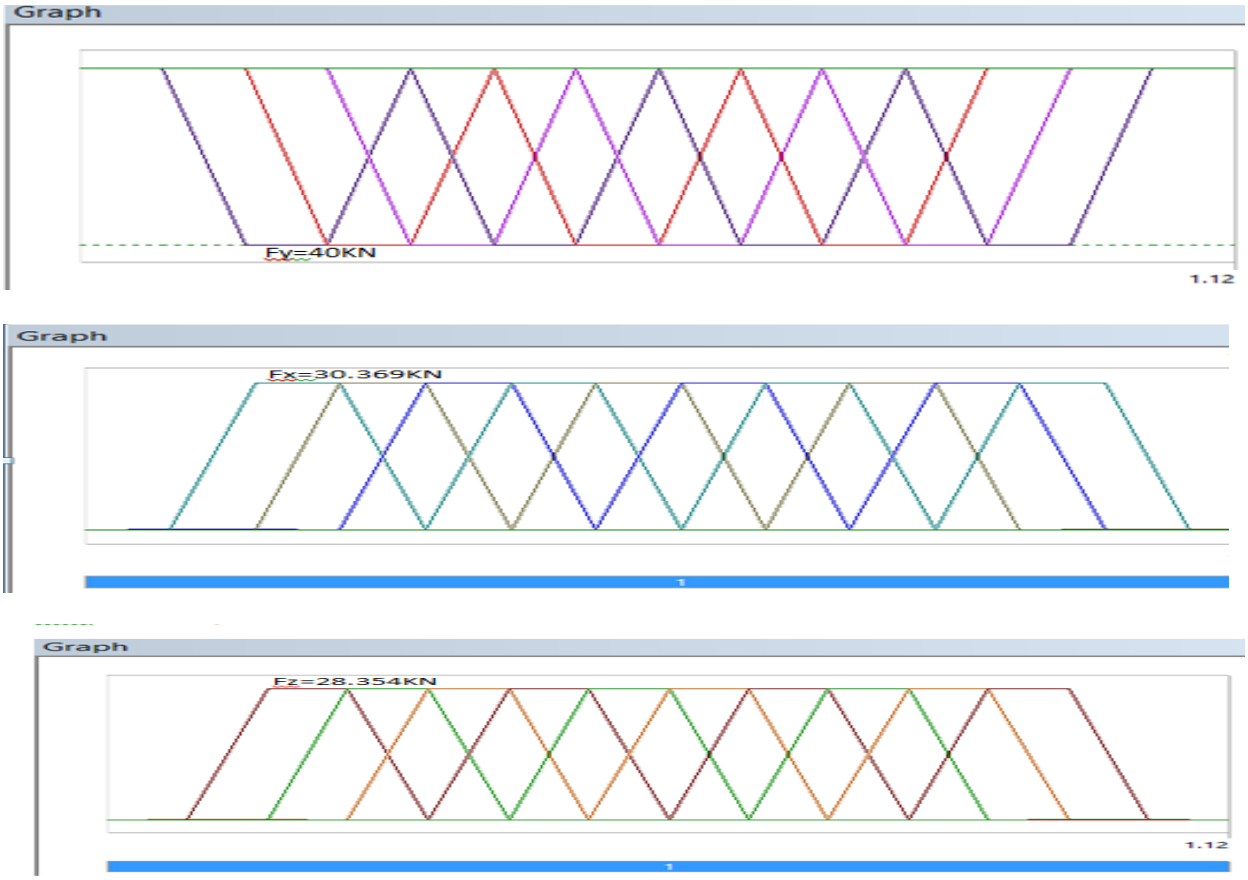

Figure3.18: Loading of pavement model

Loading Analysis

The dynamic transient structural analysis is used in this study because it provides better numerical stability and generally efficient for dynamic structural problems.

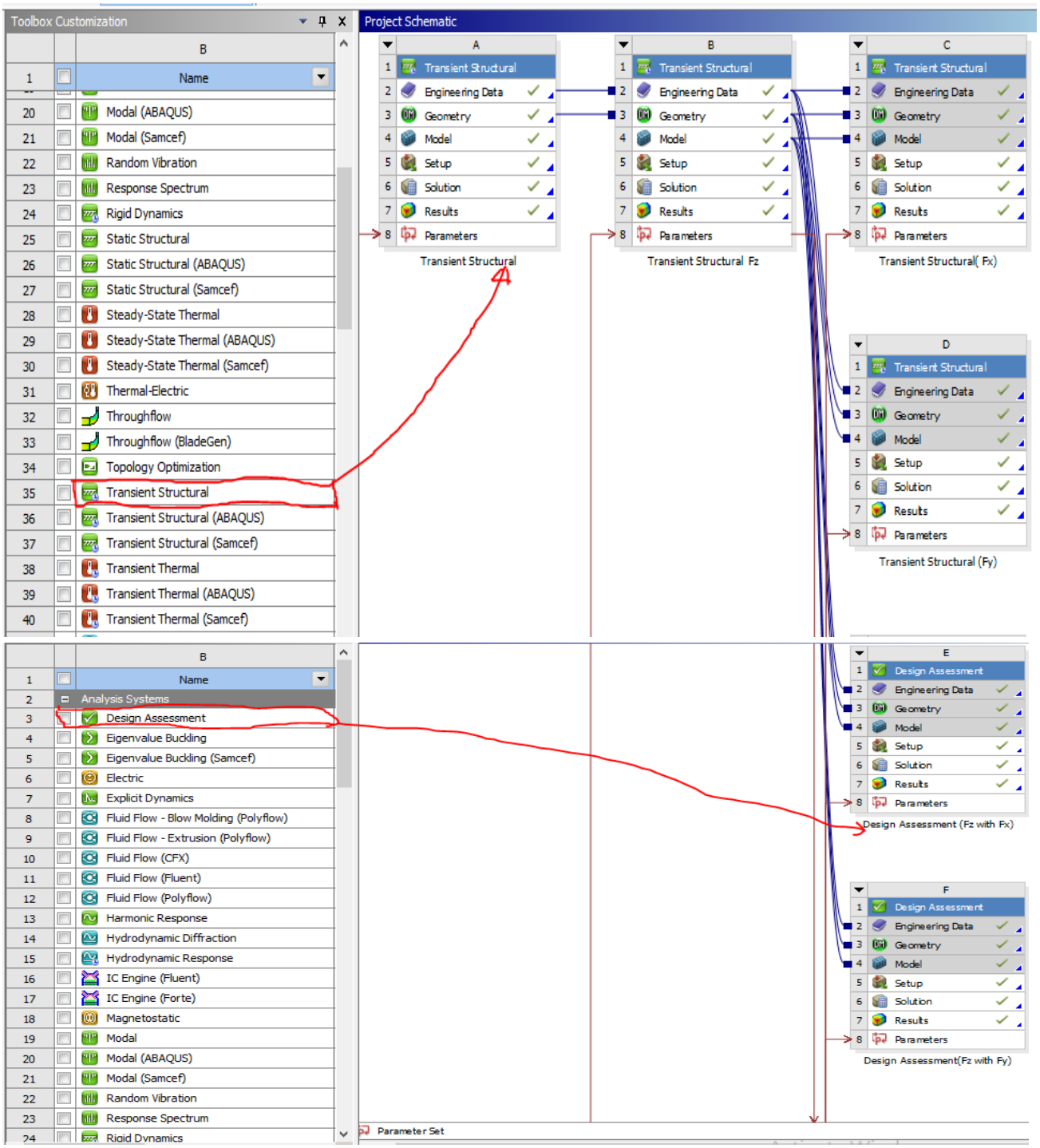

Figure 3.19: Loading analysis 1

Thickness optimization:

In this step, the depth of asphalt optimized with maximum shear stress and strains**.**

The thickness is considered as a variable, shear stresses are recalculated start from the maximum value. This shows the relationship of shear stress, strains and thickness of asphalt.

Chapter -4

4 Result and discussion

This chapter mostly discusses the result that gained from the analysis of flexible pavement model with 3-D finite element model software ANSYS and available damage model. The impacts of scuffing forces on critical responses of pavement were evaluated. The considered critical responses in this study were: tensile strains at near surface and bottom of asphalt layer, shear stresses and strains at shallow depth of asphalt layer, compressive strains at bottom and top of sub-grade and deviator stresses at the middle of base course. The criteria, location of critical point and responsibility of critical responses in damage/ failure models were presented in table 6 below. The critical responses of pavement are influenced by scuffing forces. To analyze this condition, three different cases were considered during analysis.
Case 1: free rolling condition when only vertical load was applied on the contact batch.
Case2: Braking condition when vertical along with longitudinal load applied on contact patch.
Case3: Turning/cornering condition when vertical load along with lateral load applied on the same contact batch.

The results of 3-D pavement model analysis shown as the critical responses of the flexible pavement dramatically influenced by braking and turning. Stress-strain near the surface of pavement significantly affected by scuffing forces showed that, deterioration of pavement was mainly at the top of the pavement where braking and turning of vehicle could take place.
Relative damage analysis showed that braking and turning maneuver condition are the major distress factors of the pavement. Shoving and top-down cracking are the more pavement failure type associated with scuffing force as can see from the result. The results of critical responses relative damage were summarized in tables bellow and followed by analysis. The results of critical responses were summarized in tables bellow and followed by analysis.

Table4. 1: Deviator stress on the middle of base course

Calculating point/stress value(kpa)	Maximum principal stress(σ_1)	Minor principal stress(σ_3)	Deviator stress(σ_d)= ($\sigma_1 - \sigma_3$)
Free rolling	29.887	0.45916	29.43
Braking	31.56	0.47372	31.08628
Cornering	34.854	0.46495	34.38905

Table4. 2: Compressive strain on top of sub-grade & bottom of HMA

Calculating point/strain value(micron)	Compressive strain(ε_{cv}) at top of sub-grade	Compressive strain(ε_{cv}) at bottom of HMA
Free rolling	373.91	337.45
Braking	403.44	341.89
Cornering	383.68	337.34

Table4. 3: pavement responses due to vehicle maneuvering

Responses	Free rolling	braking	turning
Longitudinal tensile strain at the bottom of asphalt layer (micron)	190.69	10%	7.28%
Transverse tensile strain at the bottom of asphalt layer (micron)	345.39	4.37%	0%
Deviator stress at the middle of base(kpa)	29.43	5.71%	16.85%
Compressive strain on top of subgrade (micro)	373.91	7.9%	2.61%

Table4. 6: Failure criteria in each pavement layer

Layer	material	criteria	Location in layer	Model of failure
surface	HMA	Tensile strain	top	Top-bottom Fatigue cracking
			bottom	Bottom-top fatigue cracking
		Shear strain	Shallow depth	Rutting caused by shear flow
		Compressive strain	bottom	Rutting caused by compression
base	Unbound aggregate	Deviator stress	middle	Shear failure from permanent deformation
Sub-grade	Native soil	Compressive strain	top	Secondary rutting

Source (Al-Qadi and Wang, 2009b).

4.1 Failure analysis with Relative Damage model of failure mechanism

Relative damage (damage ratio) is the relative observation of damage caused by one variable with respect to other variables. Relative damage used to evaluate the effect of different conditions with respect to normal condition under the same controlled variables.

In this study, the damage ratio used to evaluate the effect of scuffing forces due to pure turning and pure braking of vehicles relative to uniform motion (free rolling condition). Failure mechanisms under equation (3.11-3.18) were used to analyze the effect by using most input data

from FE analysis result and few from literature; the results were summarized in tables.

$$DR = \frac{N_{free-rolling}}{N_{Braking,Turning}} \quad (4.0)$$

Where: DR = relative damage of pavement.

The following tables summarized the calculated critical pavement response from 3-D FE for (p=0.93Mpa,F=40kN,T=22℃ & v=11.125km/hr.) and flexible relative damage ratio due to various rolling situation for HMA (fatigue cracking, rutting, shoving), base layer deformation and subgrade rutting respectively.

The relative damages were calculated as the ratio of free rolling condition to braking and turning conditions with respect to the normal traffic condition after the same number of tire loading applied on the pavement, using available damage models equations (3.11 to 3.17) & (4.0).

HMA Bottom-up and top-down Fatigue cracking

In table (4.8) & (4.9) it was found that braking causes 1.45 times bottom-up fatigue cracking, 2.04 times top-down fatigue cracking potential compared to free rolling condition. But as expected, during braking time, the pavement top part was subjected to concentrated stress that caused top-down fatigue cracking predominant of top-bottom fatigue cracking which was1.41times bottom-up fatigue cracking.

This result agrees with the study by (Wang and Al-qadi, 2011) that stated that at the braking section of the road, TCD (top-down) fatigue cracking dominant.

In a similar way, turning or cornering causes, 1.32 times bottom-up and1.09 time's top-down fatigue cracking potential compared to free rolling condition. However, bottom-up fatigue cracking was the

Table4.7: Tensile strains & fatigue relative damage of AC bottom-up cracking

Temperature	HMA thickness	Maneuver condition	Critical tensile strain bottom of HMA (micron)	Damage ratio
22℃	150mm	Free rolling	345.39	1
		Braking	360.47	1.18
		turning	345.06	1

Table4.7: Tensile strains & fatigue relative damage of AC top-down cracking

Temperature	HMA thickness	Maneuver condition	Critical tensile strain near surface(25mm) (principal maximum)of HMA (micron)	Damage ratio
22℃	150mm	Free rolling	299.75	1
		Braking	359.2	2.04
		turning	306.43	1.09

HMA rutting and shoving relative damage

In table (4.10) &(4.11) it was found that braking caused insignificant rutting of HMA with respect to free rolling which was 1.02 or 2% times, however, there was 2.85 times shoving(up and down) potential compared to normal condition. These show that pavement capacity at the braking area was largely influenced by shoving or shear flow which agreed with most research's works.

In similar ways, it was found that turning has no extra contribution to HMA rutting compared to normal movement condition; but 1.93 times shoving potential with respect to free rolling situation.

Table4.9: Compressive strain and relative damage for AC rutting (densification)

Temperature	HMA thickness	Maneuver condition	Critical compressive strains bottom of HMA (micro)	Damage ratio
22℃	150mm	Free rolling	337.45	1
		Braking	341.89	1.02
		turning	337.34	1

Table4. 1: shear stress/strain and relative damage for AC shear flow or shoving

Temperature	HMA thickness	Maneuver condition	Critical shear strain (micro) & critical shear stress (kpa) at shallow depth		Damage ratio
			Shea strain	Shear stress	
22℃	150mm	Free rolling	413.03	458.92	1
		Braking	516.26	573.62	2.85
		turning	477.26	530.29	1.93

Base permanent deformation (shear failure)

In table (4.11) it was found that the contribution of shear failure or permanent deformation of the base due to braking and turning was (7.8% & 5.8%) respectively with respect to free rolling condition. As the result shows, the impact of scuffing force on the permanent deformation is not significant relative to the normal traffic movement; this implied that scuffing force due to braking and turning are surface related damage.

Table4. 2: Deviator stress and relative damage for base shear failure

Temperature	HMA thickness	Maneuver condition	Deviator stress &Minor principal stress(kPa)		Damage ratio
			Deviator stress	Minor principal stress	
22℃	150mm	Free rolling	29.43	0.45916	1
		Braking	31.08628	0.47372	1.078
		turning	34.38905	0.46495	1.058

Subgrade rutting (secondary) relative damage

In table 4.12 it was found that braking and turning causes 1.41times and 1.12 times subgrade rutting capacity compared with free rolling conditions under controlled condition for the other variables.

Table4. 3: Compressive strain and relative damage for subgrade rutting

Temperature	HMA thickness	Maneuver condition	Critical sub-grade compressive strain(micron)	Damage ratio
22℃	150mm	Free rolling	373.91	1
		Braking	403.44	1.41
		turning	383.68	1.12

Comparison of Critical results of ANSYS analysis with 3D-Move pavement analysis.

- **Procedures to be used in 3D move.**

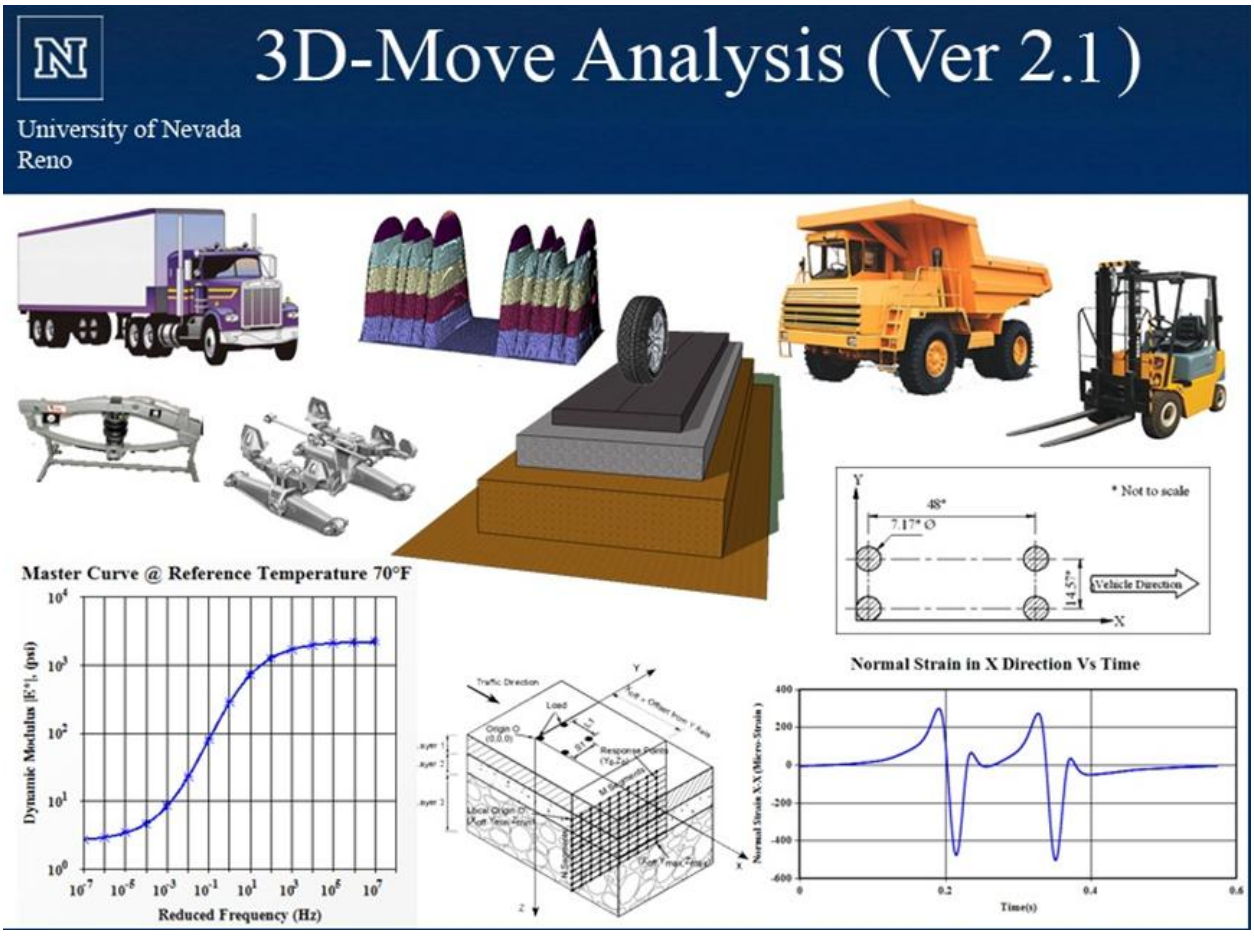

Figure4.1:3D-move profile

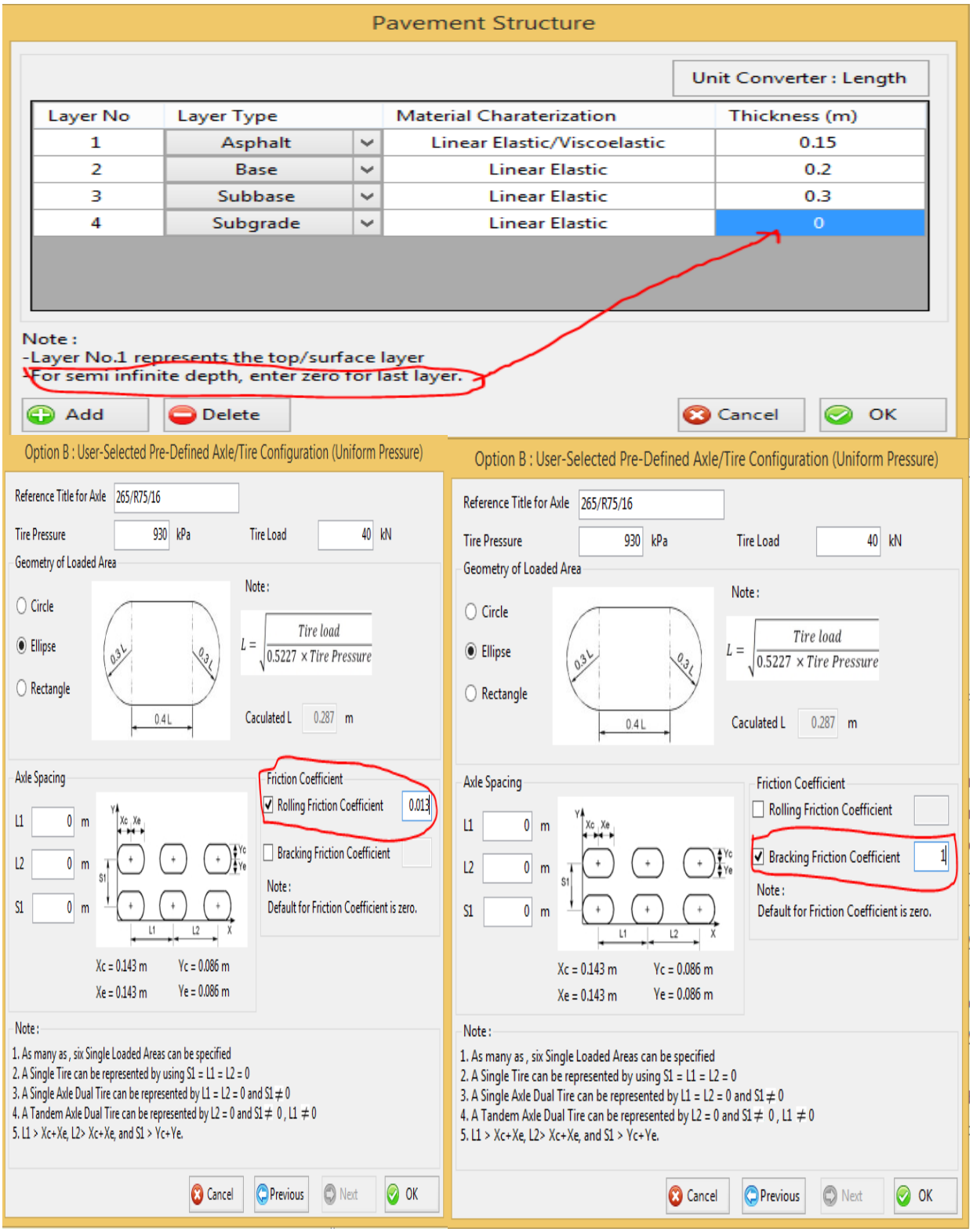

Figure 4.2:3D-Move pavement model

Note: sign convention of 3D- move is inverse of ANSYS response results.

Example 3D-move considers compression as positive and tension as negative; but ANSYS Transient, considers tension as positive & compression as negative.

Sample taken for comparison of pattern and estimated results of longitudinal normal strain and shear strain at top and bottom of asphalt for free rolling condition.

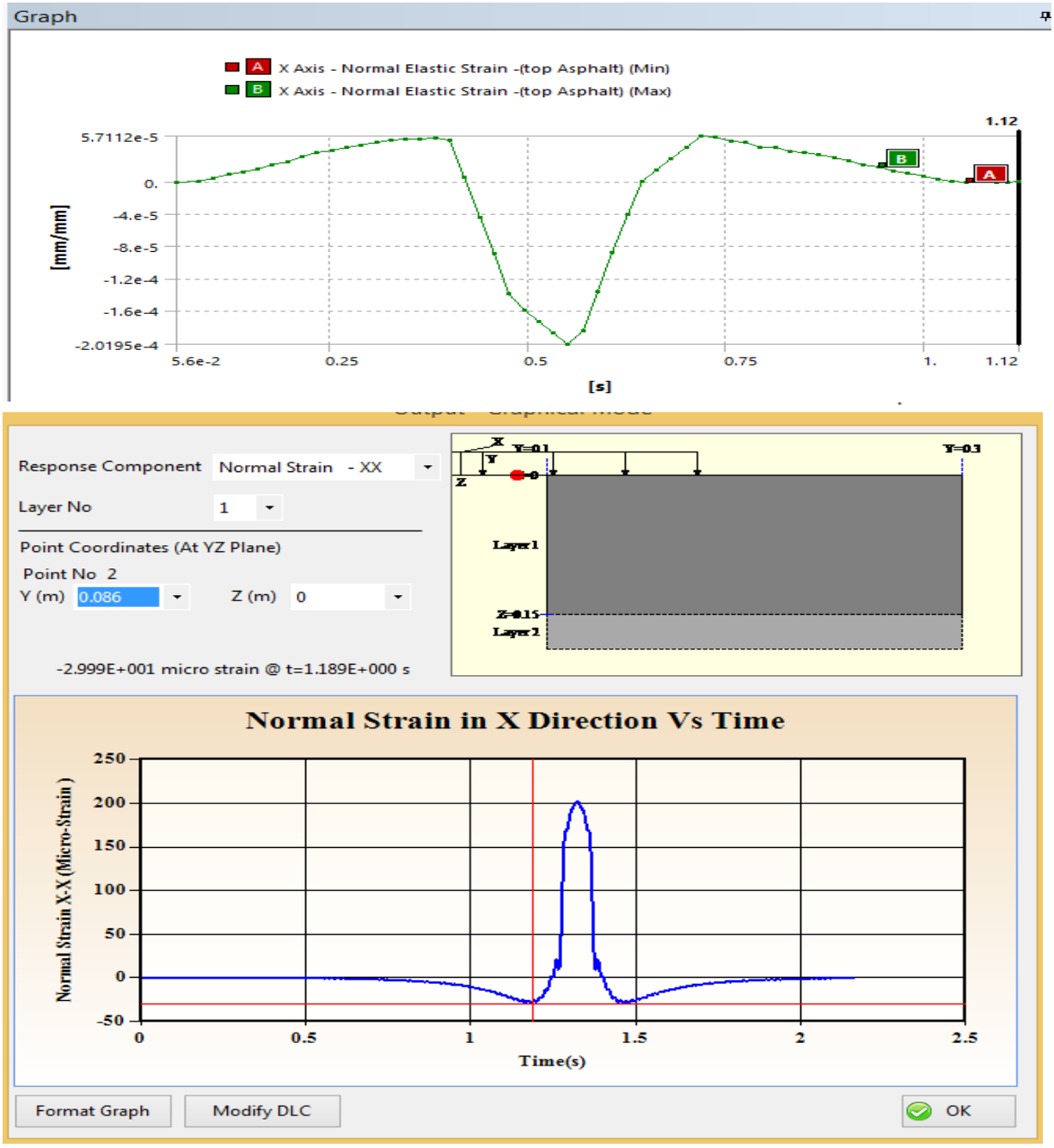

Figure4.3: Normal strain at top of asphalt

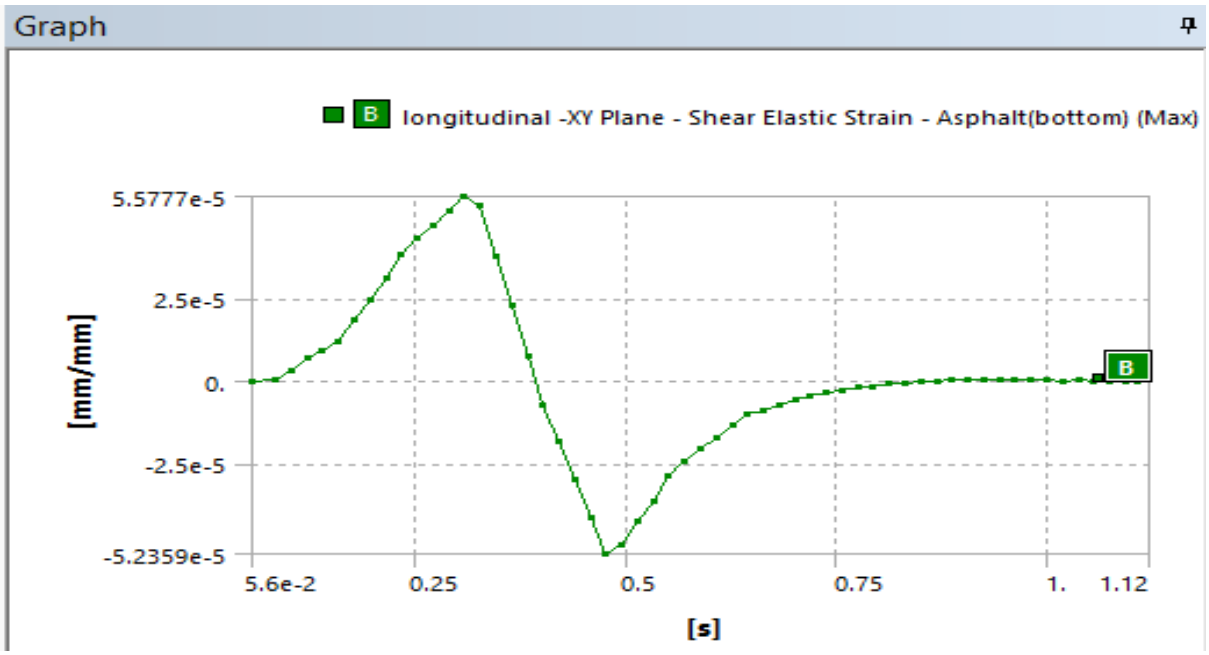

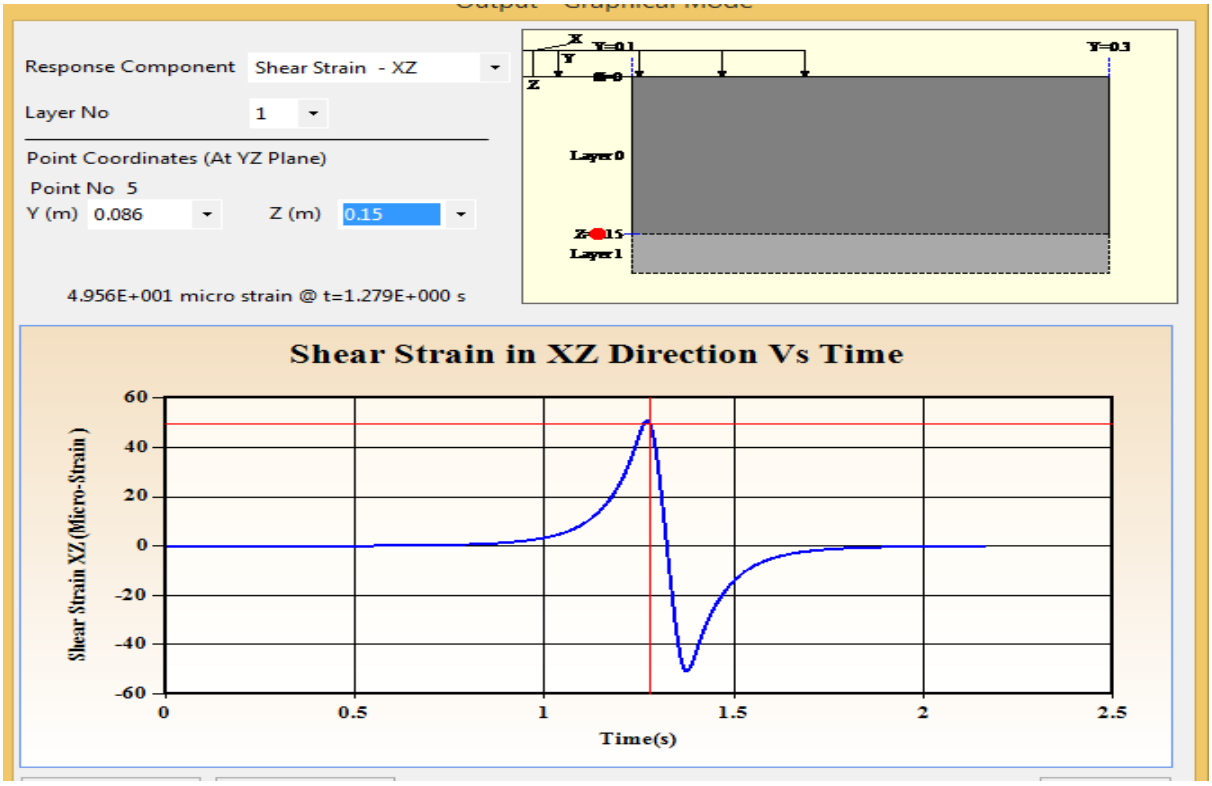

Figure4.4: Shear strain at the bottom asphalt

- Overall Comparisons of Critical Responses.

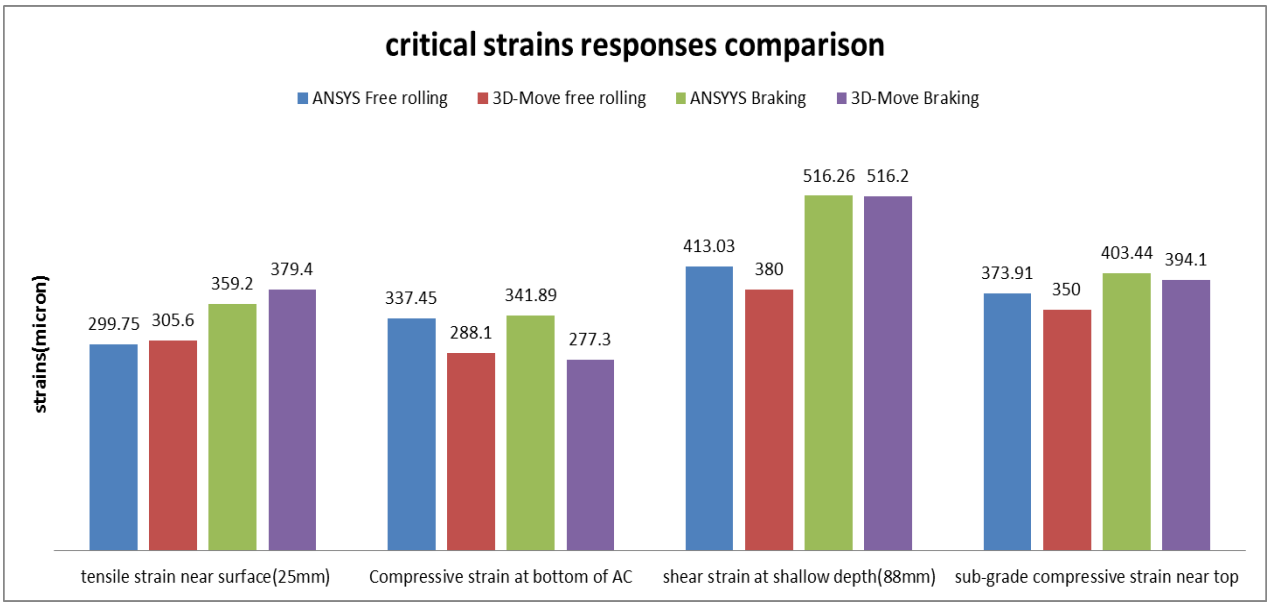

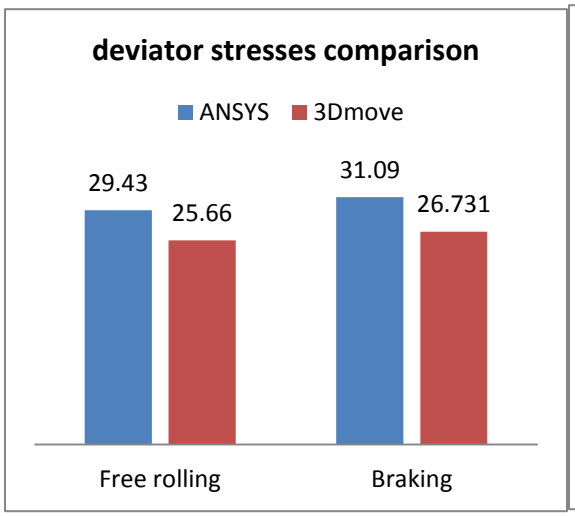

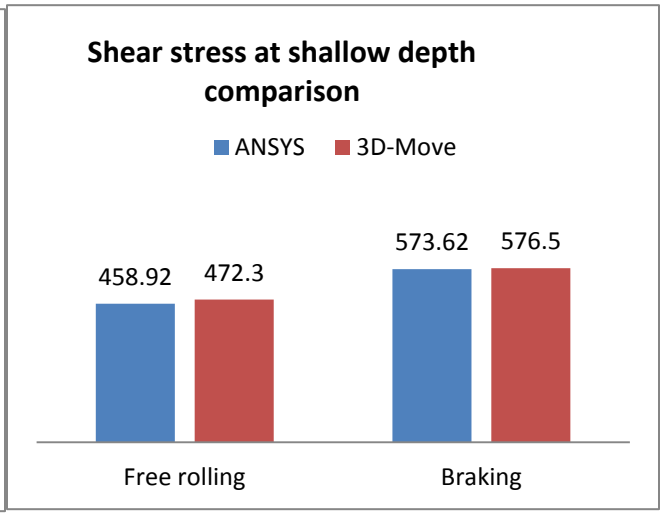

Figure 4.5: Comparison of results for validation

The only different in puts are content of bitumen and air void I asphalt.

The response of pavement calculated by ANSYS was in **surface xy**, on yz- plane.

The responses of 3D-Move were calculated at **pointes** on yz-plane.

Combined relative damage

The combined damage ratio was used to consider the overall effects of distress mechanisms caused by braking and turning relative to free rolling of vehicles. The failure type allows the lower number of load repetition is expected to cause pavement failure. But the combined damage ratio was taken individual effect and calculated as logarithmic distribution factors that balance the effect of each failure mechanism with respect to overall damage (Al-Qadi and Wang, 2009b).

The combined damage ratio is more appropriate and used for this analysis as expressed in equation 4.1

$$CRD = a_1(DR)_{fatige} + a_2(DR)_{HMA-densification} + a_3(DR)_{HMA-shove} + a_4(DR)_{base} + a_5(DR)_{rutting-subgrad} \quad (4.1)$$

$$a_i = \frac{1}{\frac{log(Ni)}{\sum_{j=1}^{n}\frac{1}{\log(Ni)}}} \quad (4.2)$$

Where: $(DR)_{fatige}$ = damage ratio of fatigue cracking

$(DR)_{HMA-densification}$ =damage ratio of HMA due to densification

$(DR)_{HMA-shear}$=damage ratio of HMA rutting (shove) due to shear flow

$(DR)_{base}$=damage ratio of base for base shear flow

$(DR)_{rutting-subgrade}$=damage ratio of subgrade due to compression.

$a_1, a_2, a_3, a_4 \& a_5$ are damage distribution factors for different failure mechanisms.

$N_i \& N_j$ are allowable number of load application for different failure mechanisms.

For this study, the value of distribution factors taken from (Al-Qadi and Wang, 2009b) and the effect of temperature difference(22℃ &25℃)is negligible and base thickness200mm& 203mm is almost equal.

Table 4.13: damage component and distribution factors

Temperature (°C)	Base thickness (mm)	Fatigue Cracking	HMA Rutting (Densificaiton)	HMA Rutting (shear)	Base Deformation	Subgrade Rutting
		a_1	a_2	a_3	a_4	a_5
25	203	0.16	0.14	0.26	0.18	0.26
	305	0.16	0.15	0.25	0.20	0.24

The total combined relative damage (CRD) due to braking was calculated as follow:

$$CRD = 0.16(2.04)_{fatige} + 0.14(1.02)_{HMArut} + 0.26(2.85)_{HMA-shove} + 0.18(1.078)_{base} + 0.26(1.41)_{rut-subgrad} = 1.77$$

$$CRD = 0.16(1.32)_{fatige} + 0.14(1)_{HMArut} + 0.26(1.93)_{HMA-shove} + 0.18(1.058)_{base} + 0.26(1.12)_{rut-subgrad} = 1.33$$

Table4.13: Distributed relative damage and ranks

Braking	CDR	Values	%	Ranks
	fatigue	0.33	18.64	3
	HMA rutting	0.14	7.91	5
	HMA shove	0.74	41.81	1
	Base deform	0.19	10.73	4
	Sub-grade rutting	0.37	20.9	2
total		1.77	100	
Turning /cornering	fatigue	0.21	15.79	3
	HMA rutting	0.14	10.53	5
	HMA shove	0.5	37.59	1
	Base deform	0.19	14.29	4
	Sub-grade rutting	0.29	21.8	2
	total	1.33	100	

Summary: deterioration of the flexible pavement subjected to braking was 1.77 times overall potential compared to of the other section of the road that subjected to free movement of vehicles.as can be seen from table 4.15,from all components of damage, HMA shoving and TDC have more than 60% contributed braking damage. This implies that top surface of pavement is vulnerable to damage because of surface induced scuffing force due to braking.

In similar fashion, the deterioration acceleration rate of curved or turning road section was 1.33 due to turning maneuver of vehicles as compared to free rolling condition. Like braking, damage because of shoving (shear flow) took the first rank and TDC fatigue cracking was also significant. Braking and turning noticeable, impacts on sub-grade rutting of flexible pavement.
Generally the service life of pavement at turning and braking section, shorten by induced scuffing force due to braking and turning of vehicles.

4.2 The effects of scuffing force on life time (service life) of pavement

Damage ratio is used to describe the effect on pavement rehabilitation time (remaining design period). For new pavement opened for service, which constructed with N design life and $ESAL_O$ equivalent standard axle load at the time of design under normal condition, that determined from traffic analysis. However, some of the pavement special sections expected to be exposed to turning or braking of vehicles enhanced load factor equivalence; this in turn increase the equivalent standard axle loads(ESALs) at this section of pavement ,that was not expected at design time. The following steps used to determine the remaining service life of flexible pavement.

A. Determine number of cumulative equivalent standard axle loads ($ESAL_o$ **)** from traffic analysis of vertical load(free rolling) that will be applied on the road in the design period.
B. Determine the number of equivalent standard axle loads (ESALs)' at braking or turning of pavement section by using damage ratio (DR) as convention factor from free rolling condition.

C. Calculate the combined number of equivalent standard axle load(ESALs) if the pavement might subject to free rolling as well as braking or free rolling as well as turning condition of vehicles movement.

If **n,** is percent of ESALo subjected to turn or brake and (1-n) percent freely move, combined ESAL can be determined as: Combined equivalent standard axle load (ESALs) =ESALo(1-n)+ESALo*n*DR

Where DR is total damage ratio of braking or total damage ratio of turning obtained from this study.

D. Rehabilitation equivalent life is the ratio of design period times original number of ESALs to combined equivalent number of ESALs(Al-Qadi and Wang, 2009b).

$$The\ remaining\ service\ life(t) = \frac{design\ life(N) * original\ number\ of\ ESALo}{combined\ number\ of\ ESALs} \qquad (4.3)$$

$$t = N * \frac{ESALo}{ESALo[1 + n(DR - 1)]}$$

$$t = \frac{N}{1 + n(DR - 1)} \quad ,n, is\ percent\ of\ turning\ or\ braking\ equivalent\ number\ of\ load$$

$$t = \frac{N}{1 + 0.77n}\ for\ braking(DR = 1.77) \quad t = \frac{N}{1 + 0.33n}\ for\ turning(DR = 1.33) \quad (4.4)$$

Using equation (4.4), the rehabilitation period of pavement is calculated for design period of 20 years and tabulated below.

Table 4.14: Effects of brakes and turns on design life

n%	N	t for braking condition	t for turning condition
0	20years	20 years	20years
35	20years	16 years	18years
55	20years	14years	17years
70	20years	13years	16years

As can be seen in table4.14 the service life of the pavement shortens at braking and turning tires of vehicles. The rehabilitation period (t) of the pavement much less than the design period (N) based on the percentage of decelerate (stops) & turning (cornering) numbers of vehicles. The result obtained from this study based on damage analysis showed that, braking condition shorten the service life of the pavement when compared to turning condition. This indicates that scuffing force significantly affect the service life of flexible pavement.

4.3 Pavement Interface Condition

A number of mechanistic pavement design approaches assume the interface layers in the flexible pavement were fully bonded. The bonded contact models assume that the condition of continuity were satisfied at the interface and vertical displacement, vertical stress, and shear stress were the same on each side of the interface.

The condition in the interface layer needs to be taken into account in pavement response analysis. Because if inadequate bonding at the pavement layers interface, the strains thought the pavement might be increased significantly and negative impact on the performance of the pavement.

Simple friction model

The strength of bond in the interface is an essential factor in determining a suitable friction model. Friction model (Coulomb model) assumes that the resistance to movement is proportional to normal pressure at interface. The interface might be resisting the movement up to some certain level & then surface at interface start to **slide relative** to each other. The coefficient of friction representing the slope of the relationship between vertical pressure and shear stress as expressed in the following equation that represents the resistance to interface movement.

$$\mu = \frac{\tau_{max}}{\sigma} \qquad (4.3)$$

μ: Coefficient of friction

τ_{max}: Maximum shear stress

σ: Normal pressure

For this study, maximum shear stress and contact pressure calculated in FE model & the values would be substituted in equation 4.3 to evaluate interface condition with (μ) between HMA and base layer only due to scuffing forces. Besides, the relative sliding is also determined from FE model as a sample of calculation for the interface of asphalt and base can be seen in the figure below for turning conditions of maneuvering. The table 14: summarize the results of FE analysis at interface of asphalt and base course for all rolling condition and give comparative analysis.

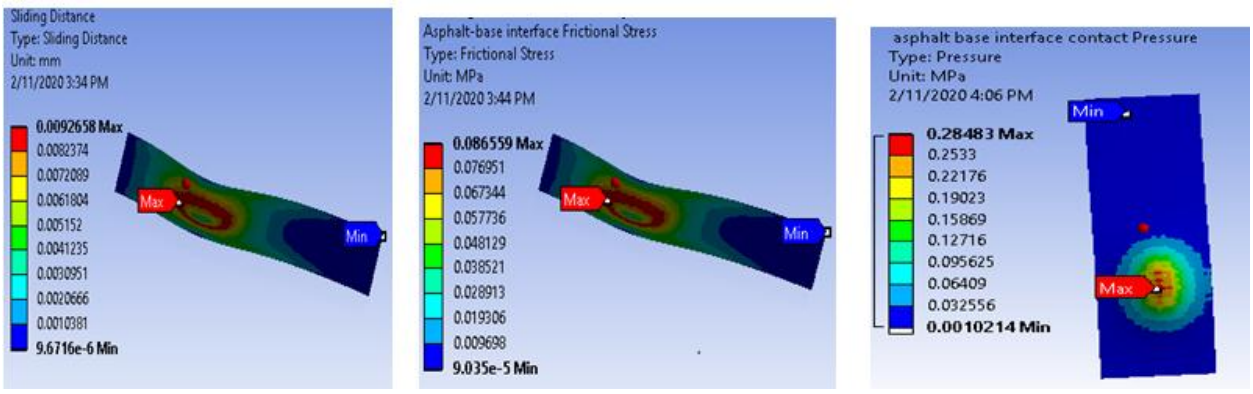

Figure 4.6: Sliding, shear stress and contact pressure at asphalt- base interface

Table4. 15: Summarize Asphalt-base course interface responses and stress ratio

Maneuver conditions	Frictional stress(τ_{max})		Normal contact pressure(kPa)		Sliding distance		Friction coefficient(μ)	
	Value (kpa)	%	Value(kpa)	%	Value($*10^{-3}$mm)	%	Value(-)	
Free rolling	76.7	-	285.4	-	8.210	-	0.27	-
Braking	91.6	19.43	289.8	1.54	9.806	19.44	0.32	18.52%
turning	86.6	12.91	284.8	-.21	9.266	12.86	0.3	11.11%

Summary: as shown in the table above, the pavement interface was affected by scuffing load and frictional stresses were increased by 19.43% and 12.91% for braking and turning respectively. But the increment of normal stress was insignificant. These show that the imbalance of disturbing force (shear) and resisting force (normal) increases the relative sliding of interface and loss bond between the surface leads to failure. The interface is very sensitive to horizontal load that causes defects at the interface which propagate to other portions of pavement that accelerate the premature failure of flexible pavement.

4.4 Effect of asphalt thickness

For Hot- Mix- Asphalt (HMA) layer of 240mm to 150mm in thickness, the maximum shear stress does not show much difference, as illustrated in figure (4.3). This shows that thinner asphalt layer doesn't lead to significantly affected by greater shear stress compared to a thicker one. It was observed that increment of asphalt thickness from 15cm to 24cm, reduced 0.155 Mpa of shear stress. In other words, 9cm of asphalt thickness, which was more than half of (15cmm), added but the reduced shear stress was 0.155 MPa.

For pavement sections that are subjected to scuffing forces, asphalt concrete thickness barely reduces the deterioration of the pavement. i.e., the thinner layer doesn't lead to be a greater risk of shoving and top-down fatigue cracking compared to a thicker one. So increasing thickness is not economical relative to its effectiveness. But increasing material quality may be the best solution.

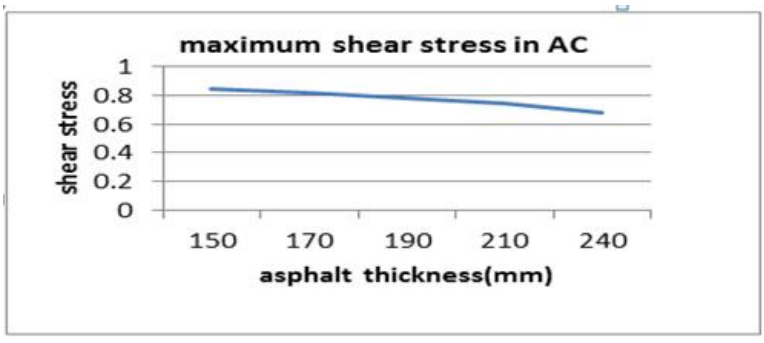

D
P7 - Maximum Shear Stress - Asphalt - End Time Maximum Maximum Value Over Time
MPa
0.83774
0.81309
0.778
0.74
0.68226

Figure 4.7: Maximum shear stress vs asphalt thickness

As shown in figure 4.4, the shear strain at transverse direction decrease as asphalt thickness increase, while shear strain along traffic is not equally affected by asphalt thickness. This shows that the effectiveness of asphalt thickness was less in the direction of traffic movement (longitudinal) to resist asphalt failure of shoving and top-down fatigue cracking relative to the transverse direction.

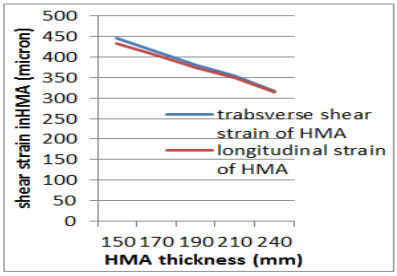

Table of Design Points

	B	C
1	P5 - h	P6 - YZ Plane - Shear Elastic Strain - Asphalt - End Time Maximum Maximum Value Over Time
2	mm	mm mm^-1
3	150	0.00044589
4	170	0.00041253
5	190	0.00038086
6	210	0.00035295
7	240	0.00031707
*		

Table of Design Points

		B	C
1		P5 - h	P7 - XY Plane - Shear Elastic Strain - Asphalt - End Time Maximum Maximum Value Over Time
2		mm	mm mm^-1
3		150	0.0043329
4		170	0.0040449
5		190	0.00037455
6		210	0.00034877
7		240	0.00031498
*			

Figure 4.8: shear strain in AC versus Asphalt thickness

4.5 Effect of elastic modulus on asphalt shear strains

shear strains from moving loads are primarily responsible for rutting and shoving/corrugation in asphalt layer(Wang and Al-qadi, 2011)& (Al-Qadi and Wang, 2019).

Reduction of shear strain is one of the ways to reduce the rate of premature pavement deterioration for flexible pavement because of tangential stresses. To reduce it, increase either material quality (modulus) or depth of the top layers. But enhancing elastic modulus of asphalt reduces the effects more when compared to thickness increment.

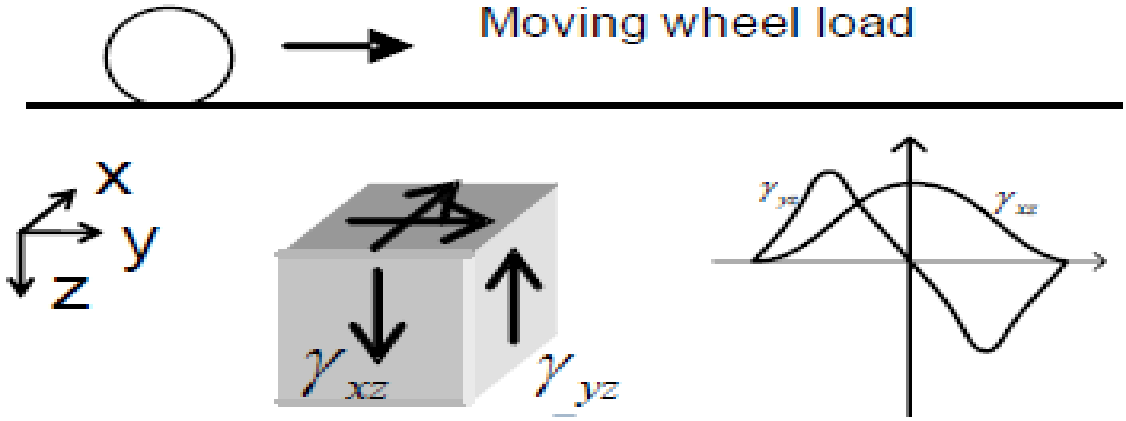

Figure 4.9: shear strains under moving load

The elastic modulus and thickness optimization of asphalt layer for shear strains shown in table below indicate that increasing either thickness of asphalt or asphalt elastic modulus, reduces the shear strain of top layer.

B	C	B	C
P8 - Young's Modulus	P6 - YZ Plane - Shear Elastic Strain - Asphalt - End Time Maximum Maximum Value Over Time	P5 - h	P6 - YZ Plane - Shear Elastic Strain - Asphalt - End Time Maximum Maximum Value Over Time
MPa	mm mm^-1	mm	mm mm^-1
3000	0.00044589	150	0.00044589
3500	0.00039052	170	0.00041253
4000	0.00034778	190	0.00038086
4500	0.00031372	210	0.00035295
5000	0.0002859	240	0.00031707

Figure 4.10: Optimized shear strain for asphalt elastic modulus and asphalt thickness

The shear strains for different asphalt elastic modulus are lower when compared to different asphalt thicknesses. As can be seen in table 4.16, increasing the modulus of asphalt causes less shear strains than does increase the thickness of asphalt for carrying the same load.

Table4.16: Shear strains at different asphalt thickness and different asphalt elastic modulus

h(mm)	Shear strains (micron)	E(Mpa)	Shear strains (micron)
150	445.89	3000	445.89
170	412.53	3500	390.52
190	380.86	4000	347.78
210	352.95	4500	313.72
240	317.07	5000	285.9

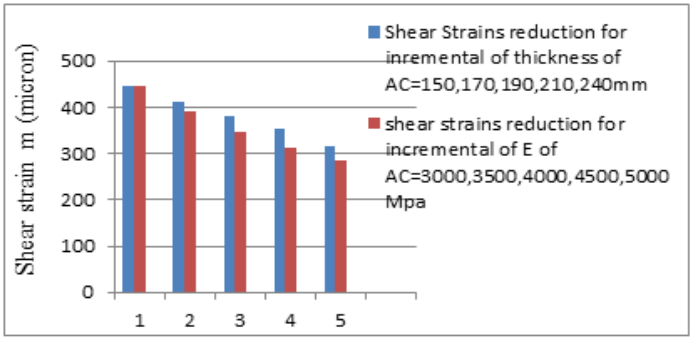

Figure 4.11: shows that the rate of reduction of shear strains increase as asphalt thickness and elastic modulus increases. However, the reduction rate of shear strains due to increasing elastic modulus is greater than that of increasing the thickness. This suggest that, increasing material quality; lesson the effect of scuffing force/tangential load on pavement distresses such as top-down cracking, slippage cracking, shoving & others distress types.

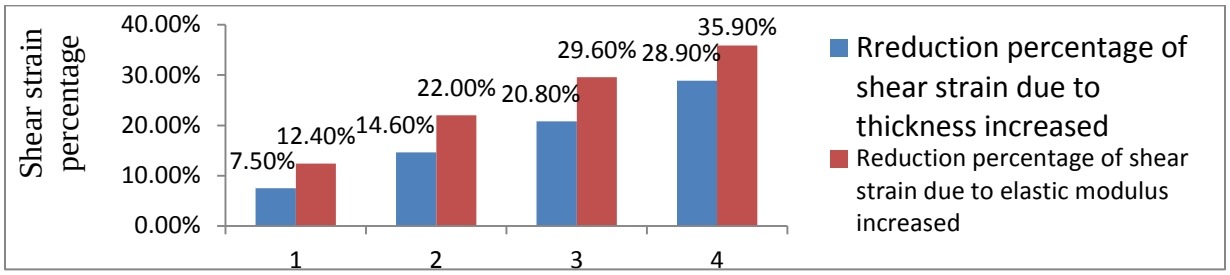

Figure 4.11: Reduction percentage of shear strains

Generally, enhancing material quality of top layer for road section where vehicles stop and turn is one of the recommended techniques to mitigate the premature failure of pavement. At tire braking and turning, surface related damage due to concentration of shear stresses at upper layer of flexible pavement could be reduced by enhancing elastic modulus of asphalt layer.

Chapter -5

5 Conclusion and recommendation

The purpose of this study was to evaluate the impact of scuffing induced at the time of braking and turning of vehicles using finite element modeling (FEM).

Three conditions are mainly investigated in this study, include relative damage, interface condition, and asphalt thickness optimization.

The maximum tangential (scuffing) forces of tire-assembly 265/75R/16 were computed using the latest Mechanical simulation software CarSim2017.1 version. The result showed that the maximum longitudinal force found at a slip ratio of (10-20) % and similarly, the maximum of transverse force found at slip angle of tire (9-14) degree. These occurred during partial braking, vehicle turning (left or right), lane change or movement on a circular path. It was observed that the factors that mainly affect the scuffing forces were tire-pavement interface coefficient of friction, slip angle (radius of turn) and slip ratio.

A 3-D FE model was developed with ANSYS to predict the pavement responses caused by the various rolling conditions. The model incorporates combined trapezoidal moving loads and transient dynamic analysis. The pavement responses and relative damage of rolling conditions were analyzed with the developed 3-D FE model and available pavement damage models. The five failure mechanisms (fatigue cracking, AC rutting (densification), AC shoving, base shear failure, and sub-grade rutting) were taken into account in relative damage analysis in order to show the impacts of scuffing forces on the capacity of flexible pavement as a whole.

The result indicated that: braking caused 2.04 times more TDC fatigue damage, 2% more AC rutting (densification), 2.85 times AC shoving (shear flow), 7.8% more base shear failure and 1.41 times more sub-grade rutting compared to free rolling condition. The contribution of braking to HMA rutting (densification) and permanent deformation of the base (base shear failure) were insignificant. Shoving/corrugation, top-down (TDC) fatigue cracking, and sub-grade rutting were the dominant distresses at the braking of a vehicle that induced by high longitudinal scuffing forces.

Similarly turning caused 9% more fatigue damage, 1.93 more AC shoving, 5.8%times more base shear failure and 1.12 times more sub-grade rutting compared to free rolling condition. But as result shows, turning condition has no contribution in AC rutting due to densification compared to free rolling condition. The pavement section under turning/cornering would be subjected mainly to shoving (up-down) and secondary rutting (sub-grade).

The results of critical responses of pavement and relative damage analysis showed that induced scuffing forces(braking & turning) caused greater surface-related damages top-down fatigue cracking and shoving/corrugation potential than did the free rolling.

Interfaces layer conditions were one of the main factors influencing pavement performance by affecting the distribution of stress-strain in the lower layer of the pavement.

To estimate the effect of scuffing forces on the layer interface condition, simple friction model(slip between layer) was used.it was found that, as tangential load increased the relative sliding of each layer of asphalt and base course were increased by 12.86% to 19.44% due to cornering and baking respectively on bonded contact relative to free rolling. The incremental value of disturbing pressure (interface shear stress) was rapidly increased by 19.43% while resisting pressure (normal contact stress) increment was very low 1.5% for braking maneuver relative to free rolling. Similarly, for turning conditions, shear (horizontal) stresses at interface of asphalt and base course that contribute to slides of the layers of pavement over each other increased by (12.91%) relative to free rolling as shown in table 14. But the incremental of normal contact load(resistive pressure) that contribute to resist the sliding of each layer , over each other is less when compared with interface shear stress but (0.21%) more relative to free rolling. General, the scuffing force could lead to increase interface shear stress, and this, in turn, increase the risk of pavement deterioration and failure.

From thickness optimization with FE, it was found that the asphalt layer has less influence on shear stress. The impact of shear stress on thin and thick asphalt layer was not much greater, and this implied that thinner asphalt layer, lead to be hardly greater risk for top-down cracking, rutting (shear flow) and other surface-related damages compared to a thicker one. Therefore, increasing the thickness of the asphalt layer for tackling the deterioration (distress) of the pavement, where braking and turning/cornering is dominant is not the best solution. For less effect reduction, it requires a high cost. The option like increasing material quality is recommended.

Generally, the investigation showed that the effects of scuffing forces due to vehicle braking and turning have a clear impact on flexible pavement capacity. So these impacts should be considered for pavement design (rehabilitation) at specific sections of the roads such as signal intersection and its legs, roundabout and its legs, vehicle station, speed barker, plaza station, curved road and other areas where full or partial braking and turning would have taken place under normal condition. This suggests that, the pavement material should be modified to attain tough enough for resisting the distortion force. Asphalt mixtures with higher elastic moduli have greater resistance of shear stress-strain effect as shown in fig 4.10-11.

5.1 Recommendation

As a result of this study, the following points are recommended:

1 The appropriate tire-pavement interaction is important to evaluate pavement deterioration (damage) caused by various tires rolling conditions.
2 The significant effect of scuffing force can’t be ignored during pavement rehabilitation and design.
3 At pavement sections that subjected to scuffing forces, increasing material quality is the best option to reduce the effect rather than increasing the asphalt thickness.

6 References:

AACRA (2004) ‘Guideline AACRA technical specification’, in *AACRA manula*.

Abdallah, I. and Nazarian, S. (2011) *Strategies to Improve and Preserve Flexible Pavement at Intersections Research Report 0-5566-1 Conducted for Texas Depar tment of Tr ansportation*. Texas at El Paso.

Adlinge, S. S. and Gupta, P. a K. (2009) ‘Pavement Deterioration and its Causes’, *Mechanical & Civil Engineering*, pp. 9–15. Available at: www.iosrjournals.org.

Al-Qadi, I. L. and Wang, H. (2009a) *E VALUATION OF P AVEMENT D AMAGE D UE TO Prepared By*.

Al-Qadi, I. L. and Wang, H. (2009b) *Pavement Damage Due to Different Tire and Loading Configurations on Secondary Roads*. Illinois.

Al-Qadi, I. L. and Wang, H. (2019) *E VALUATION OF P AVEMENT D AMAGE D UE TO Prepared By*.

Alkaissi, Z. A., Al-badran, Y. M. and Wasif, N. (2019) ‘Theoretical Analysis on the Effect of Surface Horizontal Traction on Top-Down Cracking of Flexible Pavement’, 26, pp. 170–174.

Asnake, A. (2015) *Assessment Of Road Pavement Failure Along Addis Ababa-Modjo Trunk Road Assessment Of Road Pavement Failure Along Addis Ababa-Modjo Trunk Road*.

ASPHALT INSTITUTE and No.2(Ms-2), M. series (1970) *THE THIKNESS DESIGN OF ASPHALT STRUCTURES FOR HIGHWAY*. USA.

Beskou, N. D., Tsinopoulos, S. V. and Theodorakopoulos, D. D. (2016) ‘Dynamic elastic analysis of 3-D flexible pavements under moving vehicles: A unified FEM treatment’, *Soil Dynamics and Earthquake Engineering*, 82, pp. 63–72. doi: 10.1016/j.soildyn.2015.11.013.

Blau, P. J., Qu, J. and Truhan, J. J. (2005) *A Multi-Stage Model for Scuffing of Reciprocating Components with Special Consideration of Fuel Injector Plungers*. Available at: http://www.ntis.gov/support/ordernowabout.htm.

Burmister, D. M. (1945) ‘The general theory of stresses and displacements in layered systems. I’, *Journal of Applied Physics*. doi: 10.1063/1.1707558.

Chae, S. (2006) *NONLINEAR FINITE ELEMENT MODELING AND ANALYSIS OF A TRUCK TIRE*. The Pennsylvania State University.

Doumiati, M. *et al.* (2009) ‘Lateral load transfer and normal forces estimation for vehicle safety:

Experimental test', *Vehicle System Dynamics*, 47(12), pp. 1511–1533. doi: 10.1080/00423110802673091.
ERA (2013) 'ETHIOPIAN ROADS AUTHORITY STANDARD TECHNICAL SPECIFICATIONS AND METHOD OF MEASUREMENT FOR ROADWORKS', in *ERA Manual*. Addis Ababa.
Erlingsson, S. and Ahmed, A. W. (2013) 'Road Materials and Pavement Design Fast layered elastic response program for the analysis of flexible pavement structures', (March 2013), pp. 37–41.
Gillespie, T. D. (1992) *Fundamentals of Vehicle Dynamics*. Society of Automotive Engineers, Inc. 400 Commonwealth Drive Warrendalc, PA 15096-000.
Gohring, E., Von Glasner, E. C. and Pflug, H. C. (1991) 'Contribution to the force transmission behavior of commercial vehicle tires', *SAE Technical Papers*. doi: 10.4271/912692.
Guo, M. and Zhou, X. (2019) 'Tire-Pavement Contact Stress Characteristics and Critical Slip Ratio at Multiple Working Conditions', *Advances in Materials Science and Engineering*, 2019(Article ID 5178516), p. 11. Available at: https://doi.org/10.1155/2019/5178516.
Gupta, A. and Kumar, A. (2015) 'Comparative Structural Analysis of Flexible Pavements Using Finite Element Method', *International Journal on Pavement Engineering & Asphalt Technology*, 15(1), pp. 11–19. doi: 10.2478/ijpeat-2013-0005.
Hirz, M. (2015) 'Automotive Engineering Focus : Basics of longitudinal vehicle dynamics', in. G r a z U n i v e r s i t y o f T e c h n o l o g y: FTG Institute of Automotive Engineering, p. 26. Available at: https://www.researchgate.net/publication/280303367%0ABasics.
Holanda, S. De *et al.* (2015) 'DYNAMIC ANALYSIS OF ASPHALTIC PAVEMENTS Francisco Evangelista Junior', in *Transportation*.
Hu, X. *et al.* (2017) 'Effects of tire inclination (turning traffic) and dynamic loading on the pavement stress–strain responses using 3-D finite element modeling', *International Journal of Pavement Research and Technology*. Chinese Society of Pavement Engineering, 10(4), pp. 304–314. doi: 10.1016/j.ijprt.2017.04.005.
Huang, Y. . (2004) *Pavement Analysis and Design, Ullidtz.* 2nd edn. USA: Pearson Education
Ji, X. *et al.* (2019) 'Feedback Game-based Shared Control Scheme Design for Emergency Collision Avoidance : A Fuzzy-LQR Approach Ac ce pt ed nu sc t N ot Co py ed ite d Ac ce pt t N ot Co py ed d', *Journal of Dynamic Systems, Measurement and Control*, (c). doi:

10.1115/1.4042880.
Jin, W. *et al.* (2015) 'Mechanical Effect Study of the Vehicle Braking on the Asphalt Pavement', *Applied Mechanics and Materials*, 744–746, pp. 1266–1272. doi: 10.4028/www.scientific.net/AMM.744-746.1266.
Khavassefat, P. (2014) *Pavement Response to Moving Loads*. Stockholm,sweden. Available at: http://urn.kb.se/resolve?urn=urn:nbn:se:kth:diva-145321.
Khavassefat, P., Jelagin, D. and Birgisson, B. (2015) 'Dynamic response of flexible pavements at vehicle–road interaction', *Road Materials and Pavement Design*, 16(2), pp. 256–276. doi: 10.1080/14680629.2014.990402.
Leonardi, G., Palamara, R. and Sarah, C. L. (2017) 'Numerical Analysis of Flexible Pavement Reinforced with Geogrids', *road infrastructure View project Road*. doi: 10.1061/9780784480939.036.
Madenci, E. & and Guven, I. (2006) 'THE FINITE ELEMENT METHOD AND APPLICATIONS IN ENGINEERING USING ANSYS®', p. 696.
Mannering, F. L. and Washburn, S. S. (2012) *Principles of Highway Engineering and Traffic Analysis*. 5th edn. Von Hoffman: John Wiley & Sons, Inc.
Melaku, S.1, H. Q. (2016) 'Finite Element Analysis of Pavement Design Using ANSYS Finite Element Code', in, pp. 64–69.
Monismith, C. L. and Popescu, L. (2007) 'Permanent Deformation Prediction in Asphalt Mixes and Pavements'.
NCHRP (2004) *Guide for Mechanistic-Empirical Design*. ARA, Inc., ERES Division 505 West University Avenue Champaign, Illinois 61820.
Nega, A. & and Nikraz, H. (2017) 'Evaluation of Tire-Pavement Contact Stress Distribution of Pavement Response and Some Effects on the Flexible Pavements', *Airfield and Highway Pavements*, pp. 174–185.
Pauwelussen, J. P., Dalhuijsen, W. and Merts, M. (2007) *Tyre Dynamics, Tyre as a Vehicle Component Part 1.: Tyre Handling Performance, Virtual Education in Rubber Technology (VERT), FI-04-B-F-PP-160531*.
PRADHAN, K. K. A. and CHAKRAVERTY, S. (2019) 'CHAPTER 4:Finite Element Method', in *COMPUTATIONAL STRUCTURAL MECHANICS Static and Dynamic Behaviors*, pp. 26–28. doi: 10.1016/B978-0-12-815492-2.00002-2.

Pradko, F. (2016) *Vehicle dynamics*. 7th edn, *SAE Technical Papers*. 7th edn. Edited by G. Bengt Jacobson. doi: 10.4271/620572.

R.M. Mulungye, P.M.O Owende and Mellon, K. (2005) 'Analysis of Response of Flexible Pavements Using Finite Element Method', *The ITB Journal*, 6(2), pp. 40–52. doi: 10.21427/D71T8T.

Rajamani, R. (2006) *Vehicle Dynamics and Control*. Minnesota: Springer. Available at: http://www.menet.umn.edu/-raiamani/vdc.h.

Rather, irshad ahmad and Lateef, E. mohamma. (2016) 'Road Pavement Failure of Flexible Pavement from Sanat-nagar to Pantha-Chowk', *International Journal of Advanced Research in Education & Technology (IJARET)*, 3(3), pp. 437–452. doi: 10.1016/S1059-0560(98)90031-4.

RAZA, S. (2017) *EFFECT OF HORIZONTAL SHEAR LOAD ON PAVEMENT PERFORMANCE OF ISLAMABAD – LAHORE MOTORWAY*. National University of Science and Technology Islamabad.

Reif, K. (2014) *Brakes, Brake Control and Driver Assistance Systems, Bosch Professional Automotive Information*. Edited by P. D.-I. K. R. D. H. Baden-Württemberg. Friedrichshafen, Germany: Springer Fachmedien Wiesbaden 2014. doi: 10.1007/978-3-658-03978-3.

Sarkar, A. (2015) 'Numerical comparison of flexible pavement dynamic response under different axles', *International Journal of Pavement Engineering*, 17(5), pp. 377–387. doi: 10.1080/10298436.2014.993195.

Selig, M. *et al.* (2014) 'Rubber Friction and Tire Dynamics : A Comparison of Theory with Experimental Data', *Tire Science and Technology*, TSTCA, Vol, pp. 216–262.

Seoyoung CHO, C. Tóthz. S. (2018) 'Finite Element Method analysis for mechanistic design in flexible pavement , Review : From how to build a material in FE analysis to complexity in reality', *Silicate Based and Composite Materials*, 70(6).

Shakiba, M. *et al.* (2016) 'Introducing realistic tire – pavement contact stresses into Pavement Analysis using Nonlinear Damage Approach (PANDA)', *International Journal of Pavement Engineering ISSN:*, 8436(February). doi: 10.1080/10298436.2016.1141412.

Taramoeroa, N. & and Pont, J. de (2008) *Characterising Pavement Surface Damage Caused by Tyre Scuffing Forces, Land Transport New Zealand Research Report 374*. Manakau City 1702 Auckland, New Zealand.

TEMESGEN, G. (2016) *Asphalt Road Pavement Rehabilitation and Maintenance*.

THEYSE, H. L., BEER, M. DE and RUST, A. F. C. (1996) 'Overview of South African Mechanistic', *TRANSPORTATION RESEARCH RECORD 1539*, pp. 6–17.

Thompson, M. R. and Elliott, R. P. (1985) 'ILLI-PAVE-Based Response Algorithms for Design of Conventional Flexible Pavements', *Transportation Research Record 1043*, (TRB), pp. 50–57.

Wang, Hao (2010) *Effect of Friciton on Rolling Tire – Pavement Interaction By*.

Wang, Habin (2010) *Fatigue Cracking and Rutting Development in Secondary Road Pavements due to Wide-base Tire Loading*, *@inproceeding(Wang2010Fatigue CA)*.

Wang, H. *et al.* (2014) 'Effect of Surface Friction on Tire – Pavement Contact Stresses during Vehicle Maneuvering', 140(4), pp. 1–8. doi: 10.1061/(ASCE)EM.1943-7889.0000691.

WANG, H. (2011) *ANALYSIS OF TIRE-PAVEMENT INTERACTION AND PAVEMENT RESPONSES USING A DECOUPLED MODELING APPROACH*. University of Illinois.

Wang, H. and Al-qadi, I. L. (2011) 'Evaluation of Surface-Related Pavement Damage due to Tire Braking', *Road Materials and Pavement Design*, pp. 101–121. doi: 10.3166/RMPD.11.101-121.

WHITE, T. ande and ZAGHLOUL, S. (1993) 'Use of a Three-Dimensional , Dynamic Finite Element Program for Analysis of Flexible Pavement', *TRANSPORTATION RESEARCH RECORD 1388*, (TRB), pp. 60–69.

Wong, J. Y. (2001) *THEORY OF GROUND VEHICLES*. 3rd edn. New York,: John Wiley and Sons, Inc.,.

Yoo, P. J. *et al.* (2006) 'Flexible pavement responses to different loading amplitudes considering layer interface condition and lateral shear forces', *International Journal of Pavement Engineering*, 7(1), pp. 73–86. doi: 10.1080/10298430500516074.

Yoo, P. J. and Al-Qadi, I. L. (2007) 'Effect of transient dynamic loading on flexible pavements', *Transportation Research Record*, (1990), pp. 129–140. doi: 10.3141/1990-15.

Zhu, J. J. (2011) *Study of Vehicle Dynamics with Planar Suspension Systems (PSS)*. University of Waterloo,Canada.

Zumrawi, M. M. E. (2015) 'Investigating Causes of Pavement Deterioration in Khartoum State , Sudan', 9(11), pp. 1458–1463.